



**Determination of the AIDA-I  $\beta$ -barrel crystal structure:  
getting the clue to the autotransporter secretion pathway**

Inaugural-Dissertation

zur Erlangung des Doktorgrades  
der Mathematisch-Naturwissenschaftlichen Fakultät  
der Heinrich-Heine-Universität Düsseldorf

vorgelegt von

**Iris Gawarzewski**

aus Leverkusen

Düsseldorf, November 2013

aus dem **Institut für Biochemie**  
der Heinrich-Heine-Universität Düsseldorf

Gedruckt mit der Genehmigung der  
Mathematisch-Naturwissenschaftlichen Fakultät der  
Heinrich-Heine-Universität Düsseldorf

Referent: Prof. Dr. rer. nat. Lutz Schmitt  
Korreferent: Prof. Dr. rer. nat. Joachim Jose

Tag der mündlichen Prüfung:

*„Misserfolge sind oft notwendige Umwege zum Erfolg.“*  
*N. N.*

# Contents

<b>Contents</b>	<b>I</b>
<b>Summary</b>	<b>III</b>
<b>Zusammenfassung</b>	<b>IV</b>
<b>1 Introduction</b>	<b>1</b>
1.1 Secretion systems in Gram-negative bacteria	3
1.1.1 The type I secretion system (T1SS)	3
1.1.2 The type II secretion system (T2SS)	3
1.1.3 The type III secretion system (T3SS)	3
1.1.4 The type VI secretion system (T4SS)	3
1.1.5 The type V secretion system (T5SS)	4
1.1.6 The type VI secretion system (T6SS)	5
1.1.7 The chaperone-usher (CU) pathway	6
1.1.8 The nucleation/precipitation pathway (T8SS)	6
1.2 Surface display of recombinant proteins	6
1.3 Adhesin involved in diffuse adherence (AIDA-I)	7
1.4 Structural and biochemical insights into the biogenesis of monomeric AT	9
<b>2 Aims and objectives</b>	<b>14</b>
<b>Chapter 1</b>	<b>15</b>
<b>Chapter 2</b>	<b>30</b>
<b>Chapter 3</b>	<b>56</b>
<b>Chapter 4</b>	<b>64</b>
<b>3 General discussion</b>	<b>109</b>
3.1 Crystal package	110
3.2 Structural analysis of the transport unit of AIDA-I	111
3.2.1 The overall structure of AIDA-I-linker- $\beta_2$	111
3.2.2 Comparison with other monomeric AT	112
3.2.3 A charged cluster at the extracellular side of AIDA-I-linker- $\beta_2$ serves as a binding platform for the $\beta_1$ -domain	114
3.2.4 A common secretion mechanism for monomeric AT	115
3.3 Outlook	117



---

<b>4 References</b>	<b>118</b>
<b>5 Abbreviations</b>	<b>122</b>
<b>6 Acknowledgements</b>	<b>124</b>
<b>7 Curriculum vitae</b>	<b>126</b>
<b>8 Statement</b>	<b>128</b>

## Summary

During evolution, secretion mechanisms were developed in Gram-negative bacteria to export a huge variety of proteins, which are involved bacterial communication, nutrient uptake, detoxification and pathogenicity. Among them, the type V secretion system (T5SS) is widely used by pathogenic bacteria to export adhesins, enzymes, toxins and other virulence factors but the detailed transport process is not completely known until now.

The topic of this thesis was the determination of the X-ray crystal structure of the transport unit of *adhesin involved in diffuse adherence* (AIDA-I) from enteropathogenic *Escherichia coli*, which belongs to the group of monomeric autotransporter within the T5SS. The transport unit of AIDA-I, termed AIDA-I-linker- $\beta_2$ , was fused to an N-terminal signal peptide for the transport across the inner membrane, which is subsequently cleaved off, a his<sub>6</sub>-tag and a peptide antigen tag for immunodetection and purification. According to the position of the his<sub>6</sub>-tag at the N- or C-terminus, these recombinant autotransporter were termed FP-HisN163 and FP-HisC163. The induced expression resulted in the production of two different forms of FP-HisN163 and FP-HisC163. The weakly expressed forms represented the correctly cleaved and properly folded autotransporter, which was confirmed by heat modification studies. The highly expressed forms still contained the N-terminal signal peptide. This signal peptide should have been removed by the signal peptidase during the Sec-dependent transport across the inner membrane allowing the correct folding of the autotransporter. Different expression conditions under the control of an inducible promotor and different kinds of *Escherichia coli* strains were tested to promote the expression of the correctly folded forms of FP-HisN163 and FP-HisC163. None of the tested condition was suitable for this purpose. Finally, by constitutive expression, the amount of correctly processed and folded FP-HisN163 was suitable for purification and crystallization trials. Several crystallization conditions resulted in crystals that were analysed by X-ray diffraction. A data set of one crystal was used to solve the structure of the transport unit AIDA-I-linker- $\beta_2$  at 3.0 Å resolution. AIDA-I-linker- $\beta_2$  contains a  $\beta$ -barrel, which is composed of 12  $\beta$ -strands connected by short periplasmic turns and long extracellular loops. The linker domain is accommodated in the hydrophilic pore, whereas the N-terminal part adopts an  $\alpha$ -helical fold and the C-terminal part remains unstructured. The transport unit of AIDA-I shares a high structural similarity to other monomeric autotransporter indicating a common secretion mechanism.

## Zusammenfassung

Im Laufe der Evolution entwickelten sich in Gram-negativen Bakterien Sekretionssysteme, um Proteinen, die an Prozessen wie bakterieller Kommunikation, Nährstoffaufnahme, Detoxifikation und Pathogenität beteiligt sind, zu exportieren. Darunter wird das Typ V Sekretionssystem (T5SS) vornehmlich von pathogenen Bakterien verwendet, um Adhäsine, Enzyme, Toxine und andere Virulenzfaktoren zu sekretieren. Dabei ist der genaue Transportmechanismus bis heute nicht bekannt.

Die Zielsetzung dieser Arbeit bestand in der röntgenkristallographischen Strukturaufklärung der Transporteinheit des *adhesin involved in diffuse adherence* (AIDA-I) aus enteropathogenen *Escherichia coli*, das zur Gruppe der monomeren Autotransporter innerhalb der T5SS gezählt wird. Die Transporteinheit von AIDA-I, die im Rahmen dieser Arbeit mit AIDA-I-linker- $\beta_2$  bezeichnet wird, wurde mit einem Signalpeptid für den Transport über die cytoplasmatische Membran, einem His<sub>6</sub>-Tag und einem Antigen-Tag zur Immunodetektion und Reinigung fusioniert. Der His<sub>6</sub>-Tag wurde einmal hinter dem Signalpeptid, welches nach Transport über die cytoplasmatische Membran abgespalten wird, und einmal hinter der  $\beta_2$ -Domäne am C-Terminus eingesetzt. Die resultierenden Fusionsproteine wurden mit FP-HisN163 und FP-HisC163 gekennzeichnet. Die induzierte Expression resultierte in der Bildung zweier unterschiedlich prozessierten Formen von FP-HisN163 und FP-HisC163. Die schwächer exprimierten Formen ließen aufgrund von Entfaltungsstudien darauf schließen, dass diese vollständig prozessiert und korrekt gefaltet waren. Die überwiegend gebildeten Formen der rekombinanten Autotransporter hingegen wiesen das N-terminale Signalpeptid noch auf. Dieses sollte während des Transportprozesses über die cytoplasmatische Membran durch die Signalpeptidase abgespalten werden und so eine korrekte Faltung der Autotransporterproteine ermöglichen. Um die Bildung der vollständig prozessierten und korrekt gefalteten Formen von FP-HisN163 und FP-HisC163 zu verstärken, wurden verschiedene Expressionsbedingungen und *Escherichia coli*-Expressionsstämme getestet. Dabei erwies sich keine der gewählten Bedingungen als geeignet. Durch konstitutive Expression konnten ausreichende Mengen an prozessiertem und korrekt gefaltetem FP-HisN163 zu Reinigungs- und Kristallisationszwecken produziert werden. In einer Reihe unterschiedlicher Kristallisationsbedingungen konnten Kristalle gewonnen und röntgendiffraktometrisch vermessen werden. Der Datensatz eines Kristalls wurde schließlich verwendet, um die Struktur der Transporteinheit AIDA-I-linker- $\beta_2$  mit 3.0 Å Auflösung zu lösen. AIDA-I-linker- $\beta_2$  weist ein  $\beta$ -Fass auf, das aus 12  $\beta$ -Strängen besteht. Diese sind über kurze periplasmatische und längere extrazelluläre Bereiche miteinander verbunden. Die Linkerdomäne durchzieht die Pore des  $\beta$ -Fass, wobei nur der N-Terminus eine  $\alpha$ -helikale Konformation annimmt und der C-Terminus unstrukturiert bleibt. Die Transporteinheit von AIDA-I weist eine hohe strukturelle Übereinstimmung mit anderen monomeren Autotransportern auf, was auf einen gemeinsamen Sekretionsmechanismus hindeutet.

## 1. Introduction

Within the kingdom of prokaryotic microorganisms, two groups of bacteria are distinguished by Gram staining due to the composition of their cell envelope [1]. Gram-positive bacteria possess a cytoplasmic membrane, which is surrounded by many layers of peptidoglycan resulting in a thick cell wall (Figure 1, CW) [3]. In contrast, Gram-negative bacteria are surrounded by an inner (Figure 1, IM) and an outer membrane (Figure 1, OM). Only a thin layer of peptidoglycan is located in between both membranes (Figure 1, P). During Gram staining, only the thick cell wall remains stained resulting in the differentiation of Gram-positive and Gram-negative bacteria [1; 3].

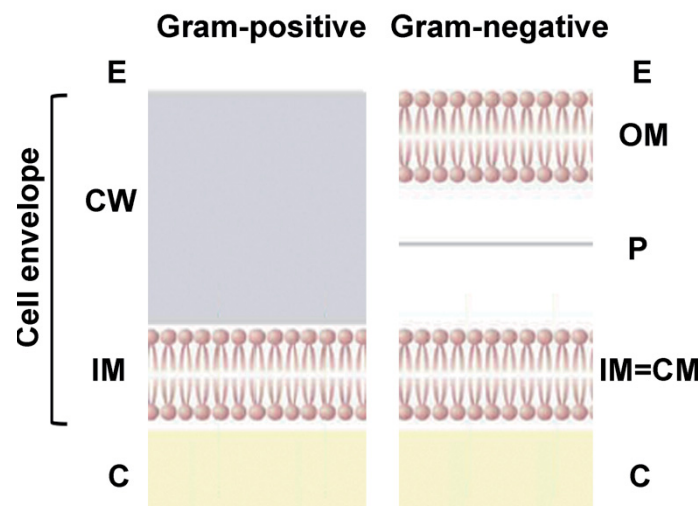


**Figure 1 Differences in cell envelope composition between Gram-positive and Gram-negative bacteria**

E: extracellular space; CW: cell wall; CM; cytoplasmic membrane; C: cytoplasm; OM: outer membrane; P: periplasm; IM: inner membrane. Picture adapted from [3].

The secretion of proteins across membranes is an essential ability for both, Gram-positive and Gram-negative bacteria. Within the group of Gram-negative bacteria a huge variety of proteins are secreted, which are involved in bacterial communication, nutrient uptake, detoxification and pathogenicity [4]. To overcome the membrane barriers different secretion mechanisms have evolved, which are divided in the type I-VIII secretion systems (T1SS-T6SS, T8SS) and the chaperone-usher pathway [3; 5-13] (Figure 2). All proteins, which are secreted, contain a signal sequence, which target them to their specific transport machinery (Figure 2, green rectangle). The T1SS, T3SS, T4SS and the T6SS are composed of specific proteins, which bridge the cytoplasm with the extracellular space. Thus, these systems act in an one-step manner without periplasmic intermediates [14].

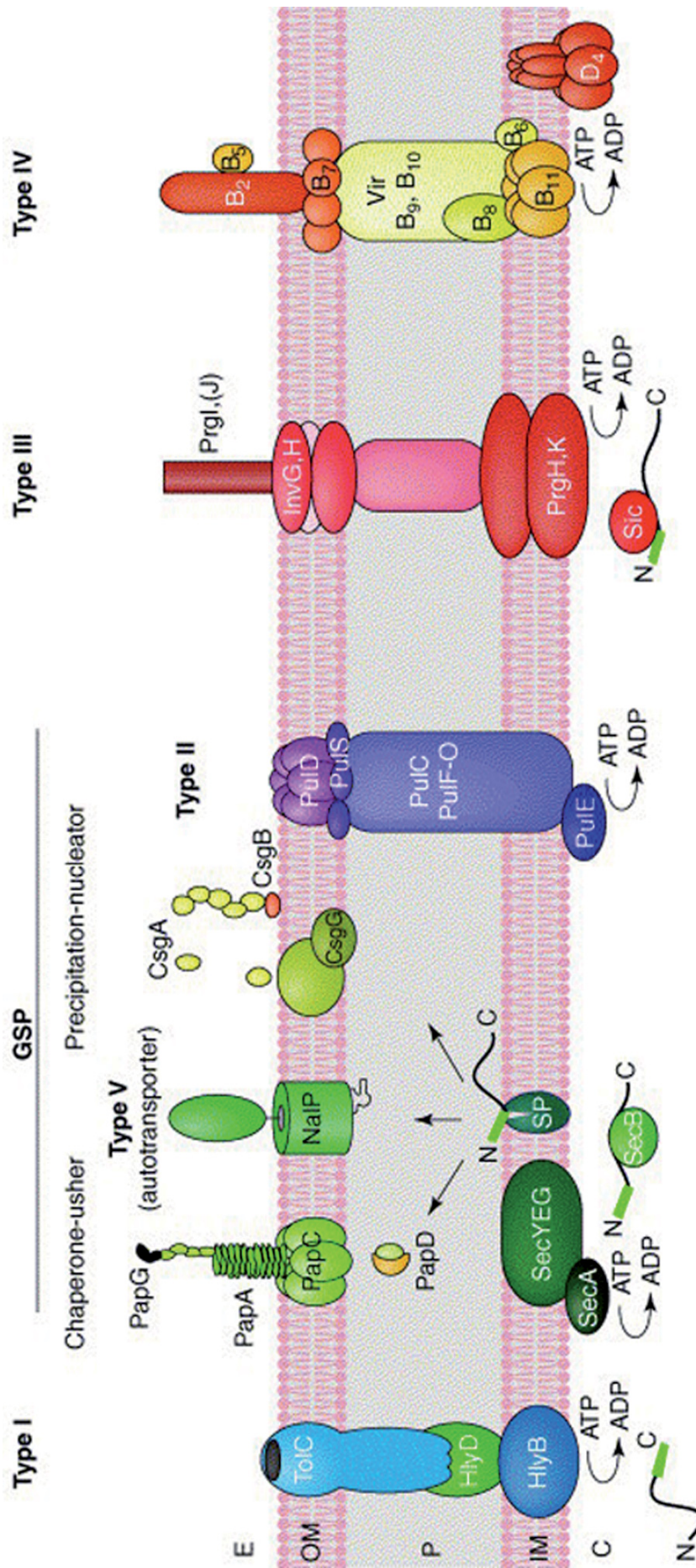


**Figure 2 Secretion systems in Gram-negative bacteria**

C: Cytoplasm; IM: inner membrane; P: periplasm; OM: outer membrane; E: extracellular space; green rectangles: signal peptide; GSP: general secretory or Sec-dependent pathway

The secretion pathways can be grouped into GSP-dependent and GSP-independent mechanisms. Sec-independent secretion systems transport their substrates directly across the outer membrane (T1SS, T3SS, T4SS and T6SS).

For the Sec-dependent secretion systems, periplasmic intermediates are observed, which are subsequently transported by their specific transport machineries located in the outer membrane (T2SS, T5SS, chaperone-usher pathway and the precipitation-nucleation pathway). Modified from [2].

On the opposite, the T2SS, T5SS, the chaperone-usher (CU) pathway and T8SS are dependent of the general secretory (GSP or Sec-dependent) or the Twin Arginine Translocation (Tat) pathway to overcome the inner membrane [15; 16]. The periplasmic intermediates are subsequently transported across the outer membrane by specific secretion machineries [3].

## **1.1 Secretion systems in Gram-negative bacteria**

### **1.1.1 The type I secretion system (T1SS)**

In general, the T1SS is composed of three different proteins: a trimeric outer membrane protein (Omp), a multimeric membrane fusion protein (MFP) and an ATP-binding cassette (ABC) protein [8]. The energy for the transport process is delivered by ATP-hydrolysis through the ABC protein. Together, the ABC protein, the MFP and the OMP form a channel connecting the cytoplasm with the cell surface. Thus, the T1SS is also termed ABC-transporter-dependent pathway, which is capable of transporting polypeptides up to 800 kDa. In Gram-negative bacteria the haemolysin ABC-transporter of *Escherichia coli* serves as a prototype. Here, TolC (Omp), HlyD (MFP) and HlyB (ABC protein) form a complex to secrete the toxin HlyA (Figure 2) [8].

### **1.1.2 The type II secretion system (T2SS)**

The T2SS is composed of at least more than 12 different proteins, which form a multimeric complex (secreton) to transport enzymes and toxins across the outer membrane [9]. A well characterized example is the secretion of the pullanase (PulA) from *Klebsiella oxytoca* (Figure 2) [17]. Here, PulD forms an oligomeric pore in the outer membrane. PulS connects PulD with a complex built up by PulC/F-O, which is anchored in the inner membrane spanning the periplasm. PulE is responsible for ATP-hydrolysis. The T2SS is capable of secreting folded proteins. These fold after Sec-dependent translocation across the inner membrane. Additional to the pilus-like structure, which is similar to the structure of type IV pili, several of the T2SS genes are homologous to genes required for type IV pili assembly. Thus, these systems seem to be evolutionary related [18].

### **1.1.3 The type III secretion system (T3SS)**

The T3SS or injectisome represents a secretion mechanism, which is mainly used by pathogenic or symbiotic Gram-negative bacteria, e.g. *Escherichia*, *Shigella* and *Yersinia*. This system is used to inject effector proteins directly into host cells (Figure 2) [7; 19]. In general, the injectisome is composed of a basal structure, a needle complex (NC) and, depending on the family, a filament, a needle or a pilus. Since the T3SS acts in an one-step manner, it harbors and ATPase activity. Furthermore, it shares common features of bacterial flagella and thus seems to be evolutionary related.

### **1.1.4 The type IV secretion system (T4SS)**

The T4SS is an important pathway for pathogenic bacteria to exchange genetic information across kingdom boundaries and deliver effector proteins to eukaryotic target cells requiring

direct cell contact [6; 20; 21]. Famous examples for the T4SS are the export machinery for pertussis toxin from *Bordetella pertussis* [6] and the T-DNA transfer systems from *Agrobacterium tumefaciens* (Figure 2) [22]: The T-DNA transfer system is composed of several proteins, which possess different functions (Figure 2): VirB4, VirB11 and VirD4 are responsible for ATP-hydrolysis, VirB1, VirB2 and VirB5 mediate cell adhesion and VirB3, VirB6, VirB7, VirB8, VirB9 and VirB10 are involved in DNA processing and transfer and in channel formation (Figure 2) [6]. The T4SS is divided in three subtypes: The first subtype comprises the conjugation system, which mediates the contact-dependent exchange of protein-bound single-stranded DNA (ssDNA) substrates after processing of the DNA at the origin of transfer (*oriT*). This exchange of DNA, integrated in the genome of the host cells, leads to dissemination of virulence and antibiotic-resistance genes and oncogenesis. The second subtype, the effector translocation system, is responsible for effector molecules delivery to host cells in a contact-dependent manner supporting bacterial colonization, survival within host cells and intoxication. Finally, the DNA uptake or release system represents the third subtype allowing the translocation of DNA to or from the extracellular milieu.

### 1.1.5 The type V secretion system (T5SS)

The T5SS enables the translocation of virulence proteins directly to the cell surface of pathogenic Gram-negative bacteria [23-25]. In general, T5SS show four functional domains: (I) a N-terminal signal peptide (SP) for Sec-dependent transport across the inner membrane, (II) a passenger domain, which harbors the biological activity outside of the cell, (III) a linker domain, which connects the passenger domain with the transport unit and the  $\beta$ -domain, which forms a  $\beta$ -barrel with a hydrophilic pore in the outer membrane. After Sec-dependent transport, the periplasmic intermediate is translocated across the outer membrane through the pore of the  $\beta$ -barrel (Figure 2). However, the exact translocation process across the outer membrane is unclear. To date, five subgroups of T5SS are differentiated: the subgroup Va comprises monomeric autotransporter (AT) harboring all information necessary for efficient translocation in one polypeptide chain. Subgroup Vb is termed the two-partner secretion system and includes proteins, where the passenger and the translocation functions are located in separated polypeptide chains. Trimeric autotransporter proteins are assigned to subgroup Vc. Here, three identical subunits contribute equally to the functional transport complex. A recently described protein, PlpD from *Pseudomonas aeruginosa*, was assigned to a new subgroup Vd, the fused two-partner secretion system. This protein shares common features of monomeric AT (Va) and those of the two-partner secretion system (Vb) fused in one polypeptide chain. The last subgroup Ve includes proteins, which contain the same functional domains of monomeric AT in one polypeptide chain, but in reversed order. Some examples for T5SS are the IgA1 protease from *Neisseria gonorrhoeae*, NalP from *Neisseria meningitidis*, BrkA from *Bordetella pertussis* and EspP and AIDA-I from *E. coli*. A detailed comparison of the transport units of T5SS as well as recent investigations on the secretion process is presented in chapter I.



### 1.1.6 The type VI secretion system (T6SS)

The T6SS is involved in contact-dependent defense (T6SS dueling) against other bacteria and phagocytic eukaryotes, which was recently discovered [26; 27]. Only less information is available but investigations have shown that this system acts as a dynamic organelle, analogous to a bacteriophage tail, attacking adjacent prey cells. It is composed of a base-plate complex, which connects the cytoplasm with the cell surface and a contractile phage sheath-like structure allowing the translocation of effector proteins comprising a spike- or tube-like fold (Figure 3) [28]. Recent studies showed that only T6SS positive cells of *Vibrio cholerae* were attacked by *Pseudomonas aeruginosa*. This system seems to be strictly regulated and capable of distinguishing between rival and neutral cells necessary, for e.g. biofilm formation.

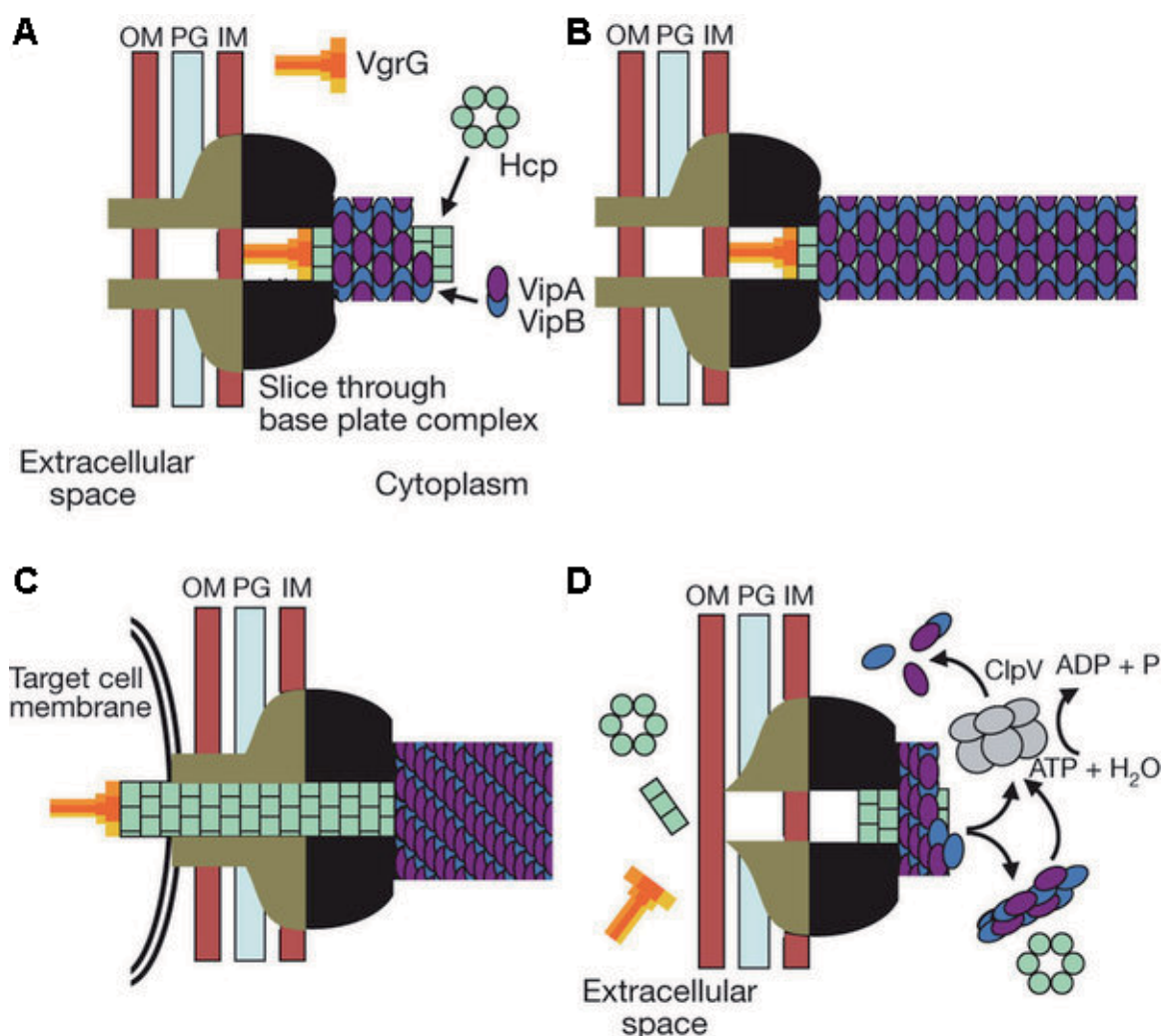


**Figure 3 Model of type VI secretion system action**

OM: outer membrane; PG: peptidoglycan; IM: inner membrane.

As a first step, the base-plate complex (black) is formed initiating the Hcp tube polymerization (A). Subsequently, the heterodimers of VipA and VipB polymerize to form the extended sheath around the Hcp tube (B). A conformational change of the base-plate complex, which is induced by an unknown extracellular signal, leads to sheath contraction and subsequent translocation of VgrG coupled to the Hcp tube across the membrane of the target cell (C). Finally, the contracted sheath is disassembled with the help of the ClpV ATPase and the released subunits are recycled. Without target cell penetration (C), Hcp and VgrG are secreted into the extracellular space (D). Modified from [28].



### 1.1.7 The chaperone-usher (CU) pathway

The CU pathway, is composed of integral outer membrane usher proteins and periplasmic chaperones, which act as accessory proteins for pilus assembly and secretion after Sec-dependent transport across the inner membrane (Figure 2) [3; 11-13]. The energy required for these processes seems to stem from the folding force of pilus subunits. The CU pathway enables the adhesion to host cells and is an important feature of pathogenic Gram-negative bacteria, such as *Pseudomonas* and *Escherichia*.

### 1.1.8 The nucleation/precipitation pathway (T8SS)

The nucleation/precipitation pathway or T8SS is responsible for curli biogenesis, which are adhesive fibrous organelles located at the cell surface of pathogenic Gram-negative bacteria [3; 29-31]. After Sec-dependent translocation, two different proteins are polymerized forming curli by a secretion platform consisting of two accessory periplasmic proteins and a lipoprotein in the outer membrane (Figure 2). These curli that show a different morphology and assembly mechanism compared to other pili, are involved in biofilm and micro-colony formation, host-specific and tissue-specific adhesion and cellular invasion. One example for the T8SS is the formation of amyloid curli in *Escherichia coli* [32].

## 1.2 Surface display of recombinant proteins

During the last decade the expression of proteins anchored to a surface has become more and more important for industrial and pharmaceutical applications, such as live vaccine development, antibody production, detoxification with bioadsorbents, whole-cell biocatalyst, biosensor development and for library screening of displayed peptides [33-35]. For this purpose, different techniques are available: (I) the phage display, (II) the yeast display and (III) the autodisplay [33; 35; 36]. The phage display technology was developed in 1985 by Smith using a filamentous fusion phage and is applied for displaying recombinant proteins [36; 37]. The yeast display, which most commonly uses *Saccharomyces cerevisiae*, focuses on the bioethanol production, chemical synthesis, adsorption of environmental pollutants and protein evolution [35]. Autodisplay is a technique, which uses autotransporter for surface display of recombinant proteins [33] and was firstly described by Maurer *et al.* (1997). Here, the transport unit of AIDA-I was used for efficient surface presentation of the cholera toxin B subunit and the peptide antigen tag PEYFK. Nowadays, the autodisplay systems using the transport unit of AIDA-I is commercially applied for the development of bioanalytical tools and biocatalysts, screening of potential molecule, protein drugs and antibodies and for the development of separation materials for peptides, proteins and chemicals (<http://www.autodisplay-biotech.com>). The surface display has several advantages, e.g. surface-exposed enzymes have direct access to their substrates in the surrounding media and expensive purification procedures of the products are redundant. Furthermore, matrix-bound proteins are more stable.

### 1.3 Adhesin involved in diffuse adherence (AIDA-I)

In 1989, Benz and Schmitt discovered a protein in an enteropathogenic *E. coli* strain from a patient suffering from infantile diarrhea, which was responsible for diffuse adherence to HeLa cells. Therefore, it was termed *adhesin involved in diffuse adherence* (AIDA-I). In 1995, AIDA-I was assigned to the group of monomeric autotransporter (AT), which belong to type V secretion systems (T5SS) [39]. Intensive research on AIDA-I revealed that it consists of five different domains (Figure 4): (I) an N-terminal signal peptide (SP) for Sec-dependent transport across the inner membrane, (II) a passenger ( $\alpha$ -) domain, which mediates diffuse adherence, (III) a predicted autochaperone ( $\beta_1$ -) domain, which is presumably involved in folding of the  $\alpha$ -domain, (IV) a linker domain and (V) a  $\beta_2$ -domain, which is predicted to form a  $\beta$ -barrel with a hydrophilic pore in the outer membrane (OM) [38; 40; 41]. A 145 kDa precursor form (preAIDA-I, Figure 4) is translated containing a SP at the N-terminus, which is removed after Sec-dependent transport across the inner membrane. The periplasmic intermediate proAIDA-I lacking the SP (Figure 4) is then glycosylated by the *autotransporter adhesin heptoyl-transferase* (Aah) [42]. Subsequently, the  $\beta_2$ -domain integrates into the outer membrane forming a pore, through which the  $\alpha$ -domain is translocated to the cell surface and adopts its active conformation possibly with the help of the  $\beta_1$ -domain, which is also found in other AT, e.g. BrkA, Hbp or IcsA [43-45]. Finally, mature AIDA-I is released by auto-proteolytic cleavage between serine<sup>846</sup> and alanine<sup>847</sup> but stays attached to the remaining AIDA<sub>C</sub> in the outer membrane (Figure 4) [46; 47]. The mature AIDA-I is responsible for adhesion, biofilm formation, aggregation and invasion into host cells [48; 49]. The translocation process across the outer membrane seems to be energized by the folding force of the  $\alpha$ -domain [50]. However, the exact mechanism of membrane integration of the  $\beta$ -barrel and  $\alpha$ -domain translocation is unclear until now.

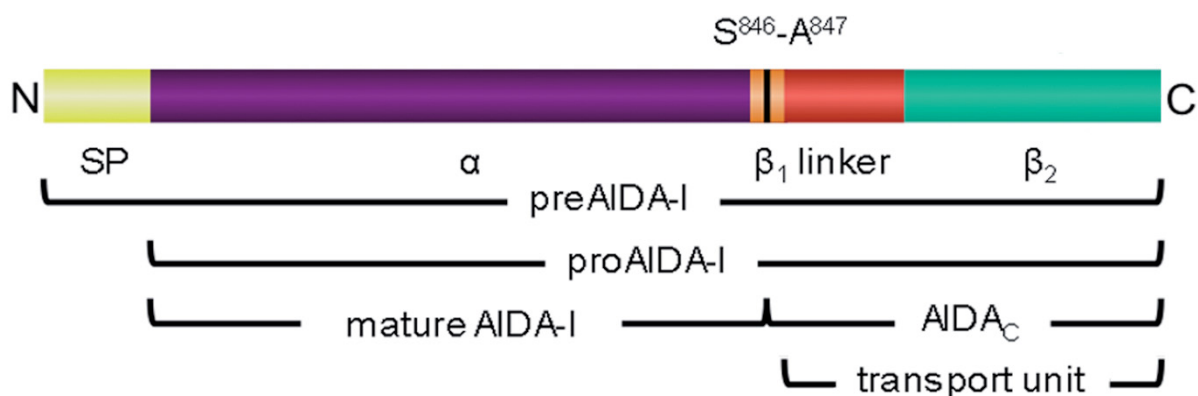


**Figure 4 Functional organization of the *adhesin involved in diffuse adherence* (AIDA-I)**

SP: signal peptide;  $\alpha$ : passenger domain;  $\beta_1$ : autochaperone domain;  $\beta_2$ :  $\beta$ -barrel forming domain in the outer membrane. AIDA-I is synthesized as preAIDA-I with a molecular weight of 145 kDa containing the SP. During Sec-dependent transport across the inner membrane, the signal peptidase cleaves off the SP resulting in proAIDA-I in the periplasm. Here, AIDA-I is glycosylated and subsequently translocated across the outer membrane. At the cell surface, the  $\alpha$ -domain is auto-proteolytically cleaved between S<sup>846</sup> and A<sup>847</sup> and mature AIDA-I is released but stays attached to AIDA<sub>C</sub>, which resides in the outer membrane. The mature AIDA-I is responsible for biological function. Picture taken from chapter IV.

In chapter I of this thesis, recent findings on the secretion process of monomeric AT are summarized and a model pathway is presented.

In the past, computational and biochemical analyses were conducted to get insights into the structure of AIDA-I. The mature AIDA-I is predicted to adopt a  $\beta$ -helical fold typical for self-associating autotransporter (SAATs) [49; 51] and the  $\beta_1$ -domain, which is also present in several AT [24], is thought to form a structure similar to the AC domain of IcsA, which was recently solved by X-ray crystallography [44]. For the transport unit of AIDA-I, several topology models were proposed [38; 47; 52]. According to Maurer *et al.* (1997), the  $\beta_2$ -domain was predicted to form a  $\beta$ -barrel in the outer membrane consisting of 14 antiparallel and amphipathic  $\beta$ -strands, connected by short periplasmic turns and longer extracellular loops (Figure 5). The linker domain was thought to form an  $\alpha$ -helix in the pore of the  $\beta$ -barrel [53]. Biochemical evidence for the membrane-integrated  $\beta$ -barrel was obtained from protease accessibility assays [40; 47]. The part of AIDA-I, which was protected by the membrane, was not accessible for protease digestion and matched AIDA<sub>C</sub>. Furthermore, it was shown by mutational analysis that all of the 14 predicted  $\beta$ -strands [39] were necessary for the outer membrane integration [54]. Additional studies focused on the analysis of the minimal linker length, which was determined to comprise 34 amino acids for sufficient translocation of a small peptide [55].

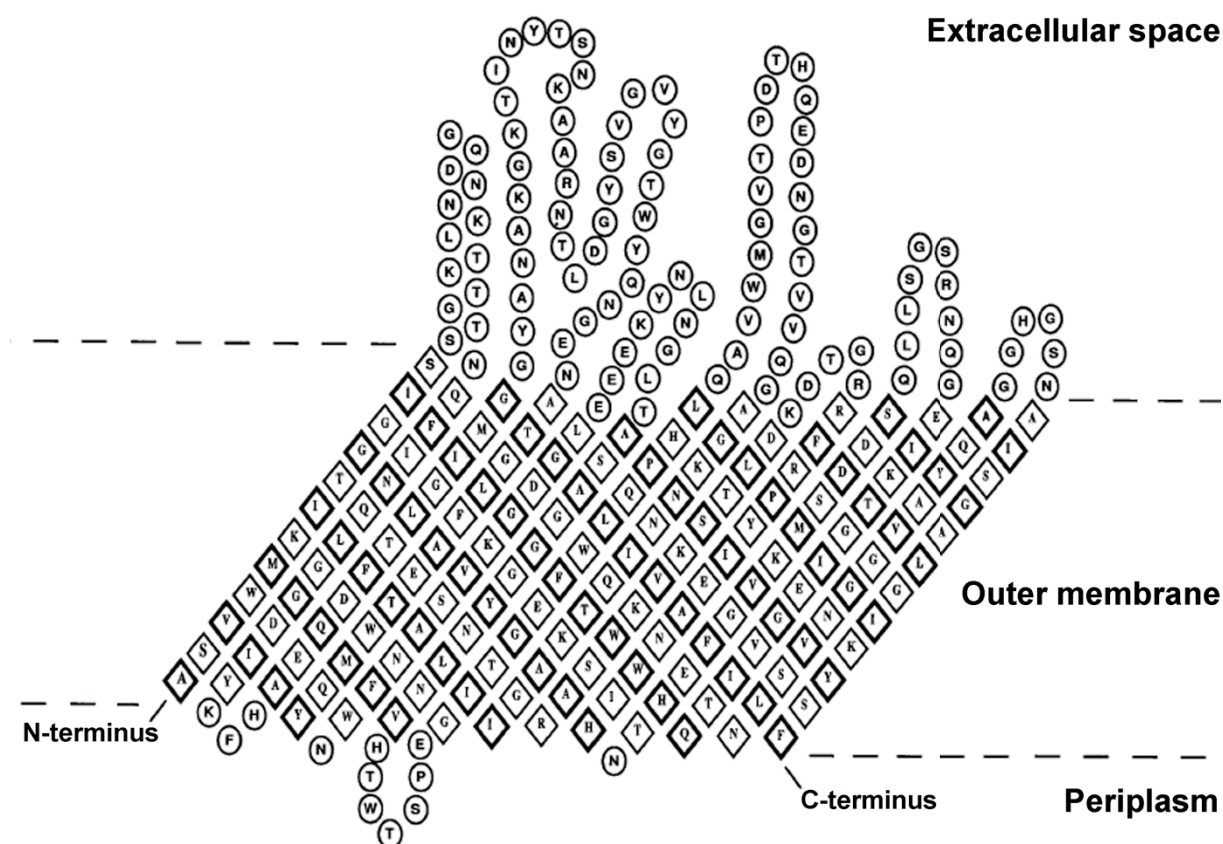


**Figure 5 Hypothetical topology model of the  $\beta$ -barrel of AIDA-I**

Amino acids (one-letter code) within the membrane are indicated by diamonds and non-membrane-embedded regions by circles. Hydrophobic (boldface typesetting) and hydrophilic (lightface typesetting) amino acids are denoted. Picture taken from [38].

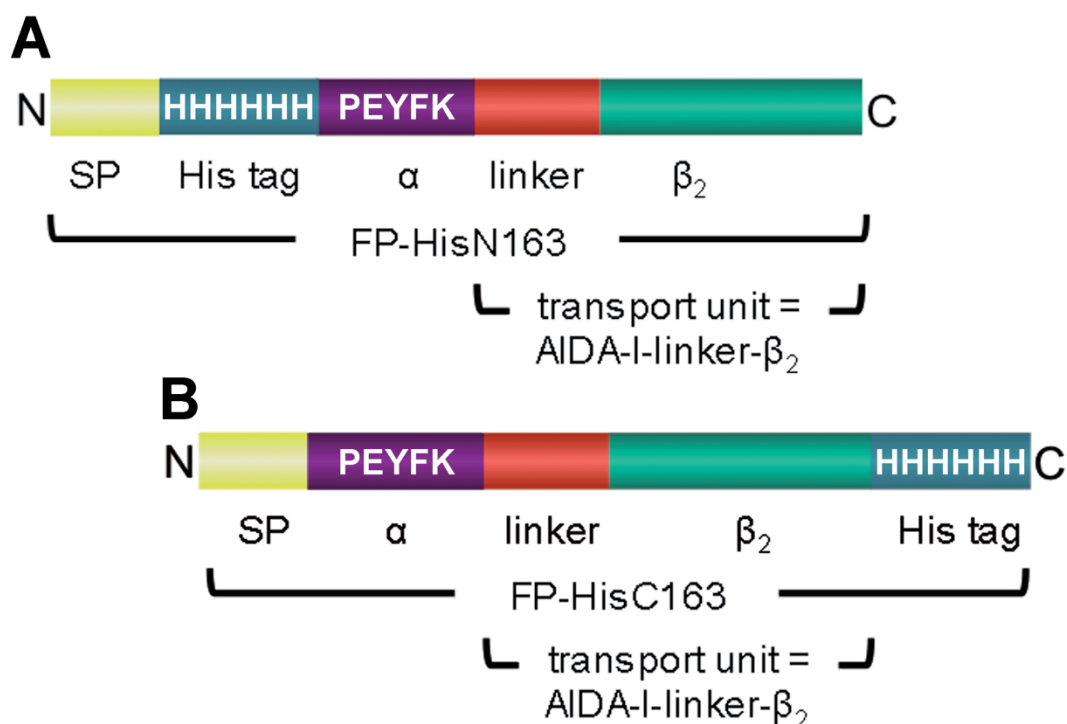


**Figure 6 Functional organization of FP-HisN163 (A) and FP-HisC163 (B)**

SP: signal peptide;  $\alpha$ : passenger domain;  $\beta_2$ :  $\beta$ -barrel forming domain in the outer membrane. The native  $\alpha$ -domain of AIDA-I was substituted by the peptide antigen tag (PEYFK) for immunodetection and the native linker and  $\beta_2$ -domains were fused at the C-terminus. For purification, a six-fold histidine tag (H) was introduced N-terminal to the PEYFK epitope (A) or C-terminal to the  $\beta_2$ -domain (B). Picture adapted from chapter IV.

Due to the lack of structural information, this thesis focuses on the structure determination of the transport unit of AIDA-I termed AIDA-I-linker- $\beta_2$  (Figure 6). For this purpose, the transport unit of AIDA-I was fused to two different tags for purification (six-fold histidine tag) and immunodetection (PEYFK). This recombinant autotransporter fusion protein was termed FP-HisN163 and FP-HisC163 carrying the histidine tag at N- or C-terminus (Figure 6) and the expression conditions were optimized as described in chapter II.

The crystal structure of AIDA-I-linker- $\beta_2$  was solved at 3.0 Å resolution (chapter III and IV). The transport unit consists of a  $\beta$ -barrel, which is composed of only 12  $\beta$ -strands contradicting the proposed topology models and a linker domain, which is accommodated in the pore of the  $\beta$ -barrel, but only the N-terminal part adopts an  $\alpha$ -helical conformation.

#### 1.4 Structural and biochemical insights into the biogenesis of monomeric AT

In contrast to the functional and structural diversity of passengers translocated by monomeric AT, the transport units share high structural similarity [56-59]. During the last decade, crystal structures of transport units of e.g. BrkA, EspP, EstA, NaIP[60-63] and Hbp (PDB code: 3AEH) were solved (Figure 7, highlighted in green). All of these structures revealed a 12-stranded  $\beta$ -barrel, which stands in contrast to the 14  $\beta$ -strands predicted not only for the transport unit of AIDA-I (see above) [52].

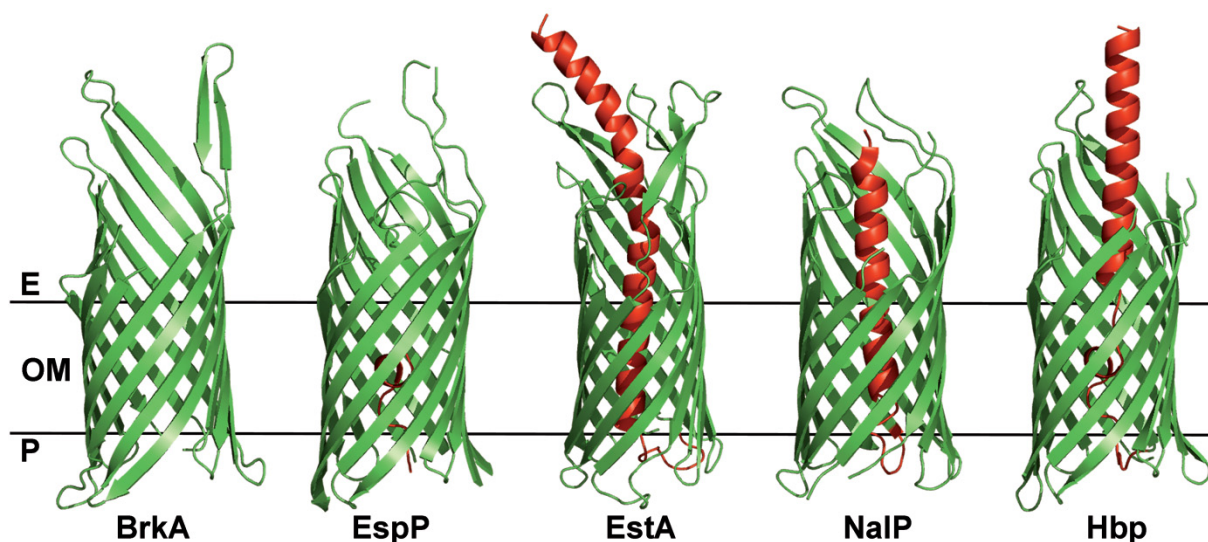


**Figure 7 Transport unit structures of monomeric AT**

Green: 12-stranded  $\beta$ -barrel; red:  $\alpha$ -helical linker; E: extracellular space; OM: outer membrane; P: periplasm

In all structures, the linker adopts an  $\alpha$ -helical conformation in the pore of the  $\beta$ -barrel, except for BrkA (Figure 7, highlighted in red). All of the structures in Figure 7 only show a fixed-image of the post-translocational state. Thus, various biochemical and mutational experiments as well as bioinformatic simulations were conducted to investigate the dynamics of the translocation process across the outer membrane. Among the different model pathways, which were proposed in the past, the hairpin (A) and the Omp85 model (B) are supported by numerous investigations (Figure 8) (chapter I).

According to the hairpin model (Figure 8A) [24], the linker domain adopts a hairpin-like conformation within the  $\beta$ -barrel, which is integrated into the outer membrane (Figure 8A, step 1). Subsequently, the unfolded passenger domain is pulled through the pore of the  $\beta$ -barrel by initial folding of the extracellular loop of the hairpin (Figure 8A, step 2). At the cell surface, the passenger domain starts to fold. After translocation, the fully folded passenger domain is presented at the cell surface (Figure 8A, step 3). In contrast to the hairpin model, the Omp85 model (Figure 8B) assumes that the outer membrane factor Omp85 is required for membrane integration of the  $\beta$ -barrel [53; 64; 65]. Subsequent to Sec-dependent transport across the inner membrane, the AT adopts a stable conformation in the periplasm interacting with chaperones and Omp85 (Figure 8B, step 1). This periplasmic intermediate is integrated into the outer membrane by Omp85, which maintains the  $\beta$ -barrel of the pre-folded autotransporter in an 'open' conformation (Figure 8B, step 2). After translocation of the passenger domain, Omp85 dissociates from the  $\beta$ -barrel and the passenger domain adopts its fully folded conformation at the cell surface (Figure 8B, step 3).

Despite experimental evidence for both models, neither the hairpin nor the Omp85 model is able to explain all data derived from structural and biochemical analyses [57; 64]. Several investigations showed that folded or modified passenger domains were detectable at the cell surface [66; 67]. Regarding the pore size of the transport units, which is too narrow to accommodate those passenger domains and an additional folded linker domain (Figure 7), these observations are inconsistent with the hairpin model [53; 64].



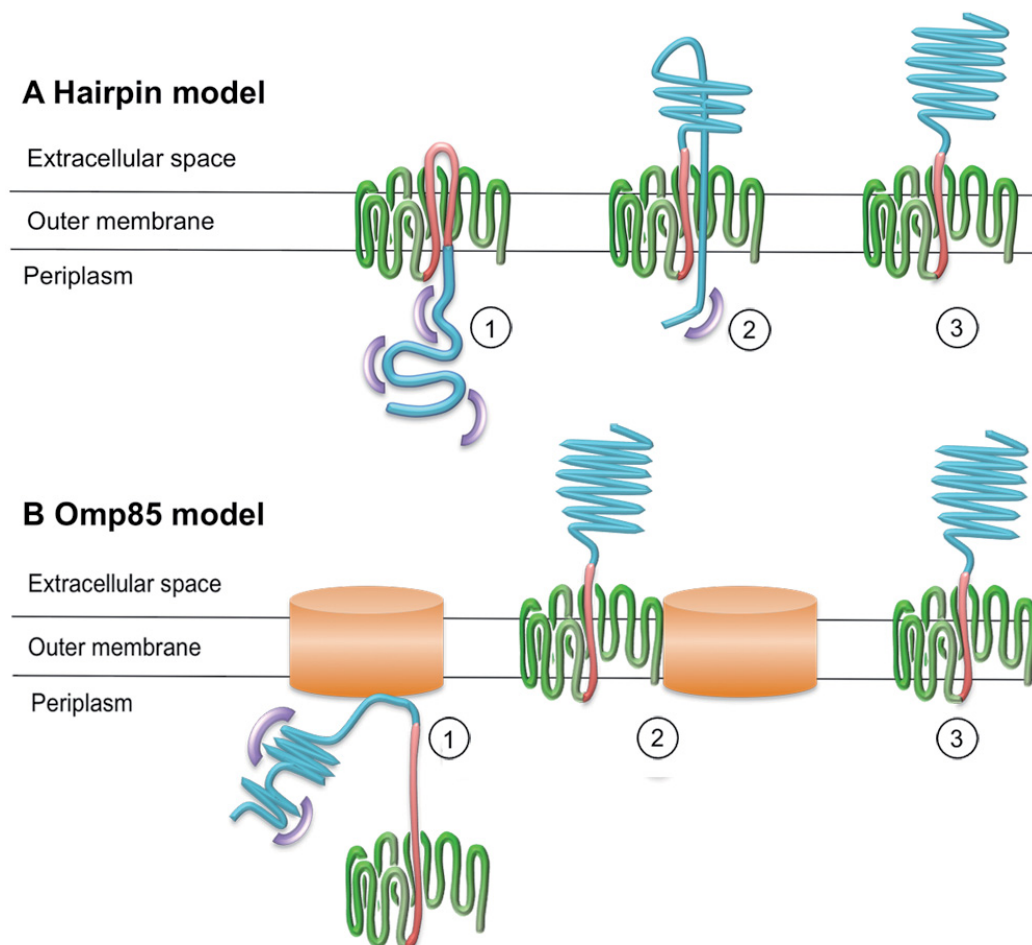


**Figure 8 Postulated mechanisms of type V translocation across the outer membrane**

Green:  $\beta$ -barrel; red:  $\alpha$ -helical linker; blue: passenger domain; orange: Omp85; violet: periplasmic chaperones. According to the hairpin model (A), the linker domain forms a hairpin-like structure in the pore of the  $\beta$ -barrel (step A1) and the passenger domain is pulled through this pore (step A2). Finally, the passenger domain adopts its fully folded conformation at the cell surface (step A3). In the Omp85 model (B), the autotransporter interacts with BamA (step B1) and is subsequently integrated into the outer membrane in an 'open' conformation (step B2), allowing transport of partially folded passengers. After translocation, across the outer membrane, the passenger domain obtains its active conformation in the extracellular space (step B3). Taken from chapter I.

Furthermore, it was shown that the C-terminus of the passenger domain is detectable at the cell surface before the N-terminus reaches the extracellular space [45; 50; 68]. These results strongly indicate a hairpin-like fold of the linker domain necessary for initiation of passenger domain translocation but contradicting the Omp85 model. Thus, a combination of both the hairpin and the Omp85 model was proposed (Figure 9) supported by recent investigations on the monomeric AT EspP and the discovery of the translocation assembly machinery (TAM) [69-72].

According to this alternative model, the AT partially folds in the periplasm after Sec-dependent transport across the inner membrane stabilized through interaction with periplasmic chaperones (Figure 9, step 1). At this point, the linker domain is incorporated in the incompletely folded  $\beta$ -barrel forming a hairpin-like structure. Afterwards, the prefolded AT is targeted to the outer membrane (Figure 9, step 2). The TAM complex stabilizes the passenger domain whilst the  $\beta$ -barrel interacts with the BAM complex.

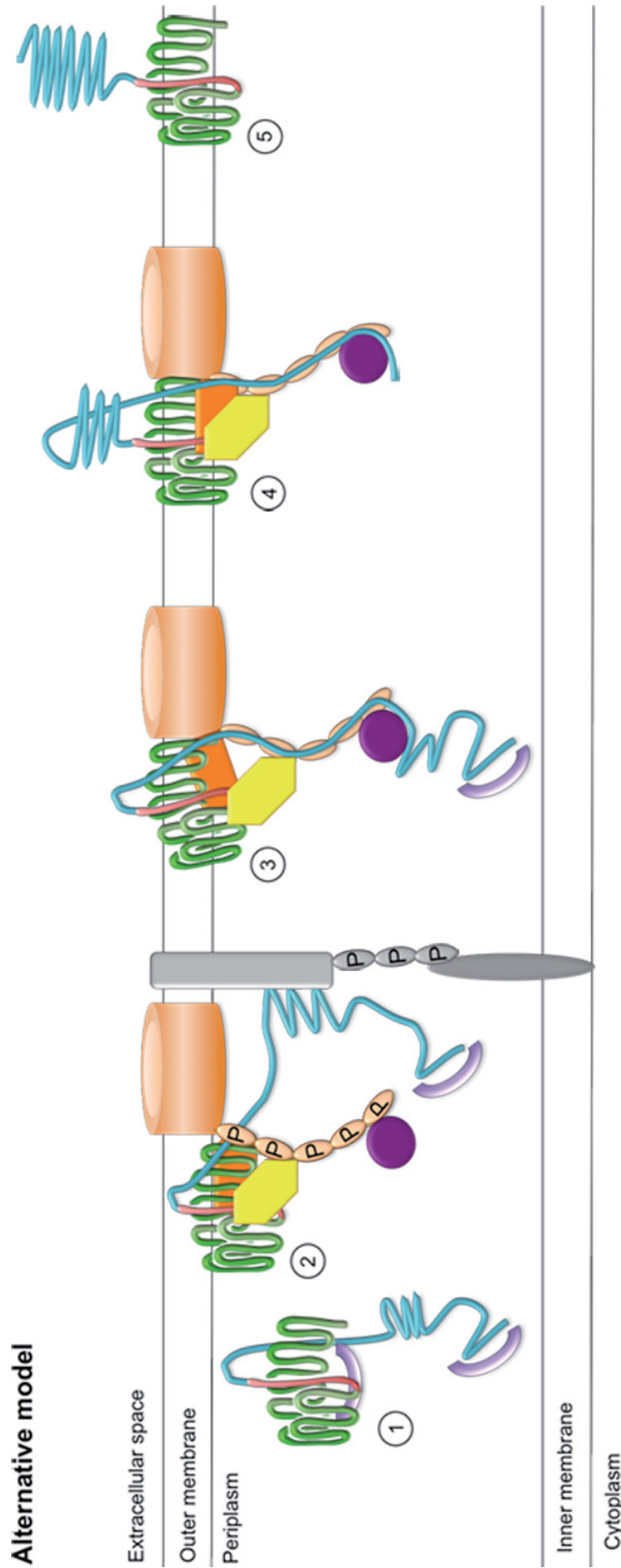


**Figure 9 Alternative model mechanism of type V passenger translocation across the outer membrane.**

Green:  $\beta$ -barrel; blue: passenger domain; red: linker domain; light gray: SurA; light gray: TamA; dark gray: BamB; yellow: POTRA domains. The autotransporter interacts with the periplasmic chaperone Skp and forms a stable intermediate with the linker domain incorporated in the pore of the prefolded  $\beta$ -barrel (step 1). This intermediate is targeted to the outer membrane interacting with TAM and the Bam complex (step 2). The prefolded  $\beta$ -barrel is integrated in the outer membrane while the passenger domain interacts with SurA and the POTRA domains of BamA (step 3), resulting in a stepwise transfer across the outer membrane (step 4). Finally, the passenger domain adopts its fully folded conformation at the cell surface (step 5). Taken from chapter I.

Due to a conformational change, the POTRA domains of Omp85 and the periplasmic chaperone SurA interact with the passenger domain, while the  $\beta$ -barrel is integrated into the outer membrane presenting the hairpin-like structure at the cell surface (Figure 9, step 3). The initial folding of the hairpin initiates the stepwise translocation of the passenger domain, which adopts its active conformation in the extracellular space (Figure 9, step 4). After completion of passenger translocation, the  $\beta$ -barrel assembly is finished resulting in the dissociation of the BAM complex (Figure 9, step 5). The periplasm and the cell surface are devoid of ATP. Thus, the translocation process seems to be energized by the folding force of AT domains [50]. All data obtained from crosslinking and mutagenesis experiments, heat modifiability and protease accessibility assays and structural analysis of monomeric AT are consistent with the alternative model, which considers several observations not explainable with only the hairpin or the Omp85 model (chapter I and general discussion).

For AIDA-I, only biochemical evidence and bioinformatic analyses were available due to lacking structural information. In 2007, Berthiaume *et al.* showed that mutations in the linker domain affected the translocation of the passenger domain, which is glycosylated in the periplasm ensuring the functional conformation of mature AIDA-I [42]. Other studies revealed that the  $\beta_2$ -domain could only fold in solution, when the  $\beta_1$ -domain or a solid support was present indicating that specific biological factors may assist correct folding [74; 75]. However, interaction with periplasmic chaperones, such as Skp, SurA or DegP [74], the outer membrane factor BamA [76] or other factors could not be observed until now.



## 2. Aims and objectives

Pathogenic Gram-negative bacteria use the type V secretion system (T5SS) to export adhesins, enzymes, toxins and other virulence factors. In recent years, lots of biochemical and structural data about monomeric AT, which are members of the subgroup 'a' of T5SS, were obtained and different model pathways were developed, which try to explain the translocation mechanisms of passenger domains across the outer membrane but detailed information of this process remains unclear. For the *adhesin involved in diffuse adherence* (AIDA-I) lots of biochemical data have been gained but no structural information is available. The aim of this doctoral thesis is to determine the structure of the transport unit of AIDA-I using X-ray crystallography allowing to investigate the AIDA-I biogenesis and to obtain a potential target for drug design against gastrointestinal diseases caused by enteropathogenic *E. coli*.

## *Chapter I*

### **Structural comparison of the transport units of type V secretion systems**

Published in: *Biological chemistry*

Impact factor: 2.965

Own proportion to this work: 70 %

Writing of the manuscript

## Review

Iris Gawarzewski, Sander H.J. Smits, Lutz Schmitt\* and Joachim Jose\*

## Structural comparison of the transport units of type V secretion systems

**Abstract:** Pathogenic gram-negative bacteria have evolved several secretion mechanisms to translocate adhesins, enzymes, toxins, and other virulence factors across the inner and outer membranes. Currently, eight different secretion systems, type I–type VIII (T1SS–T8SS) plus the chaperone-usher (CU) pathway, have been identified, which act in one-step or two-step mechanisms to traverse both membrane barriers. The type V secretion system (T5SS) is dependent first on the Sec translocon within the inner membrane. The periplasmic intermediates are then secreted through aqueous pores formed by  $\beta$ -barrels in the outer membrane. Until now, transport across the outer membrane has not been understood on a molecular level. With respect to special characteristics revealed by crystal structure analysis, bioinformatic and biochemical data, five subgroups of T5SS were defined. Here, we compare the transport moieties of members of four subgroups based on X-ray crystal structures. For the fifth subgroup, which was identified only recently, no structures have thus far been reported. We also discuss different models for the translocation process across the outer membrane with respect to recent findings.

**Keywords:** alternative model; gram-negative; hairpin model; Omp85 model; type V secretion systems.

**\*Corresponding authors:** Lutz Schmitt, Institute of Biochemistry, Heinrich Heine University Düsseldorf, Universitätsstr. 1, D-40225 Düsseldorf, Germany, e-mail: lutz.schmitt@hhu.de; and Joachim Jose, Institute of Pharmaceutical and Medical Chemistry, Westphalian Wilhelms University Münster, Corrensstr. 48, D-48149 Münster, Germany, e-mail: joachim.jose@uni-münster.de  
**Iris Gawarzewski and Sander H.J. Smits:** Institute of Biochemistry, Heinrich Heine University Düsseldorf, Universitätsstr. 1, D-40225 Düsseldorf, Germany

## Introduction

The secretion of proteins is crucial not only for pathogenic gram-negative bacteria, but also a wide variety of enzymes

are secreted for utilization of exogenous nutrients. During evolution, different secretion mechanisms developed in order to traverse the inner and outer membrane barriers; they include the type I–VIII secretion systems (T1SS–T8SS) and the chaperone-usher (CU) pathway (Desvaux et al., 2009). Among these, T1SS, T3SS, T4SS, T6SS, and T7SS are composed of protein complexes spanning both the inner and the outer membrane, promoting secretion in a single step (Rego et al., 2010). In contrast, T2SS, T5SS, T8SS, and the CU pathway are dependent on the Sec or the Tat translocon to cross the inner membrane. The final translocation is mediated by specific secretion mechanisms resulting either in the release into the extracellular space or the surface display of effector proteins (Dautin and Bernstein, 2007).

Among the two-step secretion systems, the T5SS is probably the simplest process for the export of adhesins, enzymes, toxins, and other virulence factors with varying sizes and structures (Henderson et al., 2004). Typically, members of T5SS contain a signal peptide at the N-terminus mediating Sec-dependent transport across the inner membrane and a passenger domain that exerts biological activity in the extracellular space. A linker domain connects the passenger and the  $\beta$ -domain, which forms a  $\beta$ -barrel with a hydrophilic pore in the outer membrane. Different subgroups were identified with respect to special characteristics, such as polypeptide-transport-associated (POTRA) domains, oligomerization state, and domain arrangement.

Subgroup Va is defined as the group of ‘classical’ autotransporters and includes the monomeric autotransporters containing all information required for translocation across both membranes in a single polypeptide chain (Jose et al., 1995; Desvaux et al., 2004). The two-partner-secretion (TPS) system is assigned to subgroup Vb. In this subgroup, the passenger and the transporter are expressed as two different proteins referred to as TpsA and TpsB (Clantin et al., 2007). Here, the transporter TpsB contains two POTRA domains for recognition of its corresponding passenger TpsA. A third subgroup (Vc) covers the trimeric autotransporters, which are composed of three identical

subunits (Cotter et al., 2005). Each subunit contributes four  $\beta$ -strands to the resulting 12-stranded  $\beta$ -barrel and thus deploying three passenger domains in the extracellular space. In 2010, Salacha et al. discovered a new type of autotransporter protein in *Pseudomonas aeruginosa*, termed PlpD. This protein shares the common features of classical autotransporters (Va) and TpsB proteins (Vb) in one polypeptide chain. In PlpD, the passenger domain is connected to the transport domain by only one POTRA domain. Therefore, this protein was assigned to the new subgroup Vd, termed fused TPS systems (Leo et al., 2012). Recently, the crystal structures of two adhesins, intimin of *Escherichia coli* and invasins of *Yersinia* spp., were described (Fairman et al., 2012). These structures revealed architectures similar to those of classical autotransporters of subgroup Va but in reverse order. Here, the N-terminal part of the protein chain forms a  $\beta$ -barrel domain and the C-terminal part harbors the passenger domain. Consequently, intimin and invasins were assigned to a new subgroup Ve, comprising inverted autotransporters (Leo et al., 2012).

Despite extensive biochemical and structural data, the exact mechanism of the outer membrane transport of T5SS remains unclear. Different pathways have been discussed, including the hairpin model (Henderson et al., 2004) and the BamA/Omp85 model (Voulhoux et al., 2003; Robert et al., 2006), which is based on an evolutionary ancient ensemble of periplasmic and outer membrane proteins, e.g., the Bam complex, found to have homologues even in mitochondria (Tomassen, 2010).

## The type V secretion mechanism

In T5SS, the translocation of passenger domains across both membranes of the gram-negative envelope is mediated in a two-step mechanism (Rego et al., 2010). To cross the inner membrane, the signal peptide of the protein chain is recognized by the Sec translocon (Figure 1, step 1) (Desvaux et al., 2004) and translocated therefore in an unfolded form. During translocation, the signal peptidase cleaves off the signal peptide. According to the BamA/Omp85 model (Voulhoux et al., 2003), the autotransporter protein (Figure 1, step 2), devoid of the signal peptide, adopts a stable intermediate in the periplasm by interaction with periplasmic chaperones, such as Skp and SurA, and the outer membrane Omp85/Bam complex (Brandon and Goldberg, 2001; Skillman et al., 2005; Ieva and Bernstein, 2009; Ruiz-Perez et al., 2009; Leyton et al., 2012). The  $\beta$ -domain integrates into the outer membrane in some

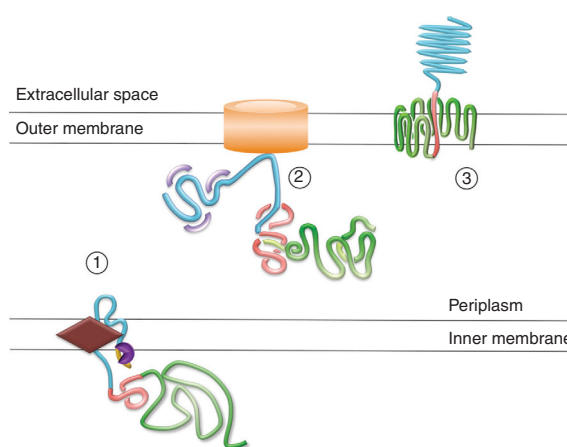


**Figure 1** Schematic overview of type V secretion mechanism. Brown: Sec translocon; purple: signal peptidase; yellow: signal peptide; green:  $\beta$ -barrel; blue: passenger domain; red: linker domain; violet: periplasmic chaperones; orange: Omp85. For simplicity, we omitted the ribosome as point of initial protein synthesis of the autotransporter. On the basis of unpublished data (JJ), one can hypothesize that some sort of co-translation mechanism in the Sec-mediated translocation of autotransporters across the inner membrane might exist. The peptide chain is transported across the inner membrane by the Sec translocon (step 1). In the periplasm, the intermediate adopts a stable conformation while interacting with periplasmic chaperones and BamA (step 2), and the passenger domain is finally translocated across the outer membrane (step 3).

way, forming a  $\beta$ -barrel with a hydrophilic pore occupied by a linker domain through which the passenger domain is apparently translocated to the cell surface (Figure 1, step 3).

## Structural and functional diversity of T5SS passengers

Passengers of T5SS are involved in major processes of gram-negative bacteria, such as virulence, bacterial motility, or nutrient acquisition and function as adhesins, enzymes, or toxins (Henderson et al., 2004; Leo et al., 2012; Jacob-Dubuisson et al., 2013). Despite varying in size with a maximum up to 500 kDa, most of the T5aSS and T5bSS passengers form extended  $\beta$ -helices after translocation, such as the passengers of pertactin, EspP, Hbp, VacA, and FHA. One exception is the passenger domain of EstA (Va), which does not contain  $\beta$ -helices (van den Berg, 2010). Each passenger undergoes one of three possible post-translocational treatments: (i) it can either remain covalently linked to the transport unit, (ii) or can be cleaved but remain attached to the cell surface, or (iii)

the passenger is released into the extracellular space after cleavage. Trimeric autotransporters (Vc), e.g., Hia and YadD, contain  $\alpha$ -helical passenger domains, which remain covalently linked after translocation across the outer membrane and function as adhesins (Cotter et al., 2005). For PlpD, which is a member of the recently defined subgroup of fused autotransporters (Vd), no structures are available. However, the passenger of the patatin-like protein D (PlpD) was predicted to fold similarly to the potato patatin Pat17 containing  $\alpha$ -helices,  $\beta$ -sheets, and connecting loops (Rydel et al., 2003; Salacha et al., 2010). The passengers of T5eSS, e.g., intimin and invasin, are released into the extracellular space and fold into several Big (bacterial immunoglobulin-like) domains and a C-type lectin-like domain at the C-terminus. Intimin and invasin mediate adhesion or the rearrangement of the host cytoskeleton (Hamburger et al., 1999; Batchelor et al., 2000; Luo et al., 2000).

In summary, a structural comparison of only the passenger domains cannot be used to differentiate between the subgroups of T5SS. Thus, it is necessary to consider the characteristics of the whole autotransporter.

## The architecture of type V transport units

In contrast to the passengers translocated by T5SS, the transport units share high structural similarity (Henderson et al., 1998; Thanassi and Hultgren, 2000; Meng et al., 2006; Leyton et al., 2012). In recent years, several crystal structures from all T5SS subgroups, except Vd, were solved (Table 1). All structures of NalP (Va), FhaC (Vb), Hia

(Vc), and intimin (Ve, Figure 2) compared here (Figures 2 and 3) consist only of the transport unit, except for FhaC (Oomen et al., 2004; Meng et al., 2006; Clantin et al., 2007; Fairman et al., 2012). For NalP and intimin, only the linker and the  $\beta$ -barrel domains were cloned, expressed, and crystallized. The structure of Hia was solved for a construct where the N-terminal part was deleted.

All type V secretion transport units localize to the outer membrane of gram-negative bacteria. These are composed of a linker and an amphipathic  $\beta$ -barrel domain, which is a common feature of proteins spanning the outer membrane of gram-negative bacteria, mitochondria, and chloroplasts (Schulz, 2002). The amphipathic  $\beta$ -barrel does not appear as a structural component in other proteins, with the peculiar exception of intracellular fatty acid-binding proteins in animal cells (Smathers and Petersen, 2011). The autotransporters  $\beta$ -barrels consist of 12 antiparallel  $\beta$ -strands in the case of NalP, Hia, and intimin (Table 1, Figure 2), and 16 strands for FhaC. The  $\beta$ -strands of the  $\beta$ -barrels are connected by short turns on the periplasmic side and larger extracellular loops. In the case of Hia, the connecting loops have the same length on both sides of the  $\beta$ -barrel (Figure 2). The central pores of the  $\beta$ -barrels are hydrophilic and occupied by the  $\alpha$ -helical linker in the case of NalP, FhaC, and Hia. For intimin, the linker domain traverses the pore in an extended conformation (Fairman et al., 2012). The diameters of these pore domains range between 10 and 20 Å, where Hia harbors the widest pore with three  $\alpha$ -helical domains in contrast to NalP and FhaC with only one (Figure 2). The surface representation illustrates the dimensions of the linker domain relative to the pore (Figure 3). For NalP, the linker domain is located in the center of the pore, resulting in dense packing of this domain close to the wall of the  $\beta$ -barrel (Figure 3B). The

**Table 1** Overview of crystal structures of type V transport units.

Protein	Organism	Type V subgroup	Pdb code	Resolution (Å)	No. of $\beta$ -strands	Passenger/function	References
BrkA	<i>Bordetella pertussis</i>	a	3QQ2	3.00	12	Serum resistance, adhesion	Zhai et al., 2011
EspP	<i>Escherichia coli</i>	a	2QOM	2.70	12	Serine protease	Barnard et al., 2007
EstA	<i>Pseudomonas aeruginosa</i>	a	3KVN	2.50	12	Esterase	van den Berg, 2011
NalP	<i>Neisseria meningitidis</i>	a	1UYN	2.60	12	Serine protease	Oomen et al., 2004
FhaC	<i>Bordetella pertussis</i>	b	2QDZ	3.15	16	FHA (filamentous hemagglutinin)	Clantin et al., 2007
Hia	<i>Haemophilus influenzae</i>	c	3EMO	2.00	12 (3×4)	Adhesion	Meng et al., 2006
YadA <sup>a</sup>	<i>Yersinia enterocolitica</i>	c	2LME		12 (3×4)	Adhesion	Shahid et al., 2012
Intimin	<i>Escherichia coli</i>	e	4E1S	1.85	12	Adhesion	Fairman et al., 2012
Invasin	<i>Yersinia pseudotuberculosis</i>	e	4E1T	2.30	12	Rearrangement of host cell cytoskeleton	Fairman et al., 2012

<sup>a</sup>Structure determination by solid-state NMR spectroscopy.

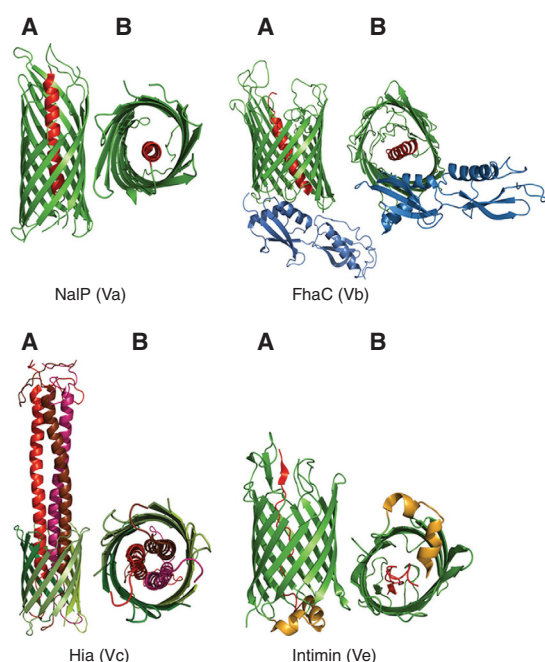


**Figure 2** Overview of transport units of type V secretion systems. Green:  $\beta$ -barrel; blue: POTRA domains; orange: periplasmic  $\alpha$ -helix; red/magenta/brown:  $\alpha$ -helices and unstructured peptide chains traversing the pore of the  $\beta$ -barrel. (A) Lateral view of crystal structures of the transport units in ribbon presentation. (B) Top view from periplasmic side of crystal structures of the transport units in ribbon presentation.

linker domain of FhaC traverses the pore in a diagonal manner owing to interactions of charged clusters of amino acids in the pore and corresponding amino acids in the linker domain, creating an asymmetric channel (Clantin et al., 2007). The pore of Hia is fully occupied by the three  $\alpha$ -helical linker domains (Figure 3). The linker domain of intimin strongly interacts with one side of the pore, which also results in an asymmetric architecture similar to the one observed for FhaC.

As shown by Struyvé et al. (1991), outer membrane proteins of gram-negative bacteria share a common C-terminal consensus sequence containing a phenylalanine or tryptophan at -1 and a hydrophobic residue at positions -3, -5, -7, and -9 (Table 2), which is recognized by Omp85 (Robert et al., 2006). Moreover, it was demonstrated for PhoE, an *E. coli* porin, that the last C-terminal amino acid in the signature sequence (a phenylalanine) is essential for the correct assembly of  $\beta$ -barrels in the outer membrane. Compared with the five conserved amino acids of the consensus signature sequences postulated by Struyvé et al. (1991), NalP, FhaC, and intimin contain all five conserved amino acids in the last  $\beta$ -strand of their  $\beta$ -barrel

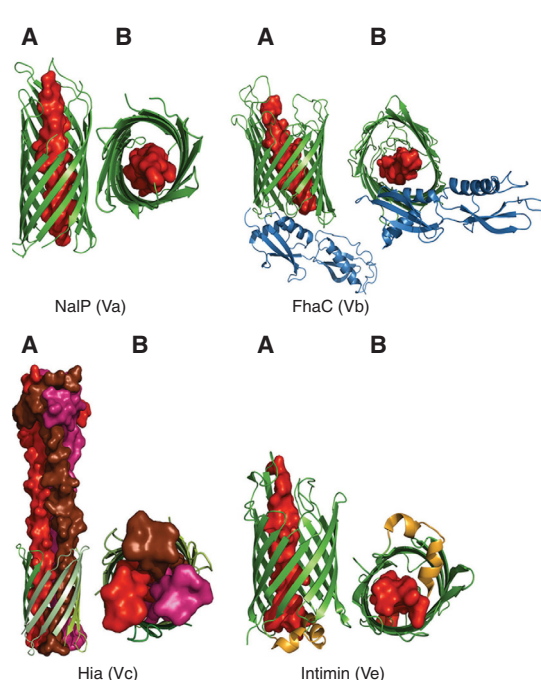


**Figure 3** Overview of transport units of type V secretion systems with surface presentation of domains traversing the  $\beta$ -barrel pore. Green:  $\beta$ -barrel; blue: POTRA domains; orange: periplasmic  $\alpha$ -helix; red/magenta/brown:  $\alpha$ -helices and unstructured peptide chains traversing the pore of the  $\beta$ -barrel. (A) Lateral view of crystal structures of the transport units as ribbon diagrams with surface presentation of domains traversing the pore. (B) Top view from the periplasmic side of crystal structures of the transport units as ribbon diagrams with surface presentation of domains traversing the pore.

(Table 2). The same is true for each subunit of the homotrimeric Hia. Loveless and Saier (1997) extended this signature sequence to the last 18 amino acids of the last  $\beta$ -strand by sequence alignment of different autotransporters. For each position, several amino acids were identified, resulting in a considerable variation of the signature sequence except for the terminal phenylalanine or tryptophan (Table 2). The highest agreement with the consensus signature sequence stated by Loveless and Saier (1997) shows the homotrimeric autotransporter Hia, which matches 13 amino acids, followed by FhaC with 12, NalP with 10, and finally intimin with 9 conserved amino acids (Table 2). These results strongly support the thesis that autotransporters are integrated in the outer membrane by a common machinery, which is also responsible for the integration of other outer membrane proteins.

Despite the high similarities of the overall architecture, the transport units contain special features that differ between the subgroups, such as POTRA domains,



Table 2 Comparison of the signature sequence of type V transport units.

Protein	18	17	16	15	14	13	12	11	10	9	8	7	6	5	4	3	2	1
NalP	G	S	K	Q	Y	G	N	H	S	G	R	V	G	V	G	Y	R	F
FhaC	G	G	A	P	R	A	P	V	W	L	Y	I	N	A	G	L	S	F
Hia	T	T	N	S	Q	G	K	T	G	V	A	A	G	V	G	Y	Q	W
Intimin	G	T	G	N	E	N	D	L	L	Y	S	M	Q	F	R	Y	Q	F
Consensus sequence (Struyvé et al., 1991)	-	-	-	-	-	-	-	-	-	B	-	B	-	B	-	B/Y	-	F/W
Consensus sequence (Loveless and Saier, 1997)	SATQRGH	AKLTQNF	FGATL	GPDSNKI	KRHNDQS	X <sub>3</sub>	DPAQH	QNDWKYFIT	ASTQN	LIVFGAS	NQHEGAIF	LIVA	NGSK	LIVMFY	RKQSTG	LIFYW	STAKRNV	F/W

B: any hydrophobic amino acid; X: any amino acid.

The numbers correspond to the amino acid position relative to the C terminus where number 18 indicates the biggest distance to the C terminal end and number 1 indicates the last amino acid of the C terminal end.

oligomerization state, and domain arrangement. For example, the TpsB protein FhaC (Vb) contains two POTRA domains (Figure 2, blue subdomains), which are responsible for the recognition of their dedicated passenger protein, filamentous hemagglutinin (FHA) (Clantin et al., 2007). Each POTRA domain consists of three  $\beta$ -strands and one short  $\alpha$ -helix. Intimin (Ve) contains a periplasmic  $\alpha$ -helix, which is located between the linker and the  $\beta$ -barrel domain (Figure 2, orange subdomains) (Fairman et al., 2012). The exchange of this helix for a short glycine-glycine linker had no influence on the heat modifiability and proteinase K sensitivity, indicating a properly folded  $\beta$ -barrel and an unaffected translocation of the passenger (Fairman et al., 2012). This helix could possibly function as a plug of the pore from the periplasmic side that avoids leakage of the cells. In contrast to members of all other subgroups, Hia (Vc) translocates its high identical passenger domains within only one  $\beta$ -barrel (Figure 2).

Next, we were interested if it is possible to distinguish between transport units of different subgroups of T5SS by a structural comparison. Therefore, the global root mean square deviation (RMSD) was calculated, which is a relative measurement for describing overall structural similarity. For that, the transport unit structures of each subgroup were compared to a reference structure of the same subgroup (Table 3). Among the monomeric autotransporters, EspP, a serine protease autotransporter (SPATE) from *E. coli*, showed the highest (RMSD of 1.20 Å) and BrkA from *Bordetella pertussis* the lowest (RMSD of 2.57 Å) structural similarity to NalP with respect to the C $\alpha$  atoms. Regarding the function of EspP, which like NalP is assigned to the SPATEs, the high structural similarity is not surprising. The structures of YadA and Hia, which both function as adhesins, are very similar over a length of 273 C $\alpha$  atoms (RMSD of 1.81 Å). The global RMSD for invasins compared with intimin is very low (0.69 Å), indicating a nearly identical structure over the whole length of the protein. Comparing structures of different subgroups, Hia and intimin to NalP, the global RMSDs of intimin (2.25 Å) and Hia (2.63 Å) are in the same range as for BrkA (Va) (2.57 Å). For FhaC, the structural identity is significantly lower (RMSD of 3.63 Å) owing to the different numbers of  $\beta$ -strands.

In consequence, the structural comparison of the transport units is not sufficient to differentiate between the subgroups of T5SS. For example, NalP and intimin share a higher structural similarity compared with NalP and BrkA, but belong to different subgroups, Va and Ve, respectively. Thus, a comprehensive analysis of the whole protein is required for the correct classification of each autotransporter.

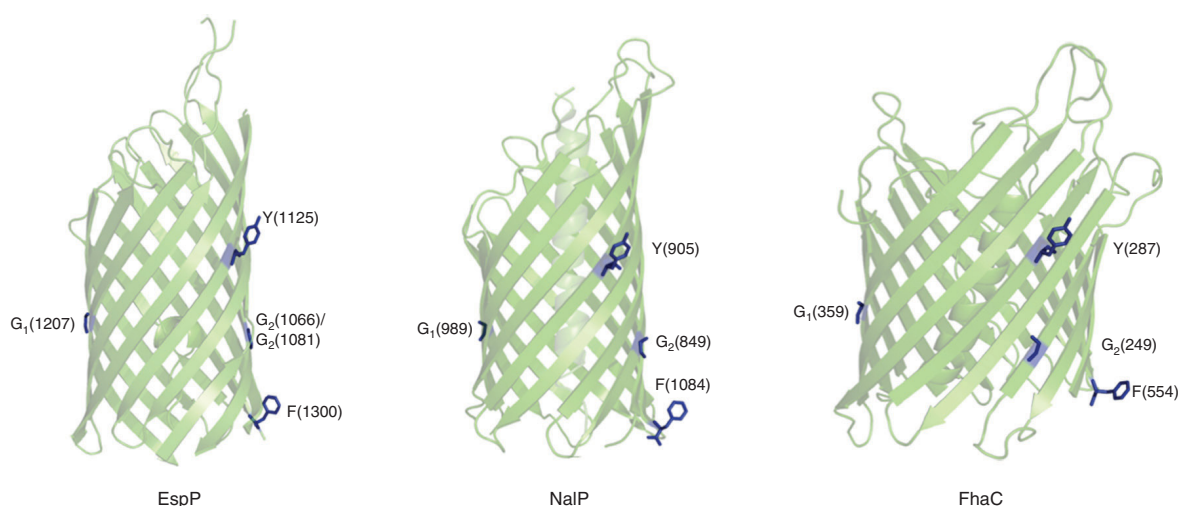
**Table 3** Global RMSD calculations of C<sub>α</sub> atoms of type V transport units.

Protein	No. of amino acids	No. of C <sub>α</sub> atoms compared	RMSD (Å)	Reference structure	No. of amino acids
BrkA	266	223	2.57	NalP	308
EspP	285	227	1.20	NalP	308
EstA	276	269	1.84	NalP	308
YadA	3×105	273	1.81	Hia	3×162
Invasin	245	236	0.69	Intimin	242
FhaC	554	191	3.63	NalP	308
Hia	3×162	186	2.63	NalP	308
Intimin	242	164	2.25	NalP	308

The smaller the RMSD, the higher the structural similarity is. For example, intimin and invasin have a high structural similarity (RMSD 0.69 Å); FhaC and NalP (3.63 Å) share a low structural similarity.

In recent years, considerable experimental data were obtained in terms of the biogenesis of the monomeric autotransporter EspP from *E. coli* (Ieva and Bernstein, 2009; Ieva et al., 2011; Pavlova et al., 2013). In these studies, several conserved amino acids were analyzed by mutational and crosslinking experiments and by bioinformatic comparison to other autotransporters. To analyze if other autotransporters contain identical amino acids at the same position in the spatial arrangement as in EspP, a structural alignment of EspP with NalP, FhaC, Hia, and intimin was performed. Indeed, four of these already investigated amino acids of EspP (Pavlova et al., 2013) were also present in NalP and FhaC, including the C-terminal phenylalanine of the conserved signature sequence (see above; Figure 4, highlighted in blue). As

depicted in Figure 4, G<sub>1</sub> and G<sub>2</sub> correspond to the glycine residues at the left and the right side of each β-barrel, to which the distance measurements listed in Table 4 refer. For EspP, heat modifiability tests revealed that mutation of G2(1066) or G2(1081) slightly interferes with the stability of the β-barrel (Pavlova et al., 2013). In consequence, the exposure of the passenger domain on the cell surface and the integration of the β-barrel into the outer membrane were delayed, as shown by crosslinking and protease accessibility tests. However, the release of the passenger domain was unaffected. The midbarrel residue Y(1125) was shown to interact with the periplasmic chaperone Skp and lipopolysaccharides from the outer membrane (Ieva et al., 2011). The role of G<sub>1</sub>(1207) in the biogenesis of EspP has not yet been determined,

**Figure 4** Conserved amino acids among the transport units of EspP, NalP, and FhaC.

Green: transport units in ribbon presentation; blue: conserved amino acids in stick presentation. For a better overview, the POTRA domains of FhaC are hidden. The conserved amino acids are labeled with one-letter code and position number. G<sub>1</sub> and G<sub>2</sub> correspond to the distance measurements in Table 4.



**Table 4** Analysis of conserved amino acids between EspP, NalP, and FhaC.

Distances (Å)	EspP	NalP	FhaC
G <sub>1</sub> -G <sub>2</sub>	26.24	24.07	24.11
G <sub>1</sub> -Y	29.70	28.90	29.70
G <sub>1</sub> -F	32.48	31.76	38.32
Y-F	27.64	28.29	27.64
Y-G <sub>2</sub>	19.26	19.74	16.88
G <sub>2</sub> -F	9.23	9.94	16.92

G<sub>2</sub>(1066) was used for distance measurements in EspP.

but this residue seems to be important for the general translocation mechanism as it is highly conserved among autotransporters (see superfamily entry pfam03797 in the Conserved Domain Database, <http://www.ncbi.nlm.nih.gov/cdd>).

Regarding the spatial arrangement, the distances between the conserved residues in EspP and NalP are very similar to each other (Table 4). Owing to the 16-stranded  $\beta$ -barrel of FhaC, the distances of G<sub>2</sub>(249) and G<sub>1</sub>(359) to F(554) and Y(287) to G<sub>2</sub>(249) differ from those observed in EspP and NalP, which are composed of 12-stranded  $\beta$ -barrels. Nevertheless, all of these amino acid side chains in each structure are exposed to the environment and thus are accessible for interactions in a comparable spatial arrangement (Figure 4). Regardless of the subgroup, these conserved amino acids could presumably play the same role in the biogenesis of T5SS.

## Translocation across the outer membrane

In the past decade, different models for translocation of passenger domains across the outer membrane of gram-negative bacteria were postulated (Veiga et al., 2002; Oomen et al., 2004; Kostakioti and Stathopoulos, 2006). Most biochemical and structural data obtained by numerous investigations support two of these models: (i) the hairpin model and (ii) the Omp85 model (Figure 5).

### The hairpin model

The hairpin model was developed on the basis of data obtained for the prototype of the type V secretion pathway, the IgA1 protease from *Neisseria gonorrhoea* (Pohlner et al., 1987). In principle, this model relied on

the discovery of a  $\beta$ -barrel structure at the C-terminus of the precursor. In addition to that observation, transport of IgA1 protease to the cell surface was observed in other gram-negative species such as *E. coli* or *Salmonella* by simply transferring the corresponding gene, indicating that translocation of these proteins are self-sufficient. This observation was later confirmed for other proteins in different species, leading to the introduction of the name 'autotransporters' (Jose et al., 1995), first for the family of IgA1 protease-like proteins (Va). According to this model, Sec-mediated translocation of the protein across the inner membrane is followed by the C-terminal part of the linker domain, forming a hairpin-like structure with the  $\beta$ -barrel during the assembly of the latter in the outer membrane (Figure 5A, step 1). This insertion of the linker is followed by the N-terminus of the protein to be transported, the so-called passenger. This results in the appearance of the passenger C-terminus at the cell surface before its N-terminus. By initial folding of the extracellular loop of this hairpin, the unfolded passenger domain is pulled through the pore of the  $\beta$ -barrel and subsequently folds at the cell surface (Figure 5A, step 2). This folding process would prevent backsliding of the passenger domain through the pore and provides an ATP-independent driving force for the translocation process (Klauser et al., 1993; Renn et al., 2012). Finally, the fully folded passenger is presented at the cell surface (Figure 5A, step 3). The hairpin model took into consideration that the periplasm and the cell surface is devoid of ATP and the only alternative, threading of the N-terminal end of the periplasmic intermediate into the pore formed by the  $\beta$ -barrel (Dautin and Bernstein, 2007), appeared to be thermodynamically unlikely.

### The Omp85 model

Recent studies have shown that the outer membrane factor, Omp85, YaeT, or BamA (Voulhoux et al., 2003; Kostakioti and Stathopoulos, 2006; Bernstein, 2007), a conserved component of the Bam complex, is required for the integration of autotransporters as well as for the assembly of outer membrane proteins in general in gram-negative bacteria, mitochondria, and chloroplasts by recognition of their C-terminal consensus signature sequence (Loveless and Saier, 1997; Robert et al., 2006; Tommassen, 2010). After translocation across the inner membrane, the autotransporter partially folds in the periplasm while interacting with periplasmic chaperones, such as Skp and SurA, and the assembly factor Omp85 (Figure 5B, step 1) (Ieva and Bernstein, 2009). In the model, this

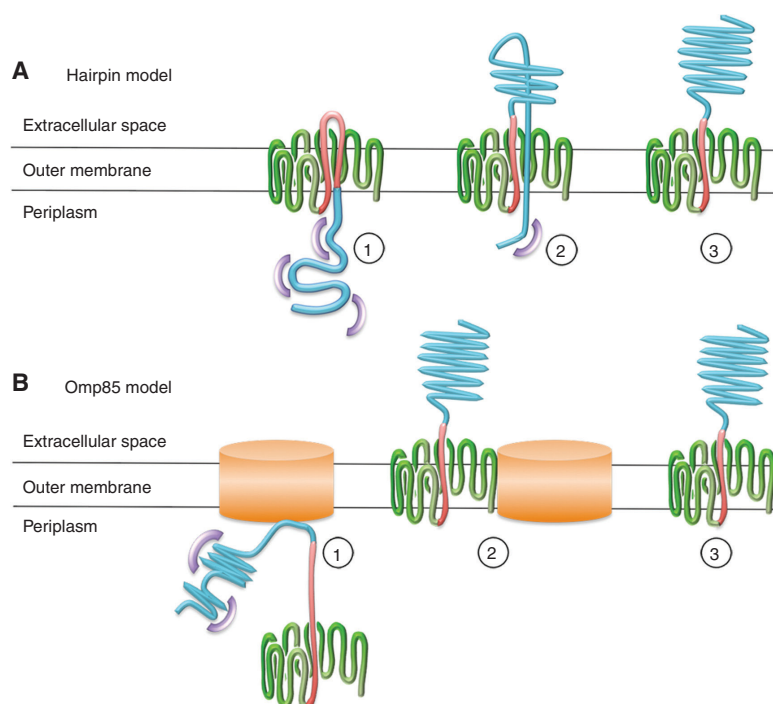


**Figure 5** Postulated mechanisms of type V passenger translocation across the outer membrane.

Green:  $\beta$ -barrel; blue: passenger domain; red: linker domain; orange: Omp85 complex; violet: periplasmic chaperones. According to the hairpin model (A), the linker domain forms a hairpin-like structure in the pore of the  $\beta$ -barrel (step A1) and the passenger domain is pulled through this pore (step A2). Finally, the passenger domain adopts its fully folded conformation at the cell surface (step A3). In the Omp85 model (B), the autotransporter interacts with BamA (step B1) and is subsequently integrated into the outer membrane in an 'open' conformation (step B2), allowing transport of partially folded passengers. After translocation, across the outer membrane, the passenger domain obtains its active conformation in the extracellular space (step B3).

periplasmic intermediate is inserted into the outer membrane by Omp85, which holds the  $\beta$ -barrel of the transport unit in an 'open' conformation, allowing translocation of partially folded passenger structures (Figure 5B, step 2; Omp85 is highlighted in orange). After translocation, Omp85 dissociates from the  $\beta$ -barrel and the passenger domain adopts its fully folded conformation in the extracellular space (Figure 5B, step 3).

### Evidence and difficulties of the hairpin model

Despite some evidence for the Omp85 model, considerable experimental data were also produced supporting the hairpin model. When the  $\beta$ -subunit of cholera toxin (CTB), which contains intramolecular disulfide bonds, was fused to the transport unit of IgA1 protease, surface translocation was not possible in *E. coli*. In contrast,

surface translocation was possible after mutation of the two cysteines to leucine and glycine, or when the gene encoding DsbA, which promotes formation of disulfide bonds in the periplasm of *E. coli*, was deleted (Jose et al., 1996). Both findings indicate that disulfide bond formation in the passenger domain is only allowed after the translocation of the IgA1 transport unit. Similar results were obtained when aprotinin, a rapid-folding Kunitz-domain-like protease inhibitor, with several disulfide bonds, was fused to the autotransporter domain of the subgroup Va autotransporter AIDA-I (Jose and Zangen, 2005). Surface translocation was only detectable when a strong reducing cell environment was provided by the addition of 1 mM 2-mercaptoethanol. Moreover, when the genes encoding the periplasmic proteases DegP or DeqQ were deleted, the aprotinin-AIDA-I fusion without the addition of 2-mercaptoethanol accumulated in the periplasm (Jose and Zangen, 2005). These results indicated that aprotinin containing disulfide bonds represented a

translocation-incompatible structure that is degraded by periplasmic proteases before it could fold into its active conformation and inhibit these proteases. Recent studies with slow-folding mutants of the wild-type autotransporter EspP in *E. coli* provided experimental evidence for the formation of a hairpin structure within the passenger domain during transport (Ieva et al., 2008; Ieva and Bernstein, 2009). In addition, after transport of the cytochrome P450 enzyme CYP106 to the cell surface by fusion to the transport unit of AIDA-I, the enzyme was found to be devoid of its prosthetic group, porphyrin. This is normally incorporated into the passenger in the periplasm of *E. coli*. As the heme group is bound to the enzyme through non-covalent interactions, it is unlikely that it is co-transported with an unfolded CYP106 enzyme, as required in the hairpin model. Porphyrin was, however, incorporated subsequently at the cell surface even without adding it to the cultures (Schumacher et al., 2012). Recent findings showed that porphyrin groups can be exported by the outer membrane channel TolC (Tatsumi and Wachi, 2008). The strongly reduced CYP106 enzyme activity in TolC mutants clearly indicates the dependency of heme export mediated by TolC. However, after addition of heme to the growth medium, the CYP106 enzyme activity could be restored (Schumacher et al., 2012). These results were a hint that surface translocation of the CYP enzyme and the export of porphyrin are independent secretion processes. Moreover, it is likely that CYP enzymes are translocated in an unfolded state across the outer membrane, thus being consistent with the hairpin model. Also in line with this model are several studies that showed that the C-terminal end of the passenger domain reaches the extracellular space before the N-terminus, driving the translocation of the passenger domain (Junker et al., 2009; Peterson et al., 2010; Soprova et al., 2010). Thus, Junker et al. (2009), working with the monomeric autotransporter pertactin from *B. pertussis*, inserted reversible cysteine pairs at different positions in the passenger domain, which stalled the secretion process at different stages. Proteinase K treatment and detection of a stable, proteinase K-resistant 28-kDa core led to the conclusion that the C-terminal end of the passenger domain reaches the extracellular space before the N-terminus and that the secretion process is vectorial. The second study (Peterson et al., 2010) was performed with the monomeric autotransporter EspP from *E. coli*. Here, the folding rate of a  $\beta$ -helix in the extracellular space was reduced by introduction of different point mutations in the C-terminal end of the passenger domain. Proteinase K treatments and immunodetection experiments revealed that this part of the passenger is translocated across the outer membrane before the rest

of the passenger domain is detected in the extracellular space. Thereby, the reduced folding rate of the  $\beta$ -helix did not abolish the translocation of the rest of the passenger domain, while in contrast deletion of this C-terminal part blocked translocation (Peterson et al., 2010). In the third study (Soprova et al., 2010), the folding behavior of the monomeric autotransporter hemoglobin protease (Hbp) from *E. coli* was analyzed. For this purpose, different mutations were introduced into the conserved C-terminal stretch of the passenger domain, which was identified as an autochaperone (AC) domain by deletion and mutagenesis experiments as well as by bioinformatic comparison to homologous autotransporters, such as BrkA (Oliver et al., 2003). Proteinase K treatments, crosslinking experiments, and immunodetection analysis showed that the amino acid tryptophan at the C-terminal end of the AC domain is crucial for the translocation of the passenger domain of Hbp (Soprova et al., 2010).

Nevertheless, the hairpin model cannot explain how some passenger domains containing disulfide bonds or glycosylated amino acids are successfully translocated across the outer membrane (Lindenthal and Elsinghorst, 1999; Skillman et al., 2005). In one study, the CTB passenger, known to fold and undergo disulfide formation in the periplasm, was fused to the transport unit of EspP (Skillman et al., 2005). Pulse-chase labeling experiments, proteinase K treatment, and immunodetection analysis revealed that the already folded passenger domains containing disulfide bonds were secreted efficiently across the outer membrane (Skillman et al., 2005). In addition, Lindenthal and Elsinghorst (1999) showed that with TibA, a monomeric autotransporter from *E. coli*, the passenger domain is translocated across the outer membrane containing glycosylated amino acids, detected by digoxigenin and proteinase K treatment of whole cells. Regarding the size constraints of the  $\beta$ -barrel pores (diameter of  $\sim 10$  Å for monomeric and  $\sim 20$  Å for trimeric autotransporters, Figure 3), only two protein chains without any modifications could be accommodated within a fully folded  $\beta$ -barrel if they are present in an extended conformation (Kostakioti and Stathopoulos, 2006; Bernstein, 2007). This fact excludes the formation of an  $\alpha$ -helical linker before or during the translocation event. In contrast, Ieva et al. (2008) assumed that such an  $\alpha$ -helical structure is achieved in the pore of EspP from *E. coli* before insertion of the  $\beta$ -barrel in the outer membrane. Accessibility tests with tobacco etch virus protease or proteinase K, cell fractionation analysis, and pulse-chase labeling experiments revealed that a 30- to 35-amino-acid segment of the linker is embedded in the  $\beta$ -barrel pore before passenger domain secretion.

## Evidence and difficulties of the Omp85 model

Today, it is known that most if not all gram-negative bacteria contain a set of periplasmic chaperones, e.g., Skp and SurA, and the Bam complex that facilitate partial folding and assembly of  $\beta$ -barrels into the outer membrane (Tomassen, 2007; Grijpstra et al., 2013). Clearly, autotransporter proteins use this machinery for the transport of their passengers to the cell surface, dependent on a specific recognition motif at the C-terminus of the  $\beta$ -barrel, as mentioned above (Robert et al., 2006). In support of the Omp85 model, Ieva and Bernstein (2009) revealed the interaction of EspP, a monomeric autotransporter, with Omp85 and periplasmic chaperones. In this study, a small linker domain was inserted into the passenger domain, creating a periplasmic intermediate by transient stalling of the translocation process. Crosslinking experiments revealed that the C-terminal part of the passenger domain and the  $\beta$ -barrel interact with Omp85 (Ieva and Bernstein, 2009). The N-terminal part of the passenger domain was shown to interact with SurA and Skp, which was later confirmed by the same group (Ieva et al., 2011).

As depicted in the model in Figure 5B, Omp85 forms a pore in which the transport unit is integrated and through which the passenger domain is transported. With liposome-swelling experiments and planar lipid bilayers, Robert et al. (2006) showed that Omp85 is able to form voltage-activated pores with a diameter of 2.5 nm.

However, this pore would be too narrow to accommodate the (partially) folded transport unit and the passenger domain. Consequently, the proposed Omp85 model cannot provide an explanation of how the translocation of folded passenger domains across the outer membrane is managed.

As mentioned above, the ensemble of chaperons and the Bam complex involved in type V secretion is an ancient machinery, existing before phylogenetic separation of the bacteria occurred. Therefore, divergent evolution of the system in different bacteria, especially of the Bam complex (Webb et al., 2012), should be considered. The heterologous expression of an autotransporter can lead to differences in transport not least owing to the lack of a 'compatible'  $\beta$ -barrel and a C-terminal recognition sequence. Finally, when recombinant passenger proteins are fused to a heterologous transport domain, this brings a third variable into play, which can also influence transport and folding. At this point, it appears important to consider that the contradictory results, e.g., the transport of passengers containing disulfide bonds (Jose et al., 1996; Skillman et al., 2005), were not obtained with identical transporter proteins in identical gram-negative bacteria. Therefore, only data obtained with constructs with identical transporter, passenger, and host gram-negative bacterium can be compared and considered valid (Jose and Meyer, 2007). Notably, data obtained from studies comparing identical systems give consistent results.

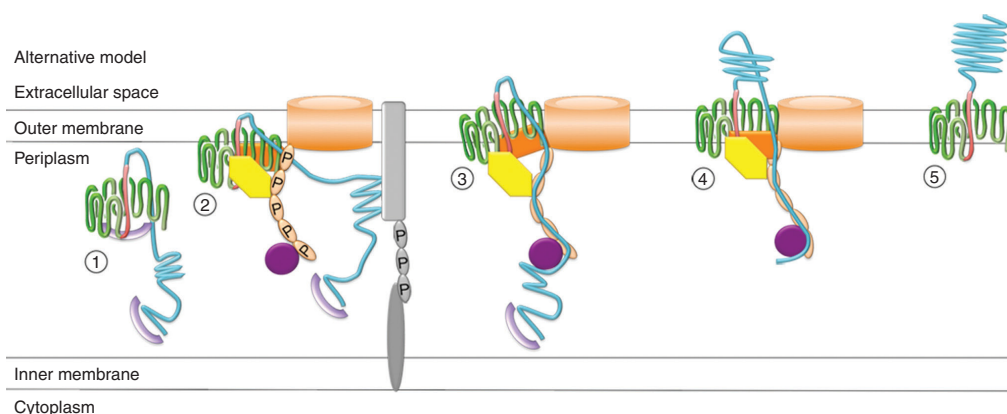


**Figure 6** Alternative model mechanism of type V passenger translocation across the outer membrane.

Green:  $\beta$ -barrel; blue: passenger domain; red: linker domain; light orange: Omp85; yellow: BamB; dark orange: BamD; violet: Skp; purple: SurA; light gray: TamA; dark gray: TamB; P: POTRA domains. The autotransporter interacts with the periplasmic chaperone Skp and forms a stable intermediate with the linker domain incorporated in the pore of the prefolded  $\beta$ -barrel (step 1). This intermediate is targeted to the outer membrane interacting with TAM and the Bam complex (step 2). The prefolded  $\beta$ -barrel is integrated in the outer membrane while the passenger domain interacts with SurA and the POTRA domains of BamA (step 3), resulting in a stepwise transfer across the outer membrane (step 4). Finally, the passenger domain adopts its fully folded conformation at the cell surface (step 5).

## Alternative model

Because neither the hairpin model nor the Omp85 model can describe a translocation mechanism consistent with all data derived from structural and biochemical analyses (Bernstein, 2007; Leyton et al., 2012), a synopsis of both appears to be worth looking at and has been proposed before (Benz and Schmidt, 2011; Ieva et al., 2011; Jose et al., 2012; Grijpstra et al., 2013; Pavlova et al., 2013).

The alternative model is a combination of both the hairpin and the Omp85 model (Figure 6), supported by recently obtained evidence from crosslinking and mutagenesis experiments, heat modifiability analysis, and protease accessibility tests with the monomeric autotransporter EspP (Ieva et al., 2011; Pavlova et al., 2013). As described below, we extend this model by the fact that a recently discovered translocation and assembly module (TAM) is involved in the translocation of autotransporters (Selkrig et al., 2012).

After translocation across the inner membrane, the autotransporter partially folds in the periplasm, interacting with the periplasmic chaperone Skp (Figure 6, step 1). At this stage, the linker domain is incorporated inside an incompletely folded  $\beta$ -barrel, forming a hairpin-like structure (Ieva et al., 2008). Subsequently, the prefolded autotransporter is targeted to the outer membrane interacting with the Bam complex in a unique orientation (Figure 6, step 2, highlighted in yellow/orange) (Ieva et al., 2011; Pavlova et al., 2013). As the midbarrel residues are accessible to crosslinking and the hairpin formed by the linker domain is not detectable at the cell surface at this stage, the  $\beta$ -barrel does not seem to be fully integrated into the outer membrane (Pavlova et al., 2013). Recently, another secretion complex, the TAM, was discovered in different proteobacteria (Selkrig et al., 2012). This module consists of TamA, an Omp85-family protein located in the outer membrane, which interacts with TamB in the inner membrane, presumably through the POTRA domains of TamA. It was shown for *Citrobacter rodentium* that mutants lacking TamA or TamB do not express the putative autotransporter protein p121. Furthermore, double mutants of *E. coli* lacking both TamA and TamB were not able to secrete the recombinant autotransporter adhesins Ag43 and EhaA. Therefore, cell-cell aggregation was abolished. Additionally, the precursor form of Ag43 accumulated in the periplasm (Selkrig et al., 2012). Moreover, crosslinking experiments with EspP in *E. coli* revealed that during the transient delay of passenger translocation, the passenger domain of EspP was crosslinked to an unidentified cellular protein with a molecular weight of 30–40 kDa (Ieva et al., 2011), which might correspond

to TamA. Consequently, the TAM is assumed to interact with the passenger domain in the periplasm, providing an essential step in the translocation process presumably by stabilizing the periplasmic intermediate (Figure 6, step 2, highlighted gray). Probably, owing to a conformational change or repositioning of this intermediate, the  $\beta$ -barrel integration into the outer membrane is completed and the hairpin is exposed at the cell surface, leading to the initiation of passenger domain translocation (Figure 6, step 3). In this way, the TAM would dissociate from the passenger domain, while a stretch of 80 amino acids of the passenger domain, as shown by crosslinking experiments, interacts with several POTRA domains of BamA/Omp85 and the chaperone SurA in the periplasm (Pavlova et al., 2013). Thus, in the alternative model, the passenger is transferred in a stepwise process through a pore composed of the autotransporter in an ‘open conformation’ mediated by the Bam complex. During another repositioning of the  $\beta$ -barrel (Figure 6, step 4), the passenger domain is fully translocated and the assembly of the  $\beta$ -barrel is completed, resulting in the dissociation of the Bam complex and the surface exposure of the passenger domain (Figure 6, step 5).

## Concluding remarks

In the last decade, more and more insight into the T5SS has been gained by structural, bioinformatic, and biochemical experiments. Comparing the crystal structures of transport units, which represent the state after translocation, the overall architecture of the type V transport units share high similarity also between the different subgroups, indicating a common translocation mechanism through the outer membrane. Different model mechanisms were discussed. Among those, the hairpin and the Omp85 model are supported by some but not all experimental results and clearly show the dependency of autotransporter proteins on additional factors, such as the Bam complex. Thus, the term ‘autotransporter’ is now redundant.

An alternative model was proposed, which is a combination of both the hairpin and the Omp85 model. Here, the fact that passengers contain disulfide bonds or modified amino acids, the interaction of the autotransporter with periplasmic chaperones and the Bam complex, and the formation of an  $\alpha$ -helical structure in the pore before insertion of the  $\beta$ -barrel in the outer membrane are taken into account. We extended this model by a novel TAM, which was discovered recently and shown to be involved



in the translocation of autotransporters across the outer membrane (Selkig et al., 2012). To determine the exact function of the TAM and its interaction partner, further investigations are obviously required. Nevertheless, our understanding of the type V secretion mechanism improved during the last decade, resulting in a more and more complete picture.

**Acknowledgments:** We thank Dr. Astrid Höppner, Crystal Farm and X-ray facility, Heinrich-Heine University

Düsseldorf, for assistance and helpful comments. We also gratefully acknowledge the support (and training) from the International NRW Research School BioStruct, granted by the Ministry of Innovation, Science and Research of the State North Rhine-Westphalia, the Heinrich-Heine University Düsseldorf, and the Entrepreneur Foundation at the Heinrich-Heine-University of Düsseldorf.

Received April 22, 2013; accepted August 6, 2013; previously published online August 7, 2013

## References

- Barnard, T.J., Dautin, N., Lukacik, P., Bernstein, H.D., and Buchanan, S.K. (2007). Autotransporter structure reveals intra-barrel cleavage followed by conformational changes. *Nat. Struct. Mol. Biol.* 14, 1214–1220.
- Batchelor, M., Prasanna, S., Daniell, S., Reece, S., Connerton, I., Bloomberg, G., Dougan, G., Frankel, G., and Matthews, S. (2000). Structural basis for recognition of the translocated intimin receptor (Tir) by intimin from enteropathogenic *Escherichia coli*. *EMBO J.* 19, 2452–2464.
- Benz, I. and Schmidt, M.A. (2011). Structures and functions of autotransporter proteins in microbial pathogens. *Int. J. Med. Microbiol.* 301, 461–468.
- Bernstein, H.D. (2007). Are bacterial ‘autotransporters’ really transporters? *Trends Microbiol.* 15, 441–447.
- Brandon, L.D. and Goldberg, M.B. (2001). Periplasmic transit and disulfide bond formation of the autotransported *Shigella* protein IcsA. *J. Bacteriol.* 183, 951–958.
- Clantin, B., Delattre, A.S., Rucktooa, P., Saint, N., Meli, A.C., Loch, C., Jacob-Dubuisson, F., and Villeret, V. (2007). Structure of the membrane protein FhaC: a member of the Omp85-TpsB transporter superfamily. *Science* 317, 957–961.
- Cotter, S.E., Surana, N.K., and St Geme, J.W., 3rd. (2005). Trimeric autotransporters: a distinct subfamily of autotransporter proteins. *Trends Microbiol.* 13, 199–205.
- Dautin, N. and Bernstein, H.D. (2007). Protein secretion in gram-negative bacteria via the autotransporter pathway. *Annu. Rev. Microbiol.* 61, 89–112.
- Desvaux, M., Parham, N.J., and Henderson, I.R. (2004). Type V protein secretion: simplicity gone awry? *Curr. Issues Mol. Biol.* 6, 111–124.
- Desvaux, M., Hebraud, M., Talon, R., and Henderson, I.R. (2009). Secretion and subcellular localizations of bacterial proteins: a semantic awareness issue. *Trends Microbiol.* 17, 139–145.
- Fairman, J.W., Dautin, N., Wojtowicz, D., Liu, W., Noinaj, N., Barnard, T.J., Udho, E., Przytycka, T.M., Cherezov, V., and Buchanan, S.K. (2012). Crystal structures of the outer membrane domain of intimin and invasins from enterohemorrhagic *E. coli* and enteropathogenic *Y. pseudotuberculosis*. *Structure* 20, 1233–1243.
- Grijpstra, J., Arenas, J., Rutten, L., and Tommassen, J. (2013). Autotransporter secretion: varying on a theme. *Res. Microbiol.* 164, 562–582.
- Hamburger, Z.A., Brown, M.S., Isberg, R.R., and Bjorkman, P.J. (1999). Crystal structure of invasins: a bacterial integrin-binding protein. *Science* 286, 291–295.
- Henderson, I.R., Navarro-Garcia, F., and Nataro, J.P. (1998). The great escape: structure and function of the autotransporter proteins. *Trends Microbiol.* 6, 370–378.
- Henderson, I.R., Navarro-Garcia, F., Desvaux, M., Fernandez, R.C., and Ala’Aldeen, D. (2004). Type V protein secretion pathway: the autotransporter story. *Microbiol. Mol. Biol. Rev.* 68, 692–744.
- Ieva, R. and Bernstein, H.D. (2009). Interaction of an autotransporter passenger domain with BamA during its translocation across the bacterial outer membrane. *Proc. Natl. Acad. Sci. USA* 106, 19120–19125.
- Ieva, R., Skillman, K.M., and Bernstein, H.D. (2008). Incorporation of a polypeptide segment into the  $\beta$ -domain pore during the assembly of a bacterial autotransporter. *Mol. Microbiol.* 67, 188–201.
- Ieva, R., Tian, P., Peterson, J.H., and Bernstein, H.D. (2011). Sequential and spatially restricted interactions of assembly factors with an autotransporter  $\beta$  domain. *Proc. Natl. Acad. Sci. USA* 108, 383–391.
- Jacob-Dubuisson, F., Guerin, J., Baelen, S., and Clantin, B. (2013). Two-partner secretion: as simple as it sounds? *Res. Microbiol.* 164, 583–595.
- Jose, J. and Meyer, T.F. (2007). The autodisplay story, from discovery to biotechnical and biomedical applications. *Microbiol. Mol. Biol. Rev.* 71, 600–619.
- Jose, J. and Zangen, D. (2005). Autodisplay of the protease inhibitor aprotinin in *Escherichia coli*. *Biochem. Biophys. Res. Commun.* 333, 1218–1226.
- Jose, J., Jahnig, F., and Meyer, T.F. (1995). Common structural features of IgA1 protease-like outer membrane protein autotransporters. *Mol. Microbiol.* 18, 378–380.
- Jose, J., Kramer, J., Klauser, T., Pohlner, J., and Meyer, T.F. (1996). Absence of periplasmic DsbA oxidoreductase facilitates export of cysteine-containing passenger proteins to the *Escherichia coli* cell surface via the IgA  $\beta$  autotransporter pathway. *Gene* 178, 107–110.
- Jose, J., Maas, R.M., and Teese, M.G. (2012). Autodisplay of enzymes – molecular basis and perspectives. *J. Biotechnol.* 161, 92–103.

- Junker, M., Besingi, R.N., and Clark, P.L. (2009). Vectorial transport and folding of an autotransporter virulence protein during outer membrane secretion. *Mol. Microbiol.* **71**, 1323–1332.
- Klauser, T., Kramer, J., Otzelberger, K., Pohlner, J., and Meyer, T.F. (1993). Characterization of the *Neisseria* IgA  $\beta$ -core: the essential unit for outer membrane targeting and extracellular protein secretion. *J. Mol. Biol.* **234**, 579–593.
- Kostakioti, M. and Stathopoulos, C. (2006). Role of the  $\alpha$ -helical linker of the C-terminal translocator in the biogenesis of the serine protease subfamily of autotransporters. *Infect. Immun.* **74**, 4961–4969.
- Leo, J.C., Grin, I., and Linke, D. (2012). Type V secretion: mechanism(s) of autotransport through the bacterial outer membrane. *Philos. Trans. R. Soc. Lond. B Biol. Sci.* **367**, 1088–1101.
- Leyton, D.L., Rossiter, A.E., and Henderson, I.R. (2012). From self sufficiency to dependence: mechanisms and factors important for autotransporter biogenesis. *Nat. Rev. Microbiol.* **10**, 213–225.
- Lindenthal, C. and Elsinghorst, E.A. (1999). Identification of a glycoprotein produced by enterotoxigenic *Escherichia coli*. *Infect. Immun.* **67**, 4084–4091.
- Loveless, B.J. and Saier, M.H., Jr. (1997). A novel family of channel-forming, autotransporting, bacterial virulence factors. *Mol. Membr. Biol.* **14**, 113–123.
- Luo, Y., Frey, E.A., Pfuetzner, R.A., Creagh, A.L., Knoechel, D.G., Haynes, C.A., Finlay, B.B., and Strynadka, N.C. (2000). Crystal structure of enteropathogenic *Escherichia coli* intimin-receptor complex. *Nature* **405**, 1073–1077.
- Meng, G., Surana, N.K., St. Geme, J.W., 3rd, and Waksman, G. (2006). Structure of the outer membrane translocator domain of the *Haemophilus influenzae* Hia trimeric autotransporter. *EMBO J.* **25**, 2297–2304.
- Oliver, D.C., Huang, G., Nodel, E., Pleasance, S., and Fernandez, R.C. (2003). A conserved region within the *Bordetella pertussis* autotransporter BrkA is necessary for folding of its passenger domain. *Mol. Microbiol.* **47**, 1367–1383.
- Oomen, C.J., van Ulsen, P., van Gelder, P., Feijen, M., Tommassen, J., and Gros, P. (2004). Structure of the translocator domain of a bacterial autotransporter. *EMBO J.* **23**, 1257–1266.
- Pavlova, O., Peterson, J.H., Ieva, R., and Bernstein, H.D. (2013). Mechanistic link between  $\beta$  barrel assembly and the initiation of autotransporter secretion. *Proc. Natl. Acad. Sci. USA* **110**, E938–947.
- Peterson, J.H., Tian, P., Ieva, R., Dautin, N., and Bernstein, H.D. (2010). Secretion of a bacterial virulence factor is driven by the folding of a C-terminal segment. *Proc. Natl. Acad. Sci. USA* **107**, 17739–17744.
- Pohlner, J., Halter, R., Beyreuther, K., and Meyer, T. F. (1987). Gene structure and extracellular secretion of *Neisseria gonorrhoeae* IgA protease. *Nature* **325**, 458–462.
- Rego, A.T., Chandran, V., and Waksman, G. (2010). Two-step and one-step secretion mechanisms in Gram-negative bacteria: contrasting the type IV secretion system and the chaperone-usher pathway of pilus biogenesis. *Biochem. J.* **425**, 475–488.
- Renn, J.P., Junker, M., Besingi, R.N., Braselmann, E., and Clark, P.L. (2012). ATP-independent control of autotransporter virulence protein transport via the folding properties of the secreted protein. *Chem. Biol.* **19**, 287–296.
- Robert, V., Volokhina, E.B., Senf, F., Bos, M.P., Van Gelder, P., and Tommassen, J. (2006). Assembly factor Omp85 recognizes its outer membrane protein substrates by a species-specific C-terminal motif. *PLoS Biol.* **4**, e377.
- Ruiz-Perez, F., Henderson, I.R., Leyton, D.L., Rossiter, A.E., Zhang, Y., and Nataro, J.P. (2009). Roles of periplasmic chaperone proteins in the biogenesis of serine protease autotransporters of Enterobacteriaceae. *J. Bacteriol.* **191**, 6571–6583.
- Rydel, T.J., Williams, J.M., Krieger, E., Moshiri, F., Stallings, W.C., Brown, S.M., Pershing, J.C., Purcell, J.P., and Alibhai, M.F. (2003). The crystal structure, mutagenesis, and activity studies reveal that patatin is a lipid acyl hydrolase with a Ser-Asp catalytic dyad. *Biochem.* **42**, 6696–6708.
- Salacha, R., Kovacic, F., Brochier-Armanet, C., Wilhelm, S., Tommassen, J., Filloux, A., Voulhoux, R., and Bleves, S. (2010). The *Pseudomonas aeruginosa* patatin-like protein PlpD is the archetype of a novel Type V secretion system. *Environ. Microbiol.* **12**, 1498–1512.
- Schulz, G.E. (2002). The structure of bacterial outer membrane proteins. *Biochim. Biophys. Acta* **1565**, 308–317.
- Schumacher, S.D., Hannemann, F., Teese, M.G., Bernhardt, R., and Jose, J. (2012). Autodisplay of functional CYP106A2 in *Escherichia coli*. *J. Biotechnol.* **161**, 104–112.
- Selkrig, J., Mosbahi, K., Webb, C.T., Belousoff, M.J., Perry, A.J., Wells, T.J., Morris, F., Leyton, D.L., Totsika, M., Phan, M.D., et al. (2012). Discovery of an archetypal protein transport system in bacterial outer membranes. *Nat. Struct. Mol. Biol.* **19**, 506–510, S501.
- Shahid, S.A., Bardiaux, B., Franks, W.T., Krabben, L., Habeck, M., van Rossum, B.J., and Linke, D. (2012). Membrane-protein structure determination by solid-state NMR spectroscopy of microcrystals. *Nat. Methods* **9**, 1212–1217.
- Skillman, K.M., Barnard, T.J., Peterson, J.H., Ghirlando, R., and Bernstein, H.D. (2005). Efficient secretion of a folded protein domain by a monomeric bacterial autotransporter. *Mol. Microbiol.* **58**, 945–958.
- Smathers, R.L. and Petersen, D.R. (2011). The human fatty acid-binding protein family: evolutionary divergences and functions. *Hum. Genomics* **5**, 170–191.
- Sopova, Z., Sauri, A., van Ulsen, P., Tame, J.R., den Blaauwen, T., Jong, W.S., and Luirink, J. (2010). A conserved aromatic residue in the autochaperone domain of the autotransporter Hbp is critical for initiation of outer membrane translocation. *J. Biol. Chem.* **285**, 38224–38233.
- Struyvé, M., Moons, M., and Tommassen, J. (1991). Carboxy-terminal phenylalanine is essential for the correct assembly of a bacterial outer membrane protein. *J. Mol. Biol.* **218**, 141–148.
- Tatsumi, R. and Wachi, M. (2008). TolC-dependent exclusion of porphyrins in *Escherichia coli*. *J. Bacteriol.* **190**, 6228–6233.
- Thanassi, D.G. and Hultgren, S.J. (2000). Multiple pathways allow protein secretion across the bacterial outer membrane. *Curr. Opin. Cell Biol.* **12**, 420–430.
- Tommassen, J. (2007). Biochemistry: getting into and through the outer membrane. *Science* **317**, 903–904.
- Tommassen, J. (2010). Assembly of outer-membrane proteins in bacteria and mitochondria. *Microbiology* **156**, 2587–2596.
- van den Berg, B. (2010). Crystal structure of a full-length autotransporter. *J. Mol. Biol.* **396**, 627–633.

Veiga, E., Sugawara, E., Nikaido, H., de Lorenzo, V., and Fernandez, L.A. (2002). Export of autotransported proteins proceeds through an oligomeric ring shaped by C-terminal domains. *EMBO J.* 21, 2122–2131.

Voulhoux, R., Bos, M.P., Geurtsen, J., Mols, M., and Tommassen, J. (2003). Role of a highly conserved bacterial protein in outer membrane protein assembly. *Science* 299, 262–265.

Webb, C.T., Heinz, E., and Lithgow, T. (2012). Evolution of the  $\beta$ -barrel assembly machinery. *Trends Microbiol.* 20, 612–620.

Zhai, Y., Zhang, K., Huo, Y., Zhu, Y., Zhou, Q., Lu, J., Black, I., Pang, X., Roszak, A.W., Zhang, X., et al. (2011). Autotransporter passenger domain secretion requires a hydrophobic cavity at the extracellular entrance of the  $\beta$ -domain pore. *Biochem. J.* 435, 577–587.



Iris Gawarzewski studied biology at the Heinrich-Heine University (HHU) Düsseldorf and finished her Diploma in 2009. In September 2009 she started her PhD in the Institute for Pharmaceutical and Medicinal Chemistry at HHU as a member of the NRW research school BioStruct. Her thesis focuses on the structure determination of the transport unit of *adhesin involved in diffuse adherence*.



Sander Smits obtained his PhD in Biochemistry at the Institute of Biochemistry, Heinrich-Heine University in 2008. Since then he works as a senior scientist with a special focus on membrane transporter. Here, especially the transporter of large unfolded proteins as well as peptides having an antimicrobial activity.



Lutz Schmitt studied Chemistry at the University of Freiburg and obtained his PhD from the Technical University Munich. After a Post Doc at Stanford University, he moved as a DFG-funded Emmy Noether Fellow to the Universities of Marburg and Frankfurt. In 2005 he was appointed as Professor of Biochemistry at Heinrich Heine University Düsseldorf where he became full professor in 2008. His research interests are recognition processes at membranes and transport across membranes.



Joachim Jose studied biology at the University Saarbrücken, and finished his PhD in 1994 with a thesis on the reaction mechanism of bacterial ureases. During his Post-Doc with Thomas F. Meyer at the MPI for Biology Tübingen (1994–1997), he was mainly involved in the discovery and description of a new family of secreted proteins: the autotransporters. From 1998 until 2003, he was a “Habilitand” in the group of Rolf W. Hartmann, Pharm. Med. Chemistry at Saarland University and obtained his habilitation with a thesis on the evolutive drug and biocatalyst design by bacterial surface display. In 2004, he accepted a call for a Professorship in Bioanalytics at the Institute of Pharm. Med. Chemistry, HHU Düsseldorf. Since March 2011 he holds a Chair in Pharm. Med. Chemistry at the WWU Münster.



## *Chapter II*

### **From cloning to crystallization – optimization of expression conditions, development of a purification protocol and crystallization of the transport unit of AIDA-I from *Escherichia coli***

Own proportion to this work: 70 %

Cloning of different expression plasmids

Expression tests with different *E. coli* strains

Preparation of outer membrane proteins and membranes

Detergent screening for solubilization

Immobilized metal ion and size exclusion chromatography

Crystallization, X-ray diffraction experiments and data analysis

## **From cloning to crystallization – optimization of expression conditions, development of a purification protocol and crystallization of the transport unit of the *adhesin involved in diffuse adherence* (AIDA-I) from enteropathogenic *Escherichia coli***

The *adhesin involved in diffuse adherence* (AIDA-I) belongs to the group of monomeric autotransporter (AT) within the type V secretion systems (T5SS) and is involved in gastrointestinal diseases caused by enteropathogenic *E. coli* (see Introduction) [1; 2]. To investigate the biogenesis of AIDA-I and the proposed common secretion process for monomeric AT, the topic of this doctoral thesis was the determination of the X-ray crystal structure of the transport unit of AIDA-I, which was termed AIDA-I-linker- $\beta_2$ . For crystallization, quantitative amounts of the pure autotransporter were needed. In order to purify the AIDA-I-linker- $\beta_2$ , a his<sub>6</sub>-tag was introduced at the N- and the C-terminus to test, whether the position of the tag had an influence on expression. For surface expression studies and localization analysis, an epitope consisting of a PEYFK motif was introduced as a passenger domain detectable by an anti-PEYFK antibody. The resulting recombinant autotransporter were termed FP-HisN163 and FP-HisC163 (see Introduction, Figure 4) [3]. The theoretical molecular weight of FP-HisN163 and FP-HisC163 containing the signal peptide was calculated to be 53.9 kDa and 50.9 kDa when the signal peptide was removed, respectively. The expression was tested with different *E. coli* strains and different promoters, applying various incubation conditions and analyzing the influence of co-expressed GFP.

### **Results**

#### **Induced surface expression of the recombinant autotransporter FP-HisN163 in *Escherichia coli***

The expression of FP-HisN163 and FP-HisC163 was analyzed by SDS-PAGE (Figure II-1). Cultures of UT5600 (DE3) pIG101 and UT5600 (DE3) pIG102 were incubated at 37 °C until an optical density of 0.5 was achieved (see experimental procedures). The expression of FP-HisN163 and FP-HisC163 was induced by adding a final concentration of 1mM Isopropyl- $\beta$ -D-thiogalactopyranoside (IPTG) to each culture with subsequent incubation at 30 °C for 60 min. Subsequently, the outer membranes were isolated (see experimental procedures) and prepared for SDS-PAGE analysis (Figure II-1). As negative controls, the outer membranes were isolated from strain UT5600 (DE3) without any plasmid and from the non-induced cultures carrying pIG101 or pIG102. The outer membrane isolation of the negative control UT5600 (DE3) showed two strong bands at 37 and 35 kDa (Figure II-1, lane 1), which could be assigned to the outer membrane proteins OmpF/C (38 kDa and 37 kDa) and OmpA (35kDa).

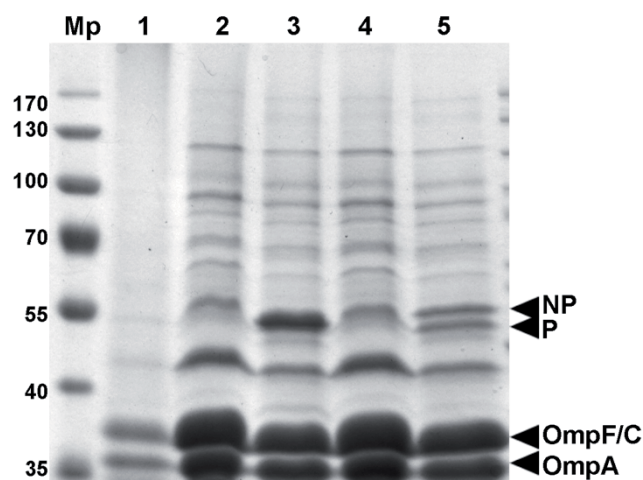


**Figure II-1 SDS-PAGE analysis of the expression of FP-HisN163 and FP-HisC163**

Mp: prestained protein ladder; 1: UT5600 (DE3); 2: UT5600 (DE3) pIG101 – not induced, 3: UT5600 (DE3) pIG101 – induced; 4: UT5600 (DE3) pIG102 – not induced, 5: UT5600 (DE3) pIG102 – induced; NP: non-processed form; P: processed form

Outer membranes of UT5600 (DE3) pIG101 and pIG102 were isolated after induction with 1 mM IPTG for 60 min at 30 °C. Aliquots were heated at 100 °C for 10 min.

These proteins serve as marker proteins for the successful outer membrane isolation and were observed in each of the other samples (Figure II-1, lane 2-5). Without induction, no protein bands at the expected molecular weight of FP-HisN163 and FP-HisC163 were observed (Figure II-1, lane 2 and 4). After induction, double bands were visible in lane 3 and 5 at an apparent molecular weight of 53 and 50 kDa, respectively (Figure II-1). These double bands indicate that two forms of the fusion proteins were expressed. One is not processed and still carries the signal peptide (upper band, indicated by NP in Figure II-1) and the other form is completely processed (lower band, indicated by P in Figure II-1), which were previously identified [4].

To verify that both of the double bands were caused by the two expression forms of FP-HisN163 and FP-HisC163, the outer membranes were analyzed with SDS-PAGE and immunodetection using an anti-His antibody (Figure II-2). The double bands in both samples were detected by the anti-His antibody (Figure II-2, lane 2) verifying the assumption that these double bands contained the two expression forms of FP-HisN163 and FP-HisC163.

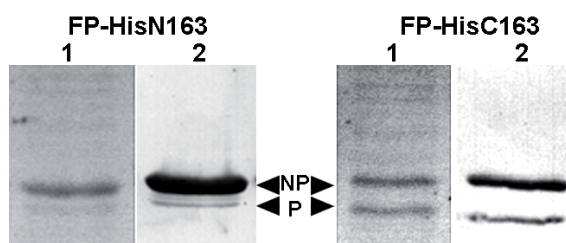


**Figure II-2 Detection of two expression forms of FP-HisN163 and FP-HisC163**

1: SDS-PAGE analysis, 2: immunodetection with anti-His antibody

The arrows indicate the double bands of the autotransporter proteins representing the non-processed form (NP, 53 kDa) and the processed form (P, 50 kDa)

The lower band was assigned to the fully processed and correctly folded form missing the signal peptide, whereas the upper band consists of the unprocessed and non-functional form carrying the signal peptide.

Outer membrane proteins, which contain  $\beta$ -barrel domains, show specific denaturation behavior and do not unfold except after addition of SDS and heating to higher temperatures [5]. To investigate this behavior of FP-HisN163 and FP-HisC163, the outer membranes were isolated from UT5600 (DE3) pIG101 and pIG102 after induction with 1 mM IPTG for 10 min at 30 °C. Aliquots were heated at different temperatures for SDS-PAGE analysis (see experimental procedures). In all lanes, a prominent protein band was observed at a molecular weight of 53 kDa (Figure II-3, indicated by NP). From a temperature of 70 °C (FP-HisN163) and 60 °C (FP-HisC163) another band appeared at a molecular weight of 50 kDa showing the expected behavior of  $\beta$ -barrel proteins (Figure II-3, indicated by P).

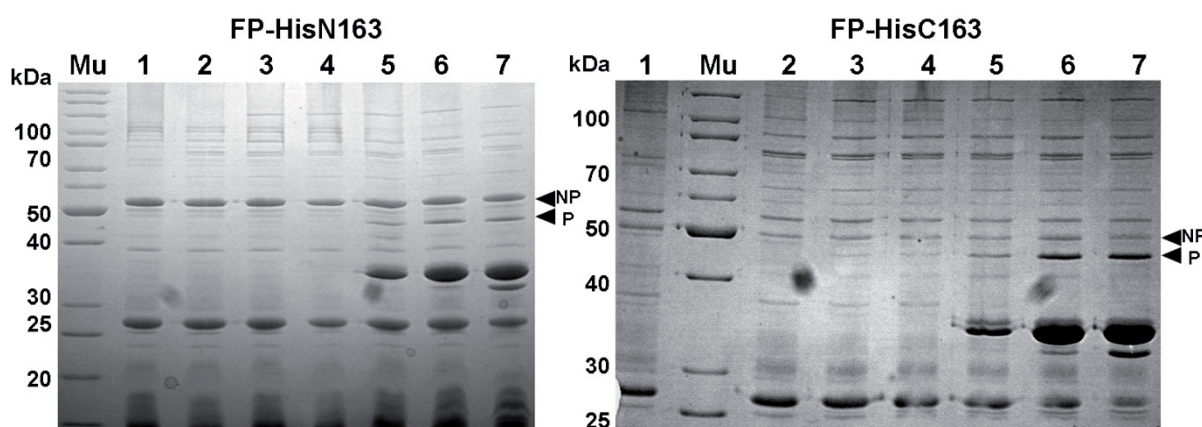


**Figure II-3 Analysis of the unfolding behavior of FP-HisN163 and FP-HisC163**

Mu: unstained protein ladder; 1: 37 °C; 2: 50 °C; 3: 60 °C; 4: 70 °C; 5: 80 °C; 6: 90 °C; 7: 100 °C; NP: non-processed form; P: processed form

Outer membranes of UT5600 (DE3) pIG101 and pI102 were isolated after induction with 1 mM IPTG for 10 min at 30 °C. Aliquots were heated at different temperatures for 10 min and analyzed by SDS-PAGE.

In summary, FP-HisN163 and FP-HisC163 could be expressed by *E. coli* and localized to the outer membrane. However, two expression forms for each of the recombinant autotransporter were observed at 53 and 50 kDa, one of them still carrying the signal peptide and thus adopts a non-native conformation.

### Optimizing of cultivation conditions

The expression conditions chosen for first expression tests resulted in two expressed forms of FP-HisN163 and FP-HisC163. To promote the expression of the fully processed forms the expression conditions had to be optimized.

As a first approach the final IPTG induction concentration was varied between 10  $\mu$ M and 1 mM and the cultures were incubated between 5 and 60 min at 30 °C. The outer membranes were isolated from the cultures expressing FP-HisN163 and FP-HisC163 and examined by SDS-PAGE and heat modification analysis (see experimental procedures).

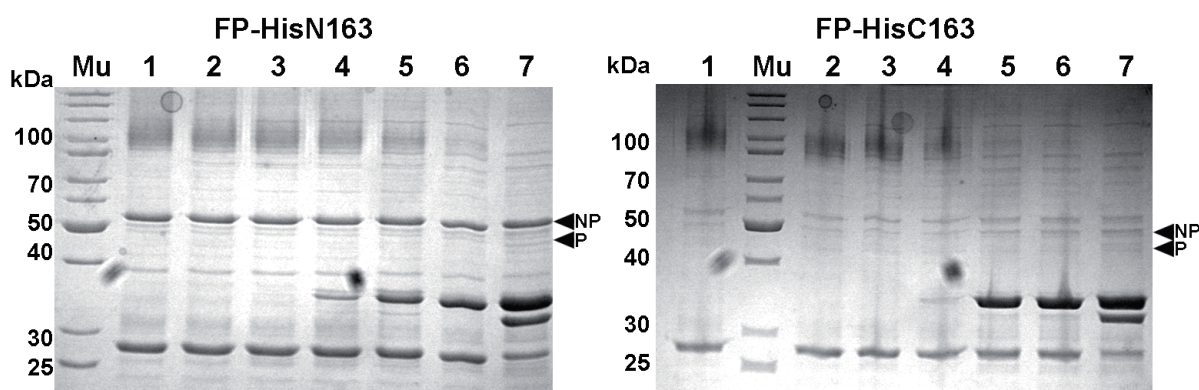


**Figure II-4 Analysis of the unfolding behavior of FP-HisN163 and FP-HisC163**

Mu: unstained protein ladder; 1: 37 °C; 2: 50 °C; 3: 60 °C; 4: 70 °C; 5: 80 °C; 6: 90 °C; 7: 100 °C; NP: non-processed form; P: processed form

Outer membranes of UT5600 (DE3) pIG101 and pI102 were isolated after induction with 10  $\mu$ M IPTG for 15 min at 30 °C. Aliquots were heated at different temperatures for 10 min and analyzed by SDS-PAGE.

As an example, the outer membrane isolations of UT5600 (DE3) pIG101 and pIG102 were shown in Figure II-4 after induction with a final concentration of 10  $\mu$ M IPTG for 15 min expressing FP-HisN163 FP-HisC163. In all lanes, the unprocessed forms with an apparent molecular weight of 53 kDa were detectable (Figure II-4, indicated by NP). Only slight protein bands were visible at a molecular weight of the processed form of FP-HisN163 and FP-HisC163 (Figure II-4, indicated by P) after denaturation at 100 °C.

All tested expression conditions resulted in the same pattern of proteins bands. Consequently, different kinds of *E. coli* strains were tested to promote the expression of the fully processed and correctly folded forms of FP-HisN163 and FP-HisC163.

#### **Suitability of different *Escherichia coli* strains for induced expression**

The induction conditions were varied as mentioned above using the *E. coli* strains BL21 (DE3) and JK321 (DE3) expressing either FP-HisN163 or FP-HisC163. The success of expression and the heat modification analyses were determined by SDS-PAGE of outer membrane isolations.

The expression analysis of BL21 (DE3) pIG101 and pIG102 after induction with a final concentration of 1 mM IPTG for one hour at 30°C showed prominent protein bands for the non-processed and incorrectly folded forms at a molecular weight of 53 kDa in all lanes (Figure II-5, indicated by NP). The fully processed and correctly folded expression forms were not detectable by Coomassie staining. All other tested expression conditions resulted in the same pattern of protein bands for FP-HisN163 and FP-HisC163.



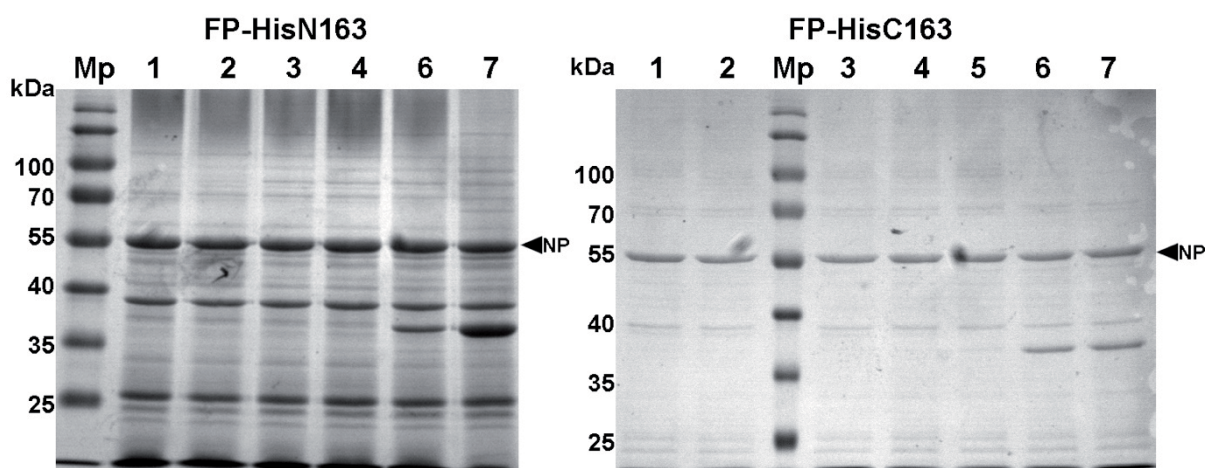


**Figure II-5 Analysis of the unfolding behavior of FP-HisN163 and FP-HisC163 after expression in BL21 (DE3)**

Mp: prestained protein ladder; 1: 37 °C; 2: 50 °C; 3: 60 °C; 4: 70 °C; 5: 80 °C; 6: 90 °C; 7: 100 °C; NP: non-processed form

Outer membranes of BL21 (DE3) pIG101 and pI102 were isolated after induction with 1 mM IPTG for 60 min at 30 °C. Aliquots were heated at different temperatures for 10 min and equal sample volumes were analyzed by SDS-PAGE. The difference of protein amounts is caused by preparation errors.

As an example, one expression analysis of JK321 (DE3) pIG101 is shown in Figure II-6. Cultures were induced with a final concentration of 0.1 mM IPTG and incubated for 60 (Figure II-6A) or 120 min (Figure II-6B). The outer membranes were isolated and analyzed by SDS-PAGE after denaturation at different temperatures. Only the non-processed form of FP-HisN163 with a molecular weight of 53 kDa was expressed (Figure II-6).

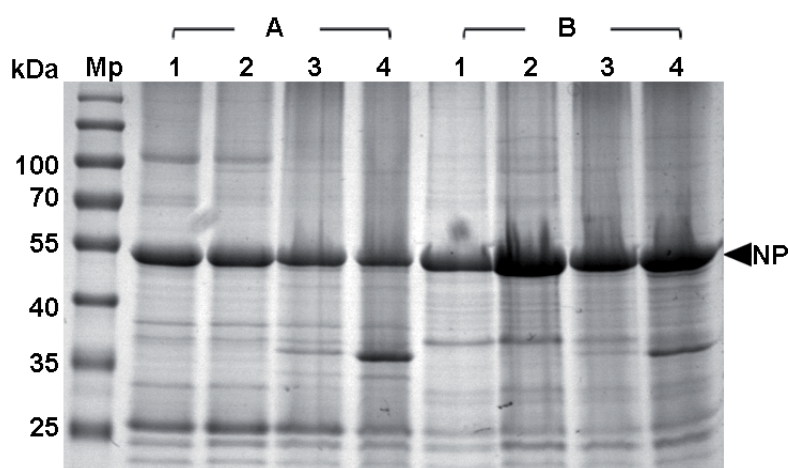


**Figure II-6 Analysis of the unfolding behavior of FP-HisN163 after expression in JK321 (DE3)**

Mp: prestained protein ladder; 1: 37 °C; 2: 70 °C; 3: 90 °C; 4: 100 °C; NP: non-processed form

Outer membranes of JK321 (DE3) pIG101 were isolated after induction with 0.1 mM IPTG for 60 (A) and 120 (B) min at 30 °C. Aliquots were heated at different temperatures for 10 min and analyzed by SDS-PAGE.

The fully processed expression form was not visible with Coomassie staining. Both strains BL21 (DE3) and JK321 (DE3) were able to express FP-HisN163 and FP-HisC163, but all tested incubation conditions resulted in a strong expression of the non-processed forms. Thus, the regulation of induced expression was tested with *E. coli* strain Lemo21 (DE3).

### Regulation of induced expression in *Escherichia coli* Lemo21 (DE3)

The variation of the IPTG concentration used to induce the expression of FP-HisN163 and FP-HisC163 always resulted in a strong production of the non-processed forms in all tested conditions. Therefore, *E. coli* Lemo21 (DE3) containing a trigger system to regulate the activity of the T7 RNA-polymerase was tested to promote the production of the fully processed forms of FP-HisN163 and FP-HisC163. The Lemo21 (DE3) strain is a derivative of BL21 (DE3), but carries a special plasmid pLysS. There, the T7 lysozyme, which is the antagonist to the T7 RNA-polymerase, is expressed under the control of a L-rhamnose inducible promotor. This L-rhamnose inducible promotor is regulated more efficiently than the T7 promotor. Expression tests were performed using 1 mM IPTG as the final concentration for induction and the L-rhamnose concentration and incubation time were varied. Cultures of Lemo21 (DE3) pIG101 and pIG102 were incubated and induced under different conditions, the outer membranes were isolated and the success of the protein expression was analyzed by SDS-PAGE after heat modification. In Figure II-7, examples from different expression test are shown.

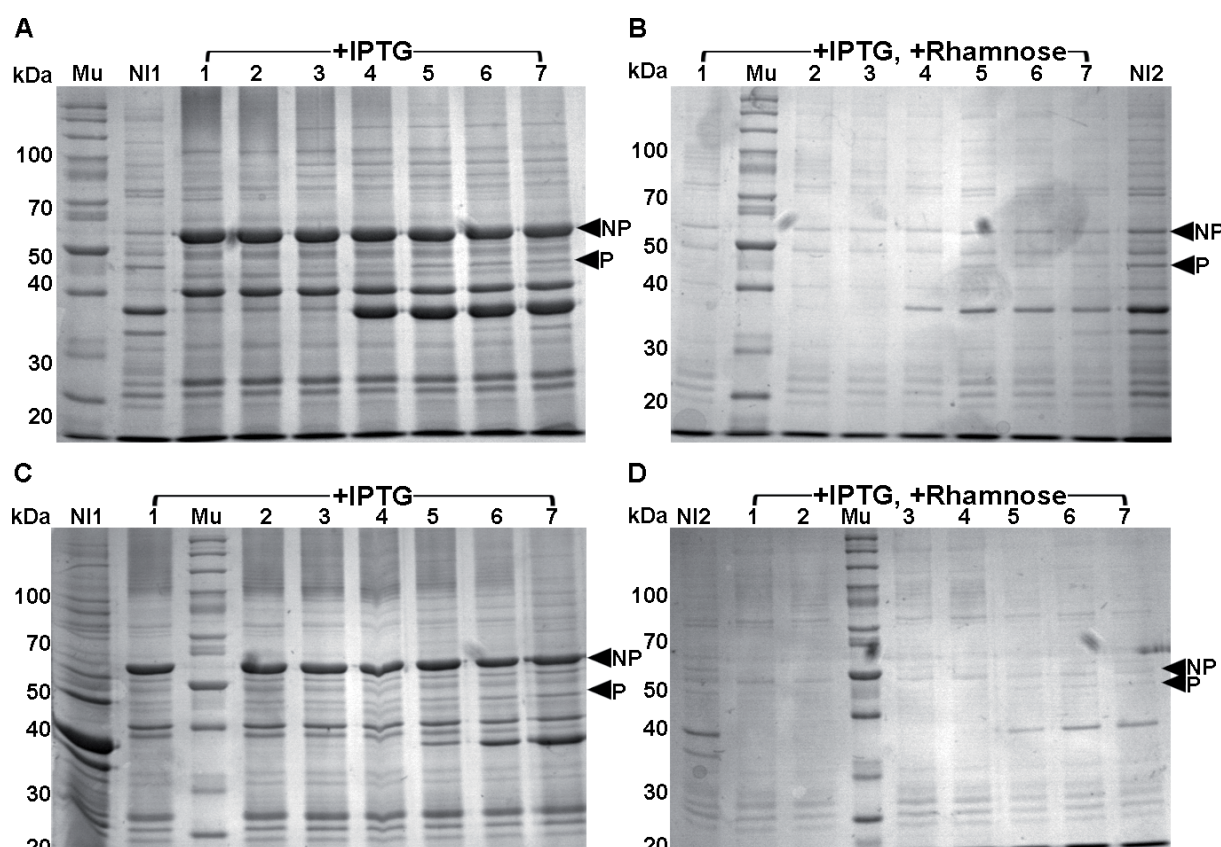


**Figure II-7 Analysis of the unfolding behavior of FP-HisN163 and FP-HisC163 after expression in Lemo21 (DE3)**

Mu: unstained protein ladder; 1: 37 °C; 2: 50 °C; 3: 60 °C; 4: 70 °C; 5: 80 °C; 6: 90 °C; 7: 100 °C; NI1: without IPTG and L-rhamnose; NI2: without IPTG and with 1 mM L-rhamnose; NP: non-processed form; P: processed form

Outer membranes of Lemo21 (DE3) pIG101 and pI102 were isolated after induction with 1 mM IPTG for 60 min at 30 °C without L-rhamnose (A/C) and with 1 mM L-rhamnose (B/D). Aliquots were heated at different temperatures for 10 min and analyzed by SDS-PAGE.



Expression tests without and with 1 mM L-rhamnose under induction with 1 mM IPTG at 30 °C were performed for FP-HisN163 (Figure II-7A/B) and FP-HisC163 (Figure II-7C/D). The negative controls NI1 (Figure II-7A/C, lane NI1) and NI2 (Figure II-7B/D, lane NI2) showed slight protein bands at 53 and 50 kDa, which indicated that the T7 promotor allows leaky expression of the FP-HisN163 and FP-HisC163 even in the absence of IPTG. The induction with 1 mM IPTG and without addition of L-rhamnose resulted in a strong expression of the non-processed forms with an apparent molecular weight of 53 kDa (Figure II-7A/C, lane 1-7, indicated by NP) and only a low expression of the processed forms (Figure II-7A/C, lane 1-7, indicated by P). When 1 mM L-rhamnose was added to the induced cultures, only slight protein bands were detectable at a molecular weight of 53 kDa (Figure II-7B/D, lane 1-7, indicated by NP). However, the amount of the fully processed protein forms of FP-HisN163 and FP-HisC163 did not increase (Figure II-7B/D, lane 1-7, indicated by P). These results indicated that the amount of L-rhamnose was not sufficient to suppress the leaky expression of FP-HisN163. Furthermore, the incubation conditions were not suitable to promote the expression of the processed forms of FP-HisN163 and FP-HisC163. In the following different final concentrations of L-rhamnose and different incubation periods at 30 °C were tested with cultures containing 1 mM IPTG. None of the tested condition resulted in satisfying expression of the fully processed and correctly folded forms of FP-HisN163 and FP-HisC163 (data not shown). In consequence, Lemo21 (DE3) was not suitable for expression of high amounts of the processed form of FP-HisN163.

Thus, a new approach concerning the velocity of the protein expression was conducted.

### **Site-specific mutagenesis of the signal peptide of FP-HisN163**

All previous results indicated that the processing machinery, which was responsible for cleavage of the signal peptide by the signal peptidase, was overcrowded after induction producing high amounts of the non-processed forms of FP-HisN163 and FP-HisC163. To slow down the translation rate [6] and enabling the correct processing, the codon usage of *E. coli* was analyzed. Regarding the codon usage in *E. coli* for the amino acid lysine (AAA: 73%, AAG: 27%, <http://www.geneinfinity.org>), two silent mutations were introduced into the signal peptide of FP-HisN163 at position 3 and 5 (see experimental procedures). The coding sequence of FP-HisN163 was introduced into pET-SH3 [3] carrying the mutated signal peptide resulting in the plasmid pIG301. Different expression conditions were tested with UT5600 (DE3) pIG301, the outer membranes were isolated and analyzed by SDS-PAGE after heat modification (Figure II-8). In this example, the induction of UT5600 (DE3) pIG301 was performed with a final concentration of 0.1 mM IPTG (Figure II-8A) and 1 mM IPTG (Figure II-8B) for 120 min at 30 °C. Both tested conditions resulted in high amount of the non-processed form with an apparent molecular weight of 53 kDa (Figure II-8, indicated by NP). Other tested conditions (data not shown) were also not sufficient to promote the expression of the fully processed and correctly folded form of FP-HisN163.

The induced expression did not result in suitable amounts of fully processed FP-HisN163 and FP-HisC163. Thus, the constitutive expression was investigated subsequently.

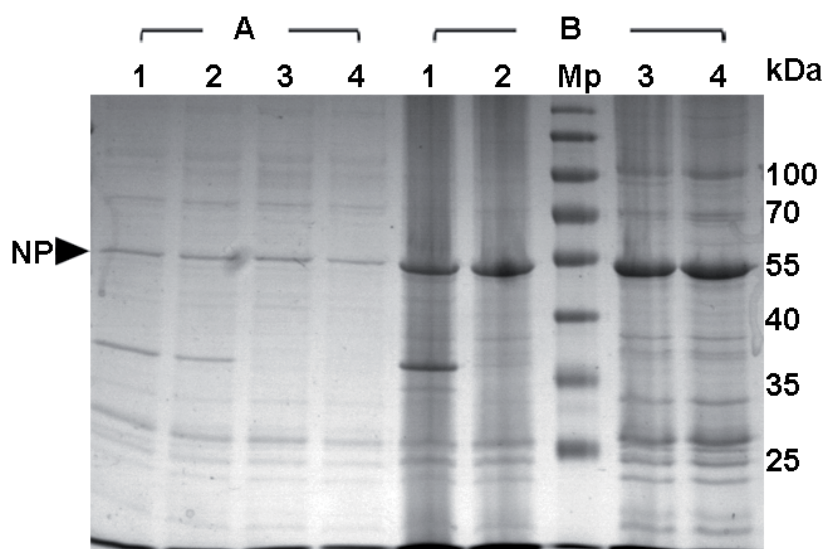


**Figure II-8 Analysis of the unfolding behavior of FP-HisN163 carrying a silent mutation in the signal peptide**

Mp: prestained protein ladder; 1: 37 °C; 2: 70 °C; 3: 90 °C; 4: 100 °C; NP: non-processed form

Outer membranes of UT5600 (DE3) pIG301 were isolated after induction with 0.1 mM IPTG (A) and 1 mM IPTG (B) for 120 min at 30 °C. Aliquots of outer membranes were heated at different temperatures for 10 min and analyzed by SDS-PAGE.

### **Constitutive surface expression of FP-HisN163 and FP-HisC163 in *E. coli* UT5600 (DE3)**

The encoding sequences of FP-HisN163 and FP-HisC163 were introduced into vector pJM007 for constitutive expression [7] resulting in the plasmids pIG501 and pIG502 (see experimental procedures). Cultures of UT5600 (DE3) pIG501 and pIG502 were incubated over 16 hours at 30°C, the outer membranes were isolated and analyzed by SDS-PAGE after denaturation at 100 °C for 10 min (Figure II-9A). The analysis of the unfolding behavior showed that only the processed forms of FP-HisN163 and FP-HisC163 with an apparent molecular weight of 50 kDa were produced by constitutive expression (Figure II-9A, indicated by P).

As an additional test, the accessibility of the PEYFK epitope was investigated by whole cell digestion with proteinase K (see experimental procedures). If FP-HisN163 and FP-HisC163 were fully processed and correctly folded, the PEYFK epitope would be exposed on the cell surface. Proteinase K is only able to cleave these parts of the autotransporter proteins, which are not protected by the outer membrane of the cells. When the PEYFK epitope is presented at the cell surface, it is cleaved by proteinase K and should not be detectable by an anti-PEYFK antibody after digestion. Cultures of both strains were incubated at 30 °C for 18 hours. After harvesting the cultures, aliquots of whole cells of both strains were digested with proteinase K (see experimental procedures). The outer membranes were isolated and applied to immunodetection with an anti-PEYFK antibody (Figure II-9B). For orientation outer membrane protein isolations of UT5600 (DE3) pIG101 and pIG102 (Figure II-2) containing the non-processed and the processed forms of FP-HisN163 and FP-HisC163 were shown (Figure II-9B, lane +). The anti-PEYFK antibody only detected the processed form of FP-HisN163 and FP-HisC163 after constitutive expression (Figure II-9B, lane 1) verifying the observation depicted in Figure II-9A.

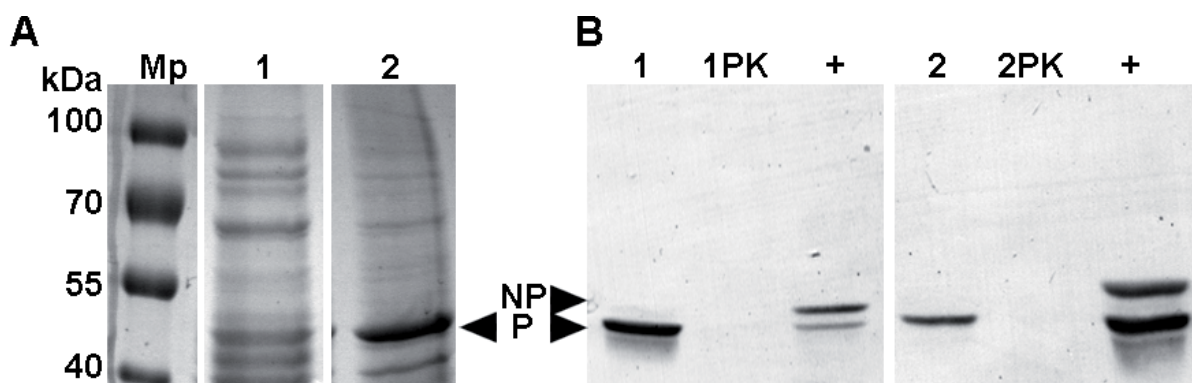


**Figure II-9 Analysis of the unfolding behavior of FP-HisN163 and FP-HisC163 after constitutive expression**

A: SDS-PAGE analysis of outer membrane isolations

Mp: prestained protein ladder; 1: UT5600 (DE3) pIG501; 2: UT5600 (DE3) pIG502; P: processed form

Outer membranes of UT5600 (DE3) pIG501 and pIG502 were isolated after incubation for 16 hours at 30 °C. Aliquots were heated at different temperatures for 10 min and analyzed by SDS-PAGE. The arrow (P) indicates the processed forms of the autotransporter proteins.

B: Immunodetection before and after digestion with proteinase K

1: UT5600 (DE3) pIG501; 2: UT5600 (DE3) pIG502; PK: whole cells were digested with proteinase K before outer membrane isolation; +: control from Figure II-2; NP: non-processed form

Outer membranes of UT5600 (DE3) pIG501 and pIG502 were isolated after incubation for 18 hours at 30 °C. Aliquots of whole cells of both strains were digested with proteinase K (1PK and 2PK). Afterwards, outer membranes were isolated and prepared for immunodetection with an anti-PEYFK antibody. Arrows indicate the non-processed (NP) and the fully processed form (P) of both autotransporter proteins. As control, outer membrane isolations of UT5600 (DE3) pIG101 for FP-HisN163 and pIG102 for FP-HisC163 (see Figure II-2) were used.

After digestion of whole cells with proteinase K, no protein bands were detected (Figure II-9B, lane 1PK and 2PK). These results confirmed that only the fully processed and correctly folded forms of FP-HisN163 and FP-HisC163 were produced by constitutive expression.

### Suitability of different *Escherichia coli* strains for constitutive expression

Cultures of BL21 (DE3) carrying pIG501 or pIG502 were incubated for 18 hours at 30 °C. As negative control BL21 (DE3) cells without any plasmid were treated in the same way. Outer membranes were isolated and analyzed by SDS-PAGE (Figure II-10). The expression level in BL21 (DE3) pIG501 for fully processed and correctly folded FP-HisN163 was quite low (Figure II-10, lane 2) compared to that produced by UT5600 (DE3) pIG501 (Figure II-9A, lane 1). For BL21 (DE3) pIG502 the amount of fully processed and correctly folded FP-HisC163 was comparable to the amount produced by UT5600 (DE3) pIG502 (Figure II-9A, lane 2). In consequence, UT5600 (DE3) was used for subsequent experiments.

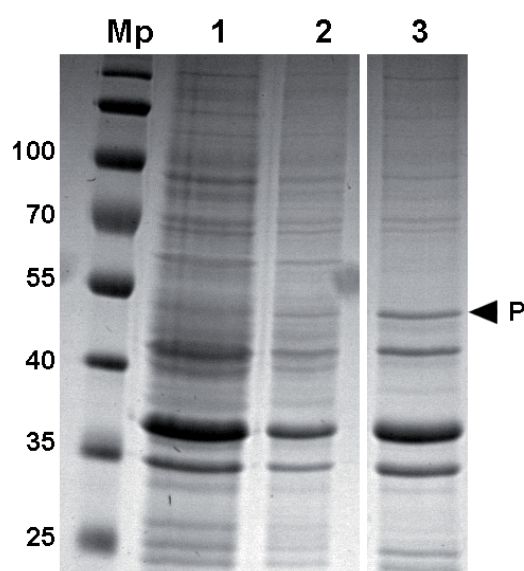


**Figure II-10 SDS-PAGE analyses of FP-HisN163 and FP-HisC163 after constitutive expression in BL21 (DE3)**

Mp: prestained protein ladder; 1: BL21 (DE3), 2: BL21 (DE3) pIG501, 3: BL21 (DE3) pIG502; P: processed form. Outer membranes of all strains were isolated after incubation for 18 hours at 30 °C. Aliquots were heated at 100°C and analyzed by SDS-PAGE.

### **Optimization of cultivation conditions for constitutive surface expression of FP-HisN163 and FP-HisC163**

Cultures of UT56000 (DE3) pIG501 and pIG502 were incubated at 30 °C for different time periods, outer membranes were isolated and analyzed by SDS-PAGE (Figure II-11). The negative control UT5600 (DE3), which was taken from the previous study (Figure II-10), showed no protein bands for at 50 kDa (Figure II-11, lane 1). For UT5600 (DE3) pIG501 the optimal incubation duration for constitutive expression was determined to last 18 hours (Figure II-11, lane 3). There, the amount of FP-HisN163 was higher than after 16 hours (Figure II-11, lane 2) or 20 hours (Figure II-11, lane 5).

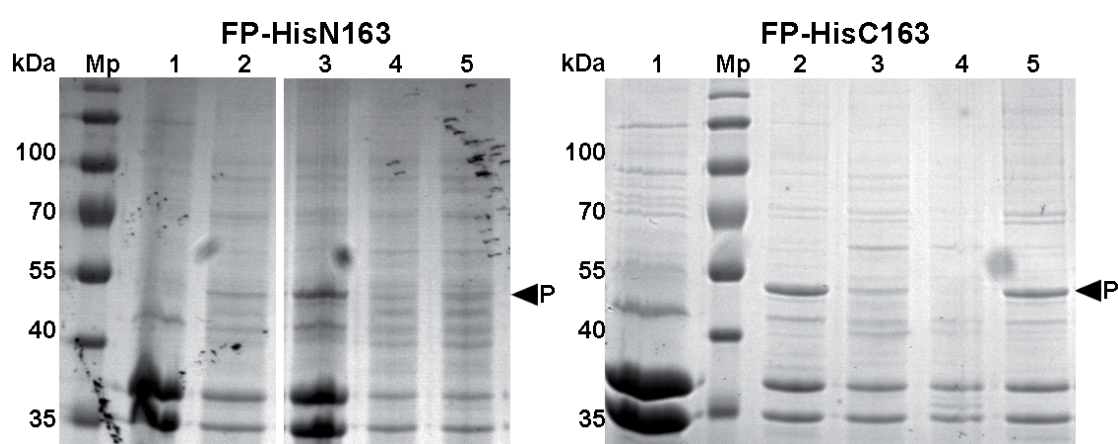


**Figure II-11 SDS-PAGE analyses of FP-HisN163 and FP-HisC163 after constitutive expression in UT5600 (DE3)**

Mp: prestained protein ladder; 1: negative control UT5600 (DE3) incubated for 18 hours at 30 °C; P: processed form

The cultures of UT5600 (DE3) carrying pIG501 or pIG502 were incubated at 30 °C for 16 (lane 1), 18 (lane 2/4) and 20 (lane 5). Whole cells of the samples in lane 4 were treated with proteinase K previous to outer membrane protein isolation. All samples were heated at 100°C for 10 min.

For the expression of FP-HisC163 by UT5600 (DE3) pIG502, the best incubation duration was determined to last 16 hours showing the highest amount of FP-HisC163 (Figure II-11, lane 2). The proteinase K treatment verified the results of the surface accessibility analysis (Figure II-9B) that the autotransporter proteins FP-HisN163 and FP-HisC163 were in a functional conformation because no protein bands at a molecular weight of 50 kDa could be detected (Figure II-11, lane 4).

### Isolation of FP-HisN163 from *Escherichia coli* UT5600 (DE3) pIG501 after constitutive expression

The following purification and crystallization experiments were performed with UT5600 (DE3) pIG501 expressing FP-HisN163 in a constitutive way under optimized incubation conditions for 18 hours at 30 °C and 200 rpm in 12 L LB medium. The membrane fractions of these cultures were isolated as described in chapter III and solubilization studies were performed to release FP-HisN163 from the outer membranes for further purification.

### Detergent screening for solubilization of FP-HisN163

For later purification, FP-HisN163 had to be released from the outer membrane into the supernatant. Different detergents were tested (see experimental procedures and chapter III). The efficacy of different detergents were analyzed by immunodetection with an anti-His antibody (Figure II-12). Sodium dodecyl-sulfate (SDS) was used as positive control. LDAO was chosen for the solubilization of FP-HisN163 because a strong band was detected in the supernatant (Figure II-12, LDAO, lane S) and only a slight band was visible in the pellet fraction (Figure II-12, LDAO, lane P). All other tested detergents showed a lower efficacy.

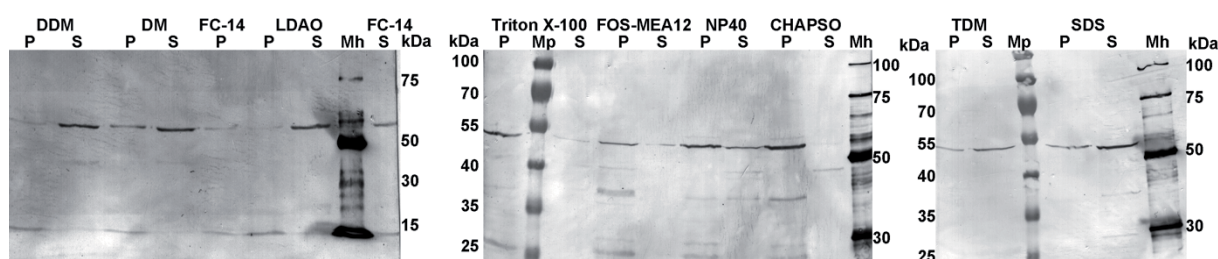


**Figure II-12 Immunodetection of FP-HisN163 after solubilization with different detergents**

Mh: anti-His protein ladder; Mp: prestained protein ladder; P: pellet; S: supernatant; Membrane fractions of UT5600 (DE3) pIG501 after incubation for 18 hours at 30 °C were isolated. Different detergents were added with a final concentration of 2 % (v/v) (Triton X-100 and SDS) or 1 % (v/v) (all others). Immunodetection with an anti-His antibody was performed.

In the next step, the optimal membrane concentration for solubilization was determined. For this purpose, outer membrane fractions were homogenized in different volumes of resuspension buffer to obtain a final concentration of 150, 125 and 100 mg/ml. Samples of these outer membrane fractions were treated as before using 1 % (v/v) LDAO as detergent. The efficacy of the solubilization process was documented by immunodetection with an anti-His antibody (Figure II-13). In the pellet fractions of the higher concentrated samples



slight protein bands at 50 kDa were detected (Figure II-13, 150mg/ml and 125mg/ml, lane P). At a concentration of 100 mg/ml no protein band was detectable in the pellet fraction at 50 kDa (Figure II-13, 100 mg/ml, lane P), but a strong protein band was visible in the supernatant fraction (Figure II-13, 100 mg/ml, lane S). Therefore, the optimal concentration was determined to be 100 mg/ml for the highest solubilization efficacy. For large-scale purification 1 % (v/v) LDAO was used to solubilize FP-HisN163 in 25 ml aliquots of membrane fractions with a concentration of 100 mg/ml at 37 °C and 70 rpm in a shaking incubator.

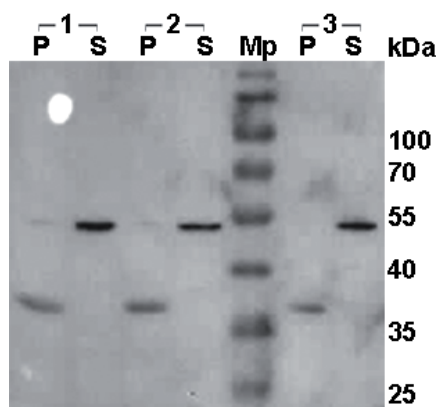


**Figure II-13 Immunodetection of FP-HisN163 after solubilization with LDAO**

Mp: prestained protein ladder; P: pellet; S: supernatant

Membrane fractions with concentrations of 150 (1), 125 (2) and 100 mg/ml (3) were incubated with 1 % (v/v) LDAO at 37 °C and 800 rpm for 60 min. The supernatants and the pellets were prepared for SDS-PAGE and immunodetection with an anti-His antibody.

### Purification of FP-HisN163

The purification of FP-HisN163 with immobilized metal ion affinity chromatography (IMAC) and subsequent size exclusion chromatography (SEC) was performed as described in chapter III. A typical chromatogram after IMAC is shown in Figure II-14. The flow rate was adjusted with 2 ml/min and fractions of 10 ml were collected until the elution step. The washing step with 15 % (v/v) IMAC buffer B (75 mM imidazole, pH 8.0) was used to remove non-specifically bound proteins and lipids (Figure II-14, peak 2). The elution was conducted in one step with 80 % (v/v) IMAC buffer B (160 mM imidazole, pH 8.0) in 2 ml fractions (Figure II-14, peak 3).

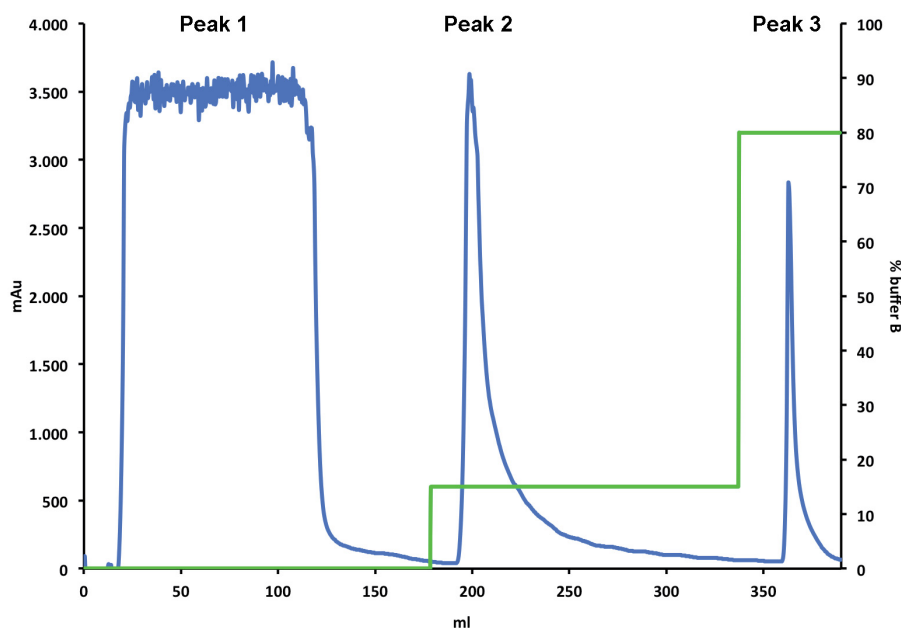


**Figure II-14 Chromatogram of an immobilized metal ion affinity chromatography**

On the x-axis the volume in ml is shown. The left y-axis shows the UV absorption signal in mAu and the right y-axis indicates the amount of imidazole containing IMAC buffer B in % (v/v). The blue curve demonstrates the behavior of the UV signal and the green curves indicates the amount of IMAC buffer B.

The signal of the flow through (peak 1) was caused by non-bound components of the applied supernatant. After a washing step with 15 % (v/v) IMAC buffer B (75 mM imidazole, pH 8.0) non-specifically bound proteins and lipids were removed from the column (peak 2). The elution of FP-HisN163 was conducted in one step with 80 % (v/v) IMAC buffer B (160 mM imidazole, pH 8.0) in one step (peak 3).

The SDS-PAGE analysis (Figure II-15) of the collected IMAC fractions showed only slight protein bands with a molecular weight of 50 kDa in the flow through fraction number 1 from peak 1 (Figure II-14) and in the wash fraction number 2 (Figure II-14, peak 2). The elution fractions contained high amounts of FP-HisN163 (Figure II-15, 4-13, indicated by an arrow). One prominent protein band above 70 kDa and several contaminants were also detectable in all elution fractions. The elution fractions 4-13 were pooled and concentrated to a final volume of 500  $\mu$ l with a protein concentration of 8.7 mg/ml for subsequent SEC.

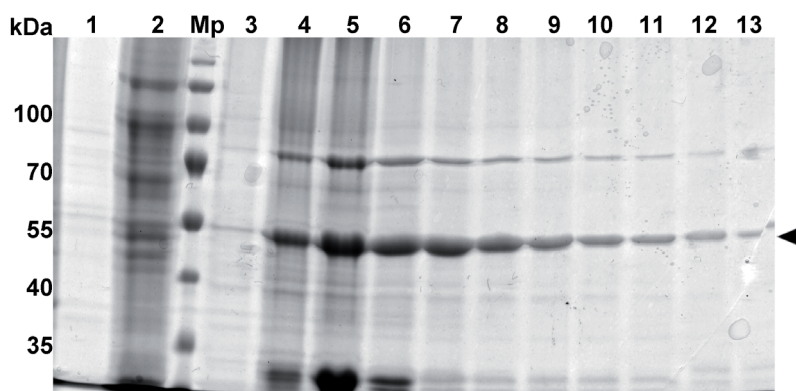


**Figure II-15 SDS-PAGE analysis of IMAC fractions**

Mp: prestained protein ladder; 1: flow through fraction (peak 1, Figure II-14); 2: washing fraction (peak 2, Figure II-14); 3-13: elution fractions (peak 3, Figure II-14)

The samples were heated at 100°C for 10 min. FP-HisN163 is indicated by an arrow.



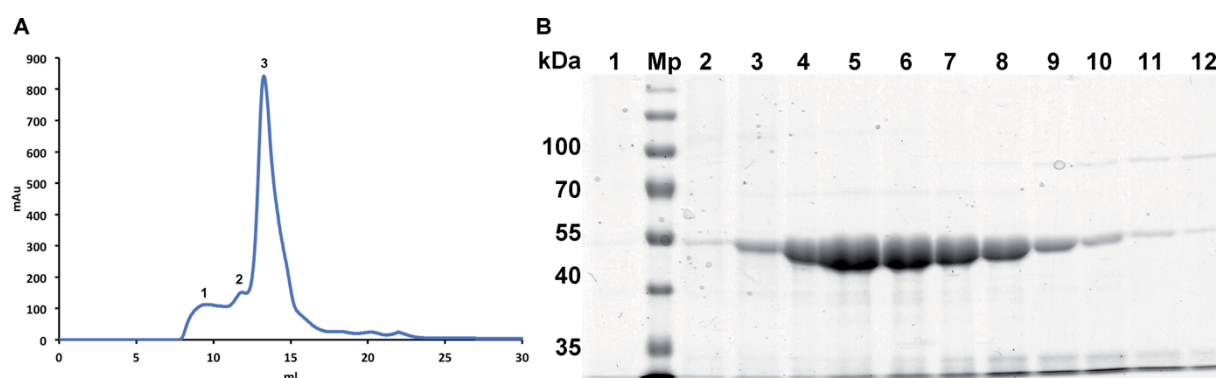


**Figure II-16 Chromatogram of a size exclusion chromatography (SEC) (A) and SDS-PAGE analysis of collected fractions (B)**

A: Between 9 and 12 ml two side peaks (1 and 2) were detectable. FP-HisN163 was eluted between 12 and 16 ml in 0.5 ml fractions (3).

B: Mp: prestained protein ladder; 1: sample of side peak 1; 2: sample of side peak 2; 3-12: elution fractions of peak 3

The samples were heated at 100°C for 10 min.

In Figure II-16A, a typical SEC chromatogram is shown. The main peak with two side peaks between 9 and 12 ml. The collected fractions were analyzed by SDS-PAGE (Figure II-16B). In the fraction of the first side peak a small protein band was detectable at 50 kDa (Figure II-16B, lane 1). For the second side peak, the same protein bands were visible but also some contaminants above 100 kDa (Figure II-16B, lane 2). The fractions from the peak 3 contained highly pure amounts of the FP-HisN163 (Figure II-16B, lane 3-9). Only some contaminants below 40 kDa and above 55 kDa were visible.

The elution fractions 3-9 were pooled and concentrated to a final of 80  $\mu$ l with a final concentration of 25 mg/ml. This sample was applied to immunodetection using an anti-His and an anti- $\beta$ -barrel antibody (Figure II-17). The SDS-PAGE analysis revealed three protein bands with a molecular weight of 50, 39 and 37 kDa. Both antibodies detected these protein bands indicating that they contained FP-HisN163, which was not fully denaturated (Figure II-17, lane 2 and 3). The prominent protein band at 50 kDa was assigned to the functional form of FP-HisN163.

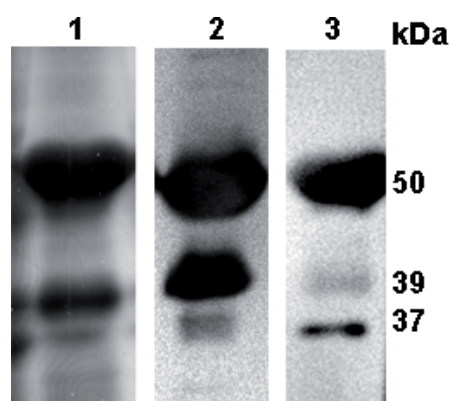


**Figure II-17 Verification of purified FP-HisN163**

After SDS-PAGE (lane 1) the immunodetection was conducted with an anti-His antibody (lane 2) and an anti- $\beta$ -barrel antibody (lane 3).

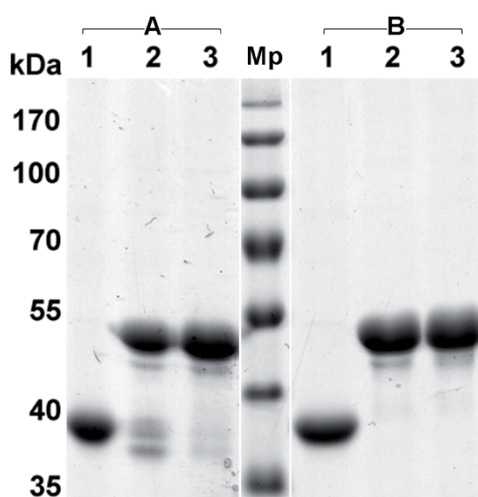


**Figure II-18 Denaturation analysis of purified FP-HisN163**

M: prestained protein ladder; A: sample buffer with 3.2 (w/v) % SDS; B: sample buffer with 6.4 /w/v) % SDS; 1: not heated; 2: heated for 5 min; 3: heated for 10 min. Adapted from chapter III.

To verify that the bands at lower molecular weight were caused by FP-HisN163, which was not fully denaturated, a denaturation analysis was performed (see chapter III). The double band at 39 and 37 kDa disappeared when a sample buffer with the doubled amount of SDS was used. In consequence, all protein samples for further SDS-PAGE analysis were prepared with SDS sample buffer containing 6.4 % (v/v) SDS and heated at 100 °C for 10 min.

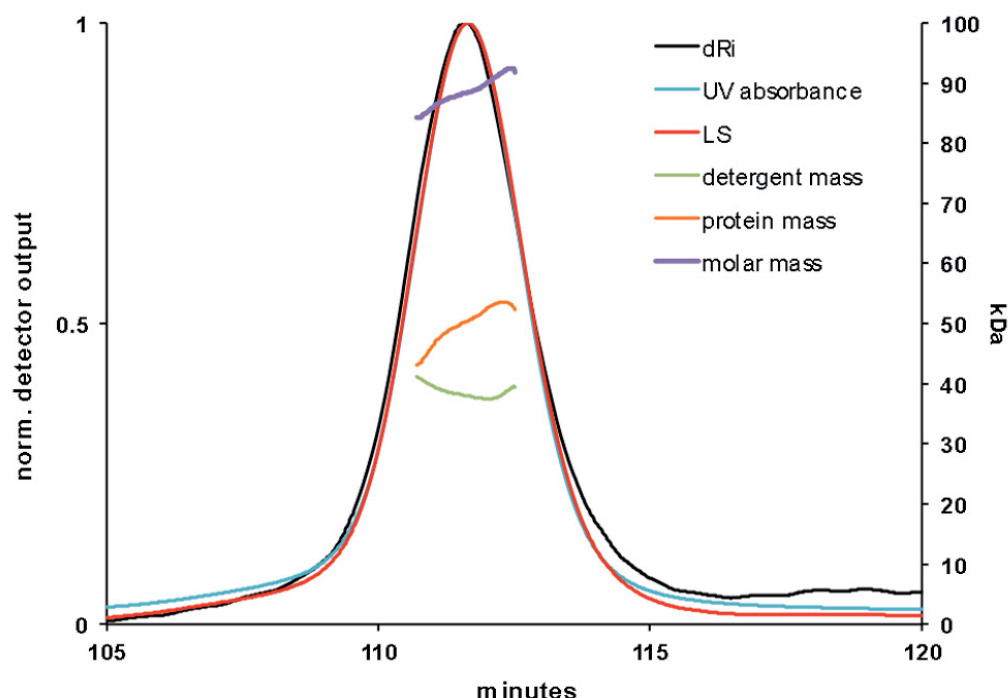


**Figure II-19 Elution profile after SEC-MALS**

Black line: refractive index detector signal; blue line: UV absorbance signal; red line: light scattering detector signal; green line: calculated detergent mass; orange line: calculated protein mass; violet line: calculated micelle mass: Picture adapted from chapter IV.

Furthermore, the oligomeric state, the monodispersity and the homogeneity of purified FP-HisN163 were determined by size exclusion chromatography coupled to a multi-angle light-

scattering detector (SEC-MALS) (see chapter IV). During solubilization and purification mixed micelles consisting of detergent, lipid and protein molecules were randomly formed in solution. After normalization of the detector outputs, one symmetric peak was observed, which demonstrate that the purified protein solution was homogeneous and monodisperse (Figure II-19, black, blue and red line). For the mixed micelles, a molecular weight of  $88.5 \pm 2.4$  kDa was calculated (Figure II-19, violet line) and for the detergent micelles  $38.6 \pm 1.0$  kDa (Figure II-19, green line). The determined molecular mass for FP-HisN163 corresponded to the monomeric form with a molecular weight of  $49.9 \pm 3.0$  kDa (Figure II-19, orange line).

### Mass spectrometric analysis of FP-HisN163

As a final verification, purified FP-HisN163 was analyzed by mass spectrometry at the BMFZ (see experimental procedures). After tryptic digestion several peptides were identified (Figure II-20), which were sequenced afterwards (Table II-1). These analyzed peptides covered 19.2 % of the FP-HisN163 sequence with 100 % identity.

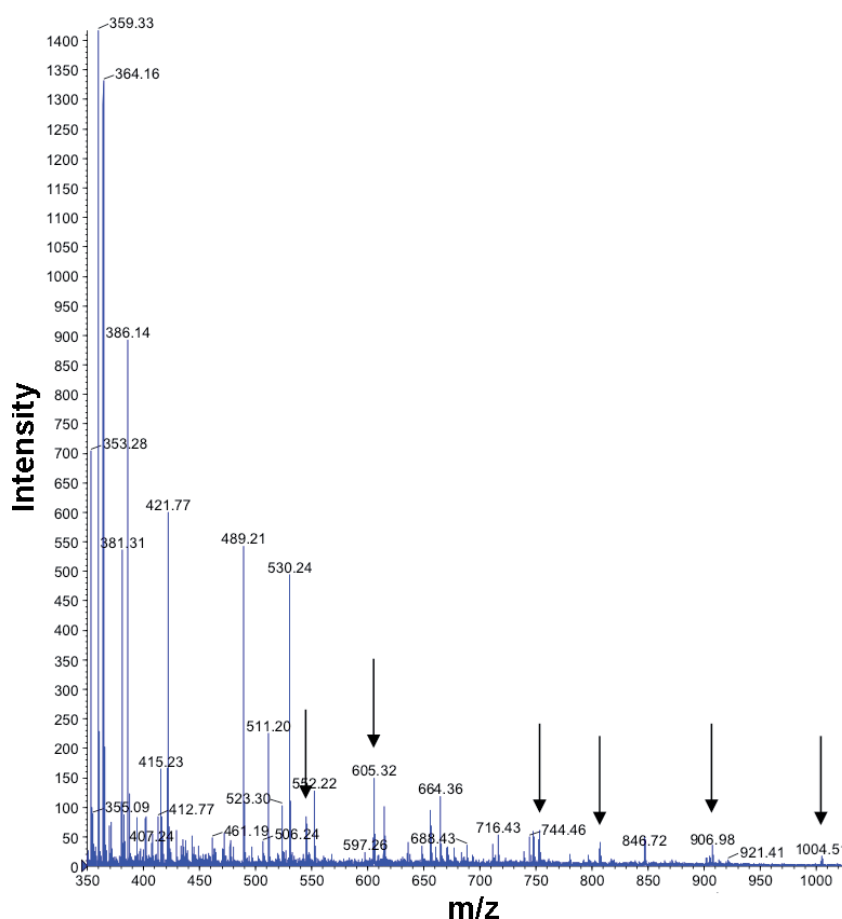


**Figure II-20 Spectrum of the mass spectrometric analysis of FP-HisN163**

On the x-axis the ratio of mass number and charge number is shown and on the y-axis the intensity of the detector signal is depicted. The numbers indicate the m/z ratio. After tryptic digestion selected peptides were sequenced (arrows).

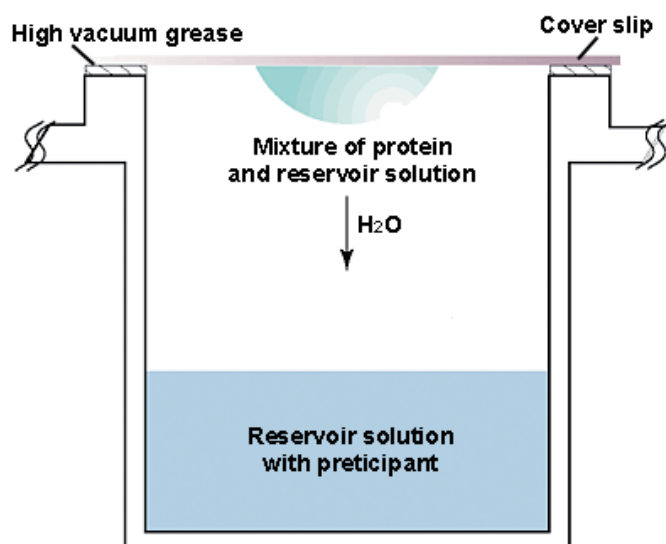
**Table II-1** Sequences of identified peptides of FP-HisN163

Mass	Charge	Molecular mass [M+H] <sup>+</sup>	Sequence
545,28	3+	1633,84	131-GWYLTSHLPTSDTR-144
752,71	3+	2256,13	224-FHAEQLGDFTLGIM <sub>ox</sub> GGYANAK-244
806,73	3+	2418,19	393-EFSPYIEANWIHNTHIEFGVK-412
906,97	2+	1812,94	208-TTTNQFINQLGGDIYK-223
1004,50	2+	2008,00	89-DGINIISVEGNSDAEFSLK-107

In conclusion, all analyses showed satisfying results in terms of purity, amount, homogeneity, monodispersity and identity of purified FP-HisN163. With the established protocols for expression, membrane isolation, solubilization and purification, the quality and quantity of FP-HisN163 was suitable for crystallization.

### Crystallization of FP-HisN163

For X-ray diffraction experiments, crystals with a high quality and large size are required. Therefore, a huge number of supplied crystallization conditions were tested using hanging drop vapor diffusion at 18 °C (Figure II-21) [8]. After observing crystals, grid screens based on the initial crystallization conditions were set up to optimize the crystallization process (see experimental procedures). Adding different additives and detergents, varying the protein-to-precipitant-ratio, seeding and incubating at different temperatures were applied to optimize the successful crystallization conditions and increase the diffraction quality.

**Figure II-21** Set-up for hanging drop vapor diffusion crystallization

The protein solution is mixed with a reservoir solution, which contains a precipitant and placed above an excess of reservoir solution in a sealed chamber. In this closed system, water diffuses from the hanging drop to the reservoir solution until equilibrium is reached, whereby the concentrations of all components in the hanging drop increases. In a successful crystallization process, nuclei form and grow to larger crystals. Picture adapted from Hampton Research (<http://www.hamptonresearch.com>).

### Initial screening of crystallization conditions

For the hanging drop vapor diffusion setup, supplied crystallization screens were tested. The initial crystals of FP-HisN163, shown in Figure II-22, were obtained at 18 °C after 4-40 days with JCSG Core I (Qiagen), MemPlus and MemGold (Molecular Dimensions). In-house X-ray diffractometry revealed that the crystals in Figure II-22A-G consisted of protein, whereas the crystals in Figure II-22H were salt crystals (data not shown).

Beside these crystallization conditions, several others were found and optimized using grid screens.

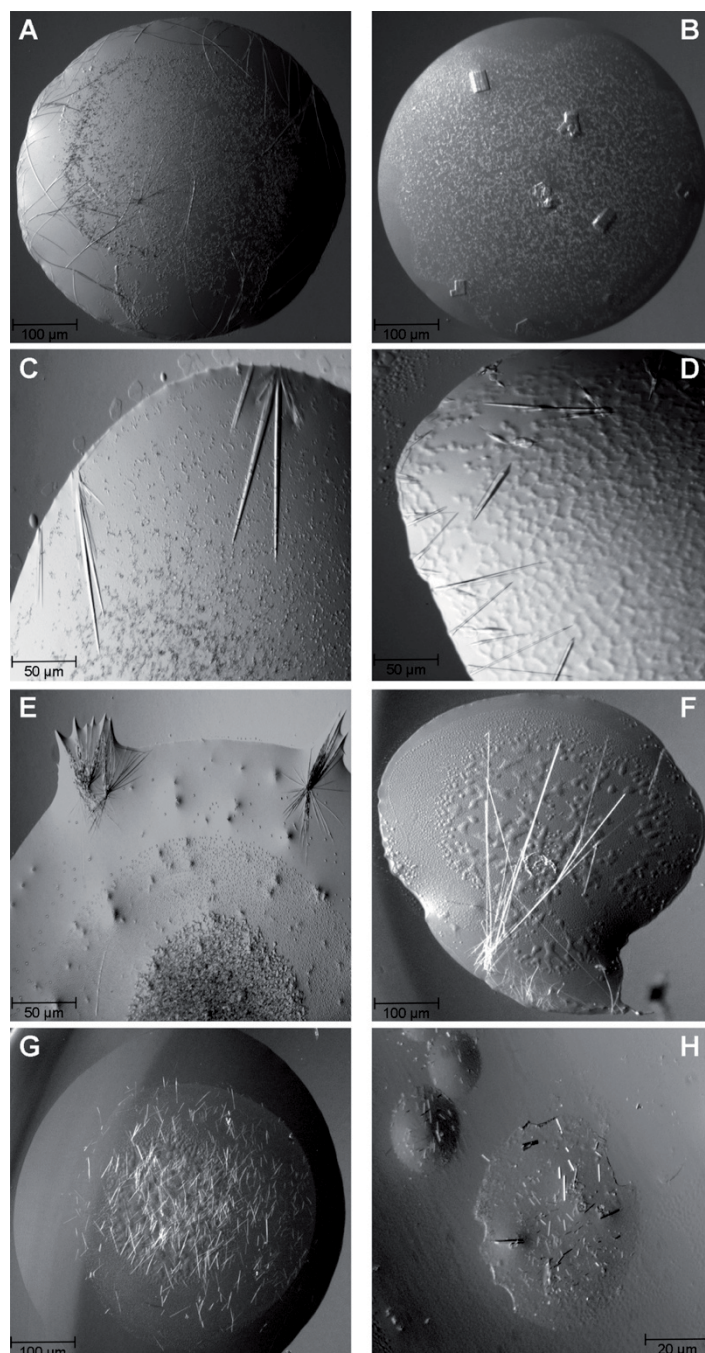


**Figure II-22 Successful crystallization after initial screening**

Crystals were obtained after 4-40 days at 18 °C by hanging drop vapor diffusion with supplied crystallization conditions. Diffraction experiments revealed that A-G were protein crystals and H were salt crystals (data not shown).



### Optimization of successful crystallization conditions

The supplied crystallization conditions were optimized in two-dimensional grid screens. Therefore pH and precipitant concentration were varied based on the initial condition (see experimental procedures). The following examples were finally taken for data collection at different synchrotrons.

Starting from the initial crystallization condition MemPlus No. 4 (Figure II-22B) several grid screens, different temperatures, additives and detergents were tested in hanging drop vapor diffusion experiments.

After four days, cuboid-shaped crystals were observed in the crystallization condition at 18 °C without any additives or additional detergents (Figure II-23A). The crystals in the same condition but with Cyclofos-5 had a pyramidal form (Figure II-23B). When Fosfen-9 was added rod-like crystals were obtained (Figure II-23C). When Fosfen-9 was added rod-like crystals were obtained (Figure II-23C).

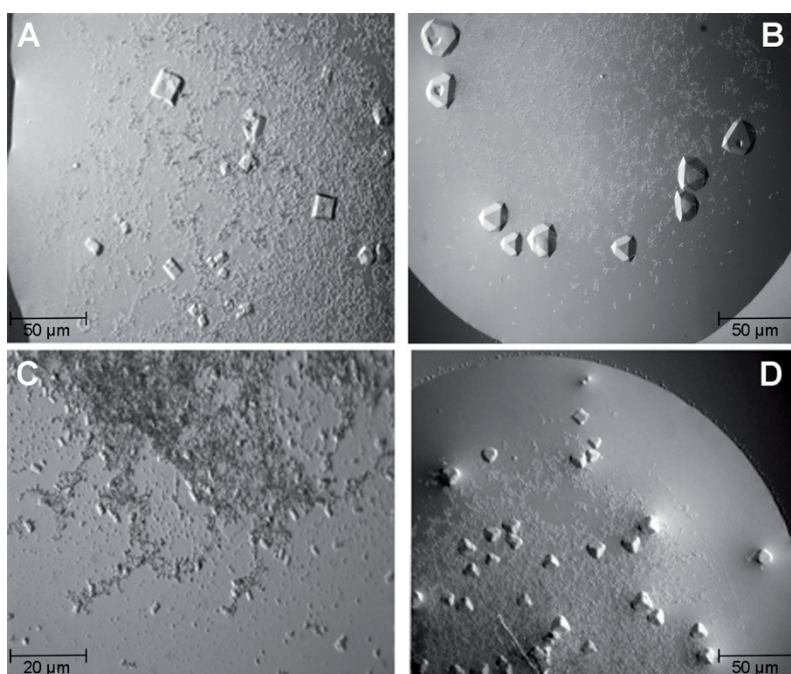


**Figure II-23 Crystals of FP-HisN163 after optimization of the initial condition MemPlus No. 4**

A: without additives and additional detergents, B: with Cyclofos-5, C: with Fosfen-9, D: with calcium acetate

Furthermore the supplied condition MemPlus No. 14 was optimized in grid screens and the same parameters, as mentioned above, were tested in hanging drop vapor diffusion experiments to obtain better diffracting crystals of FP-HisN163. Only small crystal needles grew in the supplied condition and not in the grid screens (Figure II-22D). Neither changing the temperature and the protein-to-precipitant-ratio, nor applying different additives or seeding improved the crystallization process in the supplied or optimized conditions.

Another successful crystallization condition, MemPlus No. 17 (Figure II-22E), was also optimized in grid screens and tested as mentioned above in hanging drop vapor diffusion experiments resulting in thicker crystal needles suitable for data collection (see chapter III).

Finally, cuboid-shaped small crystals grew in the AmmSO<sub>4</sub> screen after 8 weeks using microbatch plates.

### X-ray diffraction experiments with FP-HisN163 crystals

All crystals suitable for data collection were soaked in a cryo-protective buffer (crystallization condition plus an additional 10 % (v/v) of the precipitant and 10 M LDAO) and flash-cooled for X-ray diffraction experiments at different synchrotrons at 100 K (see experimental procedures).

Crystals from conditions based on MemPlus No. 4 were measured at the European Synchrotron Radiation Facility (ESRF, Grenoble) with beamline ID23-eh2 and diffracted X-rays not better than 15 Å (Figure II-24). Despite of intensive optimization efforts, these crystallization conditions were not able to produce well-diffracting crystals.

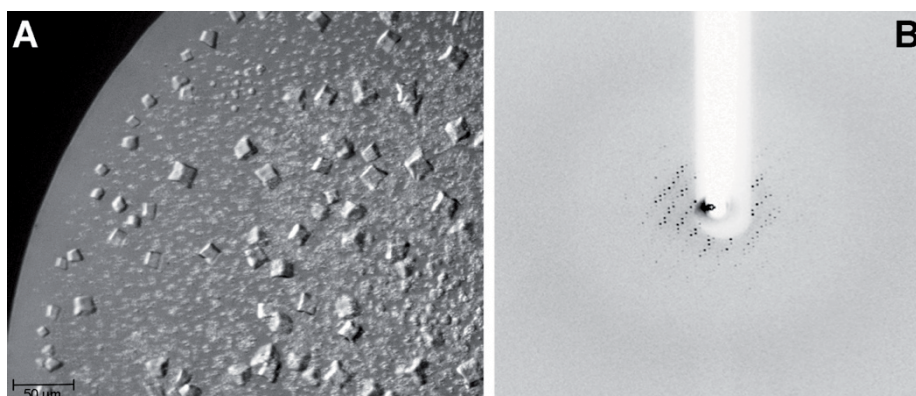


**Figure II-24 Crystal (A) and diffraction image (B) of FP-HisN163**

Cubic crystals (A) grew in a hanging drop vapor diffusion experiment using an optimized condition based on MemPlus No. 4. The crystal diffracted X-rays to a final resolution of 15 Å (B).

The crystal needles from MemPlus No. 14 (Figure II-22D) were measured at the Swiss Light Source (SLS, Villigen) with beamline PXIII to a final resolution of 3.5 Å (data not shown).

The cuboid-shaped crystals from the AmmSO<sub>4</sub> screen (Figure II-25A) were measured at the European Synchrotron Radiation Facility (ESRF, Grenoble) with the beamline ID23-eh2 and diffracted X-rays to a final resolution of 2.8 Å (Figure II-25B).

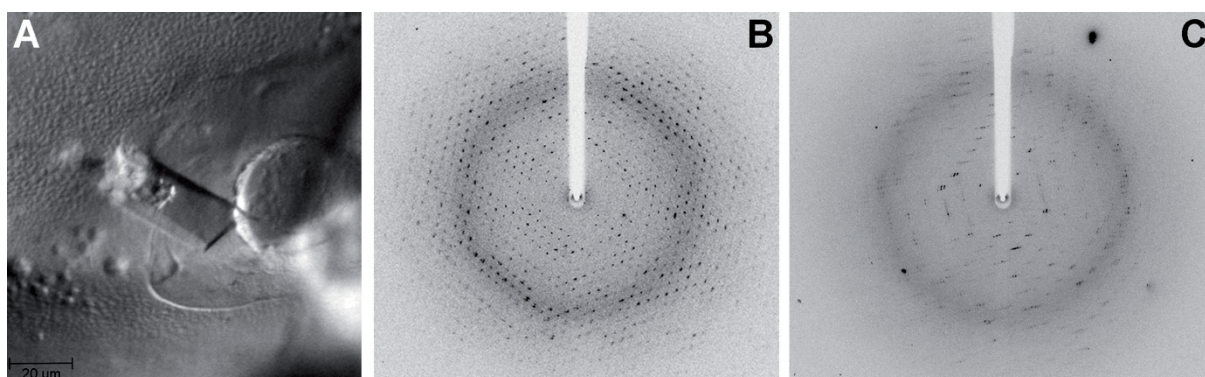


**Figure II-25 Crystal (A) and diffraction image (B) of FP-HisN163**

A cuboid crystal (A) grew in a microbatch experiment using the AmmSO<sub>4</sub> screen. The crystal diffracted X-rays to a final resolution of 2.8 Å in one direction (B) but the diffraction quality decreased when the crystal was rotated through 90° (C) showing anisotropic diffraction behavior.



However, the diffraction quality decreased when the crystal was rotated through 90 ° indicated by the anisotropic diffraction pattern (Figure II-25C). Crystal needles, which grew in optimized conditions based on MemPlus No. 17, were measured at the European Synchrotron Radiation Facility (ESRF, Grenoble) with the beamline ID23-eh2 and diffracted X-rays to a final resolution of 3.0 Å (see chapter III).

All data sets were processed with the XDS package and scaled with XSCALE [9; 10] for structure determination efforts (see experimental procedures). The data set of one crystal needle obtained in an optimized condition of MemPlus No. 17 was used to solve the structure of AIDA-I-linker- $\beta_2$  as described in chapter III and IV.

## Discussion

The aim of this doctoral thesis was the determination of the X-ray crystal structure of the transport unit of AIDA-I, which was termed AIDA-I-linker- $\beta_2$ . For this purpose, quantitative amounts of pure AIDA-I-linker- $\beta_2$  were needed. Two different fusion proteins were cloned, which carried a his<sub>6</sub>-tag at the N- (FP-HisN163) or C-terminal end (FP-HisC163). A huge variety of expression conditions, different kinds of *E. coli* strains and promoters were tested to establish an optimized expression protocol for purification. However, the position of the his<sub>6</sub>-tag had no influence on the amount of FP-HisN163 or FP-HisC163 in the outer membrane. The induced expression always resulted in huge amounts of the non-processed forms of FP-HisN163 and FP-HisC163 still carrying the signal peptide at the N-terminus for Sec-dependent transport across the inner membrane, which was previously shown [4]. The production of the processed forms of FP-HisN163 and FP-HisC163 lacking the signal peptide was not increased by all tested induced expression conditions. In consequence, constitutive expression conditions were tested. High amounts of only the processed forms of FP-HisN163 and FP-HisC163 were obtained, which were suitable for large-scale purification. After solubilization test with different detergents, LDAO was used to release FP-HisN163 from the outer membrane into the supernatant, which was applied to IMAC and SEC for purification. SEC-MALS analysis revealed that the purified FP-HisN163 was a monomer in the monodisperse and homogenous protein solution. The identity of FP-HisN163 was verified by mass spectrometry. Numerous crystallization conditions were tested and optimized to obtain well diffracting crystals of FP-HisN163. Finally, a data set of one crystal needle was used for structure determination of AIDA-I-linker- $\beta_2$ .

## Experimental procedures

### *Cloning of FP-HisN163 and FP-HisC163*

The cloning of pIG101 and pIG501 for induced and constitutive expression of FP-HisN163 was conducted as described in the supplementary information of chapter III. For cloning of pIG102, pET-SH3 [3] was used as template and two oligonucleotides (IG001: 5'-GCTCAGCGTGGTGATGATGGTGATGGAAGCTGTATTTATCCCCAG-3' and EW012: 5'-CAGACGAGATGGTATTAAT-3') were used as primers for PCR. The PCR amplificate was digested with *NsiI* and *BlnI* and fused to pET-SH3 yielding plasmid pIG102, which encodes FP-HisC163 carrying a C-

terminal, his<sub>6</sub>-tag. The sequence encoding FP-HisC163 was cut out with *NdeI/BclI* and fused with pJM007 after digestion with *NdeI/BamHI* resulting in the plasmid pIG502 for constitutive expression of FP-HisC163.

#### *Site-directed mutagenesis of the signal peptide*

To obtain correctly processed protein during induced expression the translation rate should be slowed down. Regarding the codon usage in *E. coli* for the amino acid lysine (AAA: 73%, AAG: 27%, <http://www.geneinfinity.org>), two silent mutations were introduced into the signal peptide at position 3 and 5 by using the Quick-change site-directed mutagenesis kit (Agilent Technology) referring to the manufacturers manual. Therefore, a PCR was performed with pIG101 as template and two oligonucleotides (IG004: 5'-CTTTAAGAAGGAGATATACCATGGTTAAGTTAAAGTTTGGTG-3' and IG005: 5'-CACCAAACCTTAACCTAACCATGGTATATCTCCTTCTTAAAG-3') as primers. The PCR amplificate was digested with *NdeI/BlnI* and fused with pET-SH3 [3]. The resulting plasmid was termed pIG301.

#### *Induced expression of FP-HisN163 and FP-HisC163*

Cultures of *E. coli* carrying a plasmid with an inducible promotor were incubated in LB media at 37 °C and 200 rpm until an optical density of 0.5 at was achieved. After induction by addition of Isopropyl-β-D-thiogalactopyranoside (IPTG), the cultures were incubated at 30 °C and 200 rpm. The final concentration of IPTG and the incubation time varied depending on the tested expression condition.

#### *Constitutive expression of FP-HisN163*

Cultures of *E. coli* UT5600 (DE3) pIG501 and pIG502 were cultivated in LB media at 30 °C for different time periods. Afterwards, the cultures were cooled on ice for 15 min to stop the expression of FP-HisN163 and FP-HisC163. For purification, cultures were cultivated as described in chapter III.

#### *Outer membrane (OM) isolation*

The OM was isolated as described in chapter IV.

#### *Proteinase K accessibility assay*

The proteinase K accessibility assay was conducted as described in chapter IV.

#### *Heat modification analysis*

Outer membrane samples were aliquoted, mixed with SDS sample buffer and denaturated at 37, 50, 60, 70, 80, 90 and 100 °C. Afterwards the heat modification of these outer membranes were analyzed by SDS-PAGE.

#### *SDS-PAGE analysis*

The analysis of protein samples with respect to their molecular weight was performed by SDS-PAGE of Laemmli [11].

Therefore 10 % (w/v) separating gels with stacking gels were produced (Mini Protean System, BioRad). The sample were mixed with a sample buffer containing 3.2 or 6.4 % (w/v) SDS, heated at 100 °C for 10 min and applied to the gels. Different markers were used as a standard for protein

weight analysis (Mp: PageRuler™ Prestained Protein Ladder and Mu: PageRuler™ Unstained Protein Ladder from Fermentas or Mh: anti-His Ladder from Qiagen for immunodetection).

#### *Western blotting analysis and immunodetection*

The immobilization of proteins after SDS-PAGE was performed with the help of western blotting (Mini Protean Tetra Cell, BioRad). The proteins were transferred on an activated PVDF membrane by applying 100 V for 1 hour. Afterwards the PVDF membrane was incubated in blocking solution over night at room temperature to avoid unspecific binding during immunodetection. The specific detection of proteins was carried out using an anti-His antibody, an anti-PEYFK antibody or an anti- $\beta$ -barrel antibody.

#### *Membrane preparation and screening of detergents for solubilization of FP-HisN163*

Membranes and the detergent screening were performed as described in chapter III. The tested detergents were DDM (n-dodecyl- $\beta$ -D-maltoside), DM (n-decyl- $\beta$ -D-maltoside), LDAO (Lauryldimethylamine-oxide), FC-14 (FOS-Choline 14), Triton-X100, NP40, FOS-MEA12, CHAPSO (3-[(3-cholamidopropyl)-dimethylammonio]-1-propanesulfonate) and TDM (n-tridecyl- $\beta$ -maltoside). Sodium dodecyl-sulfate (SDS) was used as positive control.

#### *Purification of FP-HisN163*

The purification was performed as described in chapter III.

#### *Mass spectrometric analysis of purified FP-HisN163*

The identity of purified FP-HisN163 was verified after tryptic digestion by ESI-MS/MS with a hybrid mass spectrometer (QqTOF) by the Biologisch-Medizinisches Forschungszentrum (BMFZ) at Heinrich Heine University Düsseldorf.

#### *Crystallization of FP-HisN163*

Initial screening of crystallization conditions were carried out with supplied crystallization screens (Qiagen, Molecular Dimensions, Hampton Research) using hanging drop vapor diffusion plates (EasyXtal 15-Well Tools, Qiagen) at 18 °C [8]. For this purpose, the protein solution was mixed with different amounts of reservoir solution containing precipitants. Conditions, in which crystals grew, were reproduced in grid screens (Table II-2). Here only some examples are listed.

Adding different additives and detergents (Hampton Research), varying the protein-to-precipitant-ratio and incubating at different temperatures were applied to optimize the suitable crystallization conditions. Furthermore another crystallization technique called microbatch was tested. Therefore, the protein and the different reservoir solutions were mixed in equal amounts and pipetted onto a 72-well microbatch plate (Terasaki Microbatch plate, Molecular Dimensions, Suffolk). The drops were covered by mineral oil that allows only little evaporation. The microbatch plates were also stored at 18 °C.

**Table II-2** Overview of suitable crystallization conditions

Supplied screen	Condition No.	Grid screen No.	Grid screen condition
MemPlus MD1-44	4  1.5 M sodium formate, pH 5.5 0.05 M sodium cacodylate 30 % (v/v) PEG 400	I	1.5 M sodium formate 0.05 M sodium cacodylate pH 5.0/5.25/5.5/5.75/6.0 PEG 400 25/30/35 % (v/v)
		II	1.5 M sodium formate 0.05 M sodium cacodylate pH 5.7/5.8/5.9/6.0/6.1 PEG 400 32.5/35/37.5 % (v/v)
		III	1.5 M sodium formate 0.05 M sodium cacodylate pH 5.8/5.85/5.9/5.95/6.0 PEG 400 25/32/35 % (v/v)
		IV	0.05 M sodium cacodylate 30 % PEG 400 (v/v) Sodium formate 1/1.5/2 M pH 5.8/5.85/5.9/5.95/6.0
		V	1.5 M sodium formate 0.05 M sodium cacodylate pH 6.1/6.2/6.3/6.4/6.5 PEG 400 25/32/35 % (v/v)
MemPlus MD1-44	14  0.02 M Tris, pH 7.5 33 % (v/v) PEG 1500	I	0.02 M Tris pH 6.8/7.2/7.4/7.75/8.0 PEG 1500 28/33/38 % (v/v)
		II	0.02 M Tris pH 7.0/7.25/7.5/7.75/8.0 PEG 1500 28/33/38 % (v/v)
		III	0.02 M Tris pH 7.0/7.25/7.5/7.75/8.0 PEG 1500/2000 (1:1) 28/33/38 % (v/v)
		IV	0.02 M Tris pH 7.1/7.2/7.3/7.4/7.5 PEG 1500 23/25/28 % (v/v)
MemPlus MD1-44	17  0.1 M sodium cacodylate, pH 6.5 12.5 % (v/v) PEG 2000 MME	I	0.1 M sodium cacodylate pH 6.0/6.25/6.5/6.75/7.0 PEG 2000 MME 12.5/22.5/32.5 % (v/v)
		II	0.1 M sodium cacodylate pH 6.0/6.25/6.5/6.75/7.0 PEG 2000 MME 27.5/32.5/37.5 % (v/v)
AmmSO <sub>4</sub> screen			0.05 M HEPES, pH 7.0 Ammonium sulfate 0.8/1.0/1.2/1.4/1.6/1.8/2.0/2.2/2.4/2.6/2.8/3.0

*X-ray diffractometry and data analysis*

To reduce the radiation damage during diffraction experiments the crystals needed to be frozen at -173.15 °C (100 K). Therefore cryoprotection buffers were prepared containing additional 10 % (v/v) of precipitant and 10 mM detergent. The crystals were transferred to the cryoprotection buffer using a nylon or litholoop (Molecular Dimensions, Suffolk), incubated for 10 to 30 seconds and subsequently frozen in liquid nitrogen.

Finally the crystals were stored in a dewar with liquid nitrogen for transport until diffraction experiments were performed. The data sets were collected at different synchrotrons at 100 K using a stream of liquid nitrogen:

- European Synchrotron Radiation Facility (ESRF, Grenoble), ID23-2 (0.873 Å)
- Deutsches Elektronen-Synchrotron (DESY, Hamburg), P14 (1.24 Å)
- Swiss Light Source (SLS, Villigen), PXIII (0.978 Å)

Data sets were processed using the *XDS* package and scaled with *XSCALE* [9; 10].

## References

1. Benz, I. and Schmidt, M. A. (1989). Cloning and expression of an adhesin (AIDA-I) involved in diffuse adherence of enteropathogenic *Escherichia coli*. *Infect Immun*, 57(5): 1506-1511.
2. Jose, J., Jahnig, F. and Meyer, T. F. (1995). Common structural features of IgA1 protease-like outer membrane protein autotransporters. *Mol Microbiol*, 18(2): 378-380.
3. Jose, J. and Handel, S. (2003). Monitoring the cellular surface display of recombinant proteins by cysteine labeling and flow cytometry. *Chembiochem*, 4(5): 396-405.
4. Winterer, E. (2009). Untersuchung zur Struktur und Funktion der Transportdomänen des Autodisplay Systems. Unpublished Dissertation: Heinrich-Heine University, Duesseldorf.
5. Maurer, J., Jose, J. and Meyer, T. F. (1999). Characterization of the essential transport function of the AIDA-I autotransporter and evidence supporting structural predictions. *J Bacteriol*, 181(22): 7014-7020.
6. Gustafsson, C., Govindarajan, S. and Minshall, J. (2004). Codon bias and heterologous protein expression. *Trends Biotechnol*, 22(7): 346-353.
7. Maurer, J., Jose, J. and Meyer, T. F. (1997). Autodisplay: one-component system for efficient surface display and release of soluble recombinant proteins from *Escherichia coli*. *J Bacteriol*, 179(3): 794-804.
8. McPherson, A. (1990). Current approaches to macromolecular crystallization. *Eur J Biochem*, 189(1): 1-23.
9. Kabsch, W. (2010). Integration, scaling, space-group assignment and post-refinement. *Acta Crystallogr D Biol Crystallogr*, 66(Pt 2): 133-144.
10. Kabsch, W. (2010). Xds. *Acta Crystallogr D Biol Crystallogr*, 66(Pt 2): 125-132.
11. Laemmli, U. K. (1970). Cleavage of structural proteins during the assembly of the head of bacteriophage T4. *Nature*, 227(5259): 680-685.

## *Chapter III*

### **Purification, crystallization and preliminary X-ray crystallographic analysis of the transport unit of the monomeric autotransporter AIDA-I from *Escherichia coli***

Published in: *Acta Crystallographica Section F*

Impact factor: 0.552

Own proportion to this work: 60 %

Cloning and expression in *E. coli*

Preparation of membranes

Detergent screening for solubilization

Purification and crystallization of the transport unit of AIDA-I

X-ray diffraction experiments and data analysis

Writing of the manuscript





Acta Crystallographica Section F

**Structural Biology  
and Crystallization  
Communications**

ISSN 1744-3091

## Purification, crystallization and preliminary X-ray crystallographic analysis of the transport unit of the monomeric autotransporter AIDA-I from *Escherichia coli*

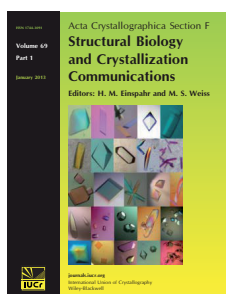
Iris Gawarzewski, Britta Tschapek, Astrid Hoepfner, Joachim Jose, Sander H. J. Smits and Lutz Schmitt

*Acta Cryst.* (2013). **F69**, 1159–1162

Copyright © International Union of Crystallography

Author(s) of this paper may load this reprint on their own web site or institutional repository provided that this cover page is retained. Republication of this article or its storage in electronic databases other than as specified above is not permitted without prior permission in writing from the IUCr.

For further information see <http://journals.iucr.org/services/authorrights.html>



*Acta Crystallographica Section F: Structural Biology and Crystallization Communications* is a rapid all-electronic journal, which provides a home for short communications on the crystallization and structure of biological macromolecules. Structures determined through structural genomics initiatives or from iterative studies such as those used in the pharmaceutical industry are particularly welcomed. Articles are available online when ready, making publication as fast as possible, and include unlimited free colour illustrations, movies and other enhancements. The editorial process is completely electronic with respect to deposition, submission, refereeing and publication.

Crystallography Journals **Online** is available from [journals.iucr.org](http://journals.iucr.org)

*Acta Cryst.* (2013). **F69**, 1159–1162

Gawarzewski *et al.* · Transport unit of AIDA-I

Acta Crystallographica Section F

Structural Biology  
and Crystallization  
Communications

ISSN 1744-3091

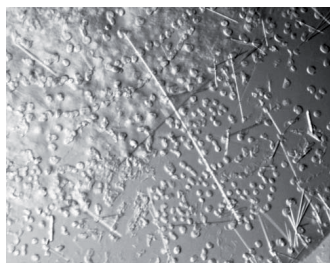
Iris Gawarzewski,<sup>a</sup> Britta  
Tschapek,<sup>a</sup> Astrid Hoepfner,<sup>b</sup>  
Joachim Jose,<sup>c</sup> Sander H. J.  
Smits<sup>a</sup> and Lutz Schmitt<sup>a\*</sup>

<sup>a</sup>Institute of Biochemistry, Heinrich-Heine-Universität, Düsseldorf, Germany, <sup>b</sup>Crystal Farm and X-ray Facility, Heinrich-Heine-Universität, Düsseldorf, Germany, and <sup>c</sup>Institute of Pharmaceutical and Medical Chemistry, Westfälische Wilhelms-Universität, Münster, Germany

Correspondence e-mail: lutz.schmitt@hhu.de

Received 4 July 2013

Accepted 1 September 2013



© 2013 International Union of Crystallography  
All rights reserved

## Purification, crystallization and preliminary X-ray crystallographic analysis of the transport unit of the monomeric autotransporter AIDA-I from *Escherichia coli*

The adhesin involved in diffuse adherence (AIDA-I) from *Escherichia coli* belongs to the group of autotransporters, specifically the type Va secretion system (T5aSS). All autotransporter systems contain a C-terminal  $\beta$ -domain, which forms a barrel-like structure in the outer membrane with a hydrophilic pore allowing passenger translocation across the outer membrane. The passenger domain harbours the biological activity in the extracellular space and functions, for example, as an adhesin, an enzyme and a toxin. The exact transport mechanism of passenger translocation across the outer membrane is not clear at present. Thus, structure determination of the transport unit of AIDA-I could provide new insights into the transport mechanism. Here, the purification, crystallization and preliminary X-ray crystallographic studies of the transport unit of AIDA-I are reported.

### 1. Introduction

Benz & Schmidt (1989) described the adhesin involved in diffuse adherence glycoprotein I (AIDA-I) of enteropathogenic *Escherichia coli* (EPEC), which was found in a patient suffering from infantile diarrhoea. Several studies revealed that AIDA-I is transported in a similar way to the IgA protease from *Neisseria gonorrhoea*, the prototype of monomeric autotransporter proteins (Pohlner *et al.*, 1987; Henderson *et al.*, 2004; Jose & Meyer, 2007). Subsequently, AIDA-I was assigned to the group of monomeric autotransporters (subgroup Va; Leo *et al.*, 2012).

In general, monomeric autotransporters consist of four functional domains encoded in one polypeptide chain: (i) an N-terminal signal peptide mediating transport across the inner membrane *via* the Sec translocon; (ii) a passenger domain harbouring the biological functionality in the extracellular space; (iii) a linker domain connecting the passenger domain and the  $\beta$ -domain; and (iv) a  $\beta$ -domain forming a  $\beta$ -barrel-like structure in the outer membrane at the C-terminus (Jose, 2006). Despite numerous studies on the autotransporter secretion pathway, the exact translocation process of the passenger domain across the outer membrane remains largely unknown. Different transport models have been proposed to try to explain recent results, *i.e.* the hairpin model and the Omp85 model (Bernstein, 2007; Shahid *et al.*, 2012). Recently, a new model mechanism was described which is a combination of both the hairpin model and the Omp85 model (Ieva *et al.*, 2011; Pavlova *et al.*, 2013). To gain further insights into this process, we crystallized the recombinant transport unit of AIDA-I for structure determination by X-ray diffraction. Here, we describe the preliminary results of the expression, purification and crystallization of the transport unit of AIDA-I from *E. coli*.

### 2. Materials and methods

#### 2.1. Cloning, expression and membrane preparation

The recombinant autotransporter protein used in this study consisted of an N-terminal His<sub>6</sub> tag, an epitope for immunodetection

## crystallization communications

as a passenger domain, the AIDA-I linker domain comprising 163 amino acids and the AIDA-I  $\beta$ -domain (see §2.1 of the Supplementary Material<sup>1</sup>). Thus, this fusion protein was termed FP-HisN163 with a theoretical molecular weight of 50.9 kDa. The gene encoding FP-HisN163 was cloned into the expression vector pJM007 (Maurer *et al.*, 1997), resulting in plasmid pIG501. The constitutive expression of FP-HisN163 was performed in 12 l cell culture with *E. coli* UT5600 (DE3) for 18 h at 303 K and 170 rev min<sup>-1</sup> to a final OD<sub>600</sub> of 4.4. Cells were harvested at 277 K and 7000g for 10 min. All subsequent steps were conducted at 277 K. Cell pellets were resuspended in 200 ml of 200 mM Tris-HCl pH 8.0, 200 mM NaCl, 0.1 mg ml<sup>-1</sup> DNase and were disrupted by several passes through a cell disrupter at 2.5 MPa (Constant Systems). Non-disrupted cells and cell debris were removed by a centrifugation step at 19 000g for 45 min. Using the supernatant, membrane fractions were isolated by ultracentrifugation at 200 000g for 1 h 15 min, homogenized in 200 mM Tris-HCl, 200 mM NaCl, 10% glycerol and diluted to a final concentration of 100 mg ml<sup>-1</sup>.

### 2.2. Detergent screen

For solubilization of FP-HisN163, aliquots of membrane fractions were mixed with a final concentration of 1% (v/v) of each tested detergent (see §2.2 of the Supplementary Material) and incubated at 310 K and 800 rev min<sup>-1</sup> for 1 h. After ultracentrifugation at 200 000g and 277 K for 30 min, pellet and supernatant fractions were applied to western blotting analysis using an anti-His antibody for subsequent immunodetection.

### 2.3. Purification

The membrane fractions were solubilized with 1% (v/v) *N,N*-dimethyldodecylamine *N*-oxide (LDAO) for 1 h at 310 K and 70 rev min<sup>-1</sup> followed by an ultracentrifugation step at 200 000g and 277 K for 30 min. All subsequent purification steps were performed at 277 K. The supernatant was first applied onto an immobilized metal-ion affinity chromatography (IMAC) column (data not shown). The collected fractions were analyzed by SDS-PAGE and concentrated with an Amicon Ultra Centrifugal Filter device (30 kDa molecular-weight cutoff, Millipore) to a final concentration of 4 mg ml<sup>-1</sup>. In the second purification step size-exclusion chromatography (SEC) with a Superdex 200 10/30 column (GE Healthcare) was performed with 20 mM HEPES pH 7.5, 150 mM NaCl, 2.8 mM LDAO (data not shown). Fractions were collected, analyzed by SDS-PAGE and concentrated with an Amicon Ultra Centrifugal Filter device (30 kDa molecular-weight cutoff, Millipore) to achieve final concentrations between 7 and 28 mg ml<sup>-1</sup>. The purification procedure yielded 2 mg pure protein from 12 l culture. Protein concentration was determined with a NanoDrop device (PeqLab Biotechnology GmbH) using the molecular mass of FP-HisN163 (50.90 kDa including the His<sub>6</sub> tag) and its calculated extinction coefficient (84.80 M<sup>-1</sup> cm<sup>-1</sup>; <http://web.expasy.org/protparam>).

### 2.4. Denaturation analysis

The purified protein samples of FP-HisN163 were prepared for SDS-PAGE analysis with sample buffers A [3.2% (w/v) SDS] and B [6.4% (w/v) SDS]. These samples were heated at 373 K for 0, 5, 10, 15, 20, 25 and 30 min, respectively.

<sup>1</sup> Supplementary material has been deposited in the IUCr electronic archive (Reference: WD5224).

### 2.5. Crystallization and preliminary X-ray analysis

Initial screening for crystallization conditions was performed at 291 K using the hanging-drop vapour-diffusion method combined with commercially available buffer screens (MemPlus from Molecular Dimensions and JCSG Suites I-IV from Qiagen). Needle-like crystals were observed after 2–3 weeks by mixing equal volumes of protein and precipitant solution. The primary crystallization condition [100 mM sodium cacodylate pH 6.5, 12.5% (v/v) PEG 2000 MME] was optimized to a final condition consisting of 100 mM sodium cacodylate pH 6.5, 27.5% (v/v) PEG 2000 MME, resulting in rod-like crystals with maximum dimensions of 20 × 20 × 200  $\mu$ m. Crystals were soaked in cryoprotective buffer [the crystallization condition plus an additional 10% (v/v) PEG 2000 MME and 10 mM LDAO] and flash-cooled in liquid nitrogen. A data set was collected from a single crystal on ESRF beamline ID23-eh2. The data set was processed using the XDS package (Kabsch, 2010b) and scaled with XSCALE (Kabsch, 2010a).

## 3. Results

The recombinant autotransporter protein FP-HisN163 carrying the transport unit of the monomeric autotransporter AIDA-I was expressed in *E. coli* UT5600 (DE3). Since FP-HisN163 is embedded in the outer membrane a suitable detergent had to be found for solubilization, for which a screen was performed using membrane fractions and different detergents at a final concentration of 1% (v/v) (see §2.2). Of all of the detergents tested, LDAO showed the highest solubilization efficiency. LDAO is likewise the detergent that was used for the solubilization and crystallization of other membrane proteins (Camara-Artigas *et al.*, 2002; Yue *et al.*, 2003; van den Berg *et al.*, 2004). Thus, LDAO was used in all subsequent purification steps. FP-HisN163 was first isolated using IMAC (see §2.3; data not shown). As a second purification step SEC was performed with the concentrated fractions of the elution peak resulting from IMAC (see §2.3; data not shown). The pooled fractions were concentrated to a final concentration of between 7 and 28 mg ml<sup>-1</sup>.

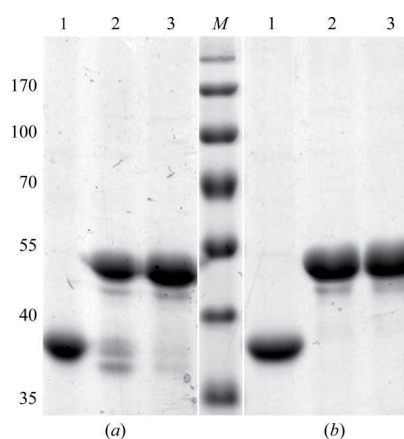


**Figure 1**  
Denaturation analysis of purified FP-HisN163 by Coomassie-stained SDS-PAGE. (a) SDS sample buffer with 3.2% (w/v) SDS (lanes 1–3). (b) SDS sample buffer with 6.4% (w/v) SDS (lanes 1–3). Lane M, PageRuler Prestained Protein Ladder (Fermentas; labelled in kDa on the left); lane 1, not heated; lane 2, heated for 5 min; lane 3, heated for 10 min. The samples were heated to 373 K.

## crystallization communications

**Table 1**

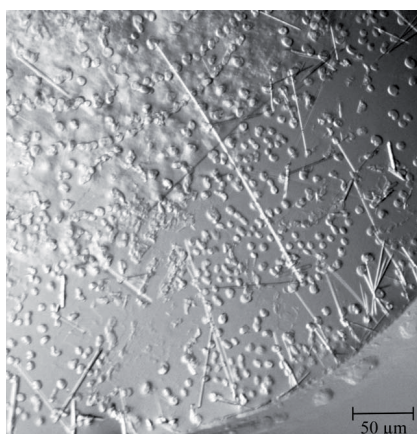
Data-collection statistics.

Values in parentheses are for the outermost resolution shell.

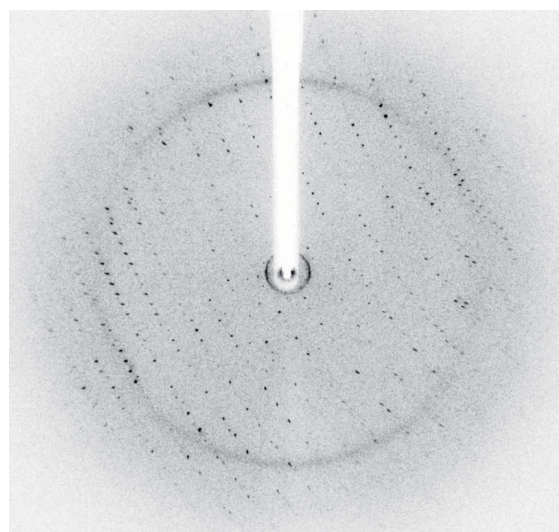
No. of crystals	1
Beamline	ID23-eh2, ESRF
Temperature (K)	100
Wavelength (Å)	0.8726
Detector	MAR Mosaic 225 mm
Crystal-to-detector distance (mm)	375.71
Rotation range per image (°)	1.35
Total rotation range (°)	108
Exposure time per image (s)	2.168
Resolution range (Å)	50–3.15 (3.20–3.15)
Space group	$P2_12_12_1$ or $P2_12_12_1$
Unit-cell parameters	
$a$ (Å)	40.33
$b$ (Å)	85.85
$c$ (Å)	134.05
$\alpha = \beta = \gamma$ (°)	90
Mosaicity (°)	0.78
Total No. of measured intensities	36648 (1606)
Unique reflections	7899 (348)
Multiplicity	4.64 (4.61)
Completeness (%)	92.3 (94.3)
$R_{\text{meas}}$ † (%)	9.5 (49.7)
$R_{\text{p.i.m.}}$ ‡ (%)	4.0 (18.2)
$\langle I/\sigma(I) \rangle$	15.38 (3.34)
Overall $B$ factor from Wilson plot (Å <sup>2</sup> )	48.29

†  $R_{\text{meas}} = \sum_{hkl} \{N(hkl)/[N(hkl) - 1]\}^{1/2} \sum_i |I_i(hkl) - \langle I(hkl) \rangle| / \sum_{hkl} \sum_i I_i(hkl)$ .  
 ‡  $R_{\text{p.i.m.}} = \sum_{hkl} \{1/[N(hkl) - 1]\}^{1/2} \sum_i |I_i(hkl) - \langle I(hkl) \rangle| / \sum_{hkl} \sum_i I_i(hkl)$ .

It is known that outer membrane proteins are very stable at room temperature even upon addition of SDS and show abnormal migration behaviour during SDS–PAGE analysis owing to their compact folding (de Cock *et al.*, 1996; Sugawara *et al.*, 1996; Maurer *et al.*, 1999). When analyzing the sample by SDS–PAGE, FP-HisN163 migrates at a lower molecular mass than expected (Fig. 1). The different sample buffers *A* and *B* were added to aliquots of purified FP-HisN163 and then heated at 373 K for different time periods (see §2.4). The non-heated protein was detected at a molecular weight of 39 kDa independently of the applied sample buffer (Fig. 1, lane 1). After 5 min of heating at 373 K in sample buffer *A* three bands were observed at molecular weights of 50, 39 and 37 kDa (Fig. 1*a*, lane 2). The protein bands at 37 and 39 kDa disappeared with increased heating time in sample buffer *A* and were identified as denaturation artifacts. These protein bands were not detected using sample buffer

**Figure 2**

Needle crystals of FP-HisN163 with dimensions of 20 × 20 × 200 μm.

**Figure 3**

Diffraction image collected with a rotation width of 1.35°.

*B* even at the shortest heating time (Fig. 1*b*, lane 2). Therefore, for all other samples and SDS–PAGE analysis buffer *B* and a short heating procedure were used.

Crystals grew in various crystallization conditions using the hanging-drop vapour-diffusion method (see §2.5). Well diffracting crystals were obtained after 40 d at 291 K in 100 mM sodium cacodylate pH 6.5, 27.5% (v/v) PEG 2000 MME (Fig. 2). Crystals were transferred into cryobuffer, flash-cooled and a native data set was collected. The crystals diffracted to a resolution of 3.15 Å (Table 1; Fig. 3).

Preliminary processing of the data set using the *XDS* package and self-rotation analysis using the data processed in *P1* revealed that the crystals belonged to a primitive orthorhombic space group with unit-cell parameters  $a = 40.33$ ,  $b = 85.85$ ,  $c = 134.05$  Å. At present we cannot distinguish between space group  $P2_12_12_1$  and  $P2_12_12_1$ , since the systematic absences observed are not conclusive (see Table 1 for data statistics). The unit-cell content analysis suggests the presence of one monomer (50.10 kDa) in the asymmetric unit with a  $V_M$  value of  $2.32 \text{ Å}^3 \text{ Da}^{-1}$  and a solvent content of 47% (v/v) (Matthews, 1968). Structure determination is currently in progress.

We thank the staff of ESRF beamline ID23-eh2 and the EMBL Hamburg staff for support and assistance during crystal screening and data collection. We also gratefully acknowledge support (and training) from the International NRW Research School BioStruct granted by the Ministry of Innovation, Science and Research of the State North Rhine-Westphalia, Heinrich-Heine-University Düsseldorf and the Entrepreneur Foundation at Heinrich-Heine-University Düsseldorf.

## References

- Benz, I. & Schmidt, M. A. (1989). *Infect. Immun.* **57**, 1506–1511.  
 Berg, B. van den, Black, P. N., Clemons, W. M. Jr & Rapoport, T. A. (2004). *Science*, **304**, 1506–1509.  
 Bernstein, H. D. (2007). *Trends Microbiol.* **15**, 441–447.  
 Camara-Artigas, A., Brune, D. & Allen, J. P. (2002). *Proc. Natl Acad. Sci. USA*, **99**, 11055–11060.

## crystallization communications

- Cock, H. de, van Blokland, S. & Tommassen, J. (1996). *J. Biol. Chem.* **271**, 12885–12890.
- Henderson, I. R., Navarro-Garcia, F., Desvaux, M., Fernandez, R. C. & Ala'Aldeen, D. (2004). *Microbiol. Mol. Biol. Rev.* **68**, 692–744.
- Ieva, R., Tian, P., Peterson, J. H. & Bernstein, H. D. (2011). *Proc. Natl Acad. Sci. USA*, **108**, E383–E391.
- Jose, J. (2006). *Appl. Microbiol. Biotechnol.* **69**, 607–614.
- Jose, J. & Meyer, T. F. (2007). *Microbiol. Mol. Biol. Rev.* **71**, 600–619.
- Kabsch, W. (2010a). *Acta Cryst. D* **66**, 133–144.
- Kabsch, W. (2010b). *Acta Cryst. D* **66**, 125–132.
- Leo, J. C., Grin, I. & Linke, D. (2012). *Philos. Trans. R. Soc. Lond. B Biol. Sci.* **367**, 1088–1101.
- Matthews, B. W. (1968). *J. Mol. Biol.* **33**, 491–497.
- Maurer, J., Jose, J. & Meyer, T. F. (1997). *J. Bacteriol.* **179**, 794–804.
- Maurer, J., Jose, J. & Meyer, T. F. (1999). *J. Bacteriol.* **181**, 7014–7020.
- Pavlova, O., Peterson, J. H., Ieva, R. & Bernstein, H. D. (2013). *Proc. Natl Acad. Sci. USA*, **110**, E938–E947.
- Pohlner, J., Halter, R., Beyreuther, K. & Meyer, T. F. (1987). *Nature (London)*, **325**, 458–462.
- Shahid, S. A., Bardiaux, B., Franks, W. T., Krabben, L., Habeck, M., van Rossum, B. J. & Linke, D. (2012). *Nature Methods*, **9**, 1212–1217.
- Sugawara, E., Steiert, M., Rouhani, S. & Nikaido, H. (1996). *J. Bacteriol.* **178**, 6067–6069.
- Yue, W. W., Grizot, S. & Buchanan, S. K. (2003). *J. Mol. Biol.* **332**, 353–368.



## Supplementary Material

### S2.1 Cloning of FP-HisN163

The plasmid pET-SH3, which encodes the transport unit of AIDA-I and a PEYFK epitope as passenger domain for immunodetection (Jose and Handel, 2003), was digested with the restriction enzymes *Nde*I and *Bgl*II and fused with a synthetic oligonucleotide:



As a result, a six-fold histidine tag was introduced at the N-terminus downstream of the signal peptide gaining the plasmid pIG101. Subsequently, the sequence encoding FP-HisN163 was cloned into the plasmid pJM007 (Maurer et al., 1997) using the restriction sites *Nde*I and *Bam*HI, which results in the plasmid pIG501. The expression was controlled by the constitutive  $T_K$  promoter.

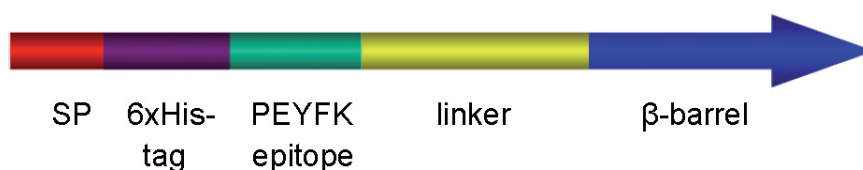


**Figure S1 Schematic representation of FP-HisN163**

SP: signal peptide; His: histidine

### S2.2 Detergent screen

The detergent screen includes the following detergents, each at a final concentration of 1 % (v/v):

n-Dodecyl β-D-maltoside (DDM), n-Decyl β-D-maltoside (DM), Fos-Choline 14, N,N-Dimethyldodecylamine N-oxide (LDAO), FOS-MEA12, NP 40, 3-[(3-cholamidopropyl) dimethylammonio]-1-propanesulfonate (CHAPSO) and n-Tridecyl β-D-maltoside (TDM).



AIDA-I	NKAYSIIWHSRQAWIVASELARGHGFVLAKNTLLVLAVVSTIGNAFVAVNISGTVSSGG 60
FP-HisN163	-----
AIDA-I	TVSSGETQIVYSGRGNSNATVNSGGTQIVNNGGKTTATTVNSSGSQNVGTSGATISTIVN 120
FP-HisN163	-----
AIDA-I	SGGIQRVSSGGVASATNLSGGAQNIYNLGHASNTVIFSGGNQTFISGGITDSTNISSGGQ 180
FP-HisN163	-----
AIDA-I	QRVSSGGVASNTTINSSGAQNILSEEGAISTHISSGGNQYISAGANATETIVNSGGFQRV 240
FP-HisN163	-----
AIDA-I	NSGAVATGTVLSGGTQNVSSGSAISTSVYNSGVQTVFAGATVTDTTVNSGGNQNISSGG 300
FP-HisN163	-----
AIDA-I	IVSETTVNVSGTQNIYSGGSALSANIKGSQIVNSEGTAINTLVSDGGYQHIRNGGIASGT 360
FP-HisN163	-----
AIDA-I	IVNQSGYVNISGGYAESTIINSGGTLRVLSDG YARGTILNNSGRENVSNGGVSYNAMIN 420
FP-HisN163	-----
AIDA-I	TGGNQYIYSDGEATAAIVNTSGFQRINSGGTAPVQNSVVVTRTVSSAAKPFDAEVYSGGK 480
FP-HisN163	-----
AIDA-I	QTVYLWRGIWYSNFLTAVWSMFPGTASGANVNLSGRLNAFAGNVVGTILNQEGRQYVYSG 540
FP-HisN163	-----
AIDA-I	ATATSTVGNNEGREYVLSGGITDGTVLNSGGLQAVSSGGKASATVINEGGAQFVYDGGQV 600
FP-HisN163	-----
AIDA-I	TGTNIKNGGTIRVDSGASALNIALSSGCNLTSTGATLPELTMAALSVSQNHASNVILE 660
FP-HisN163	-----
AIDA-I	NGGLLRVTSGGTATDTTVNSAGRLRIDGGGTINGTTTINADGIVAGTNIQNDGNFILNLA 720
FP-HisN163	-----
AIDA-I	ENYDFETELSGSGVLVKDNTGIMTYAGTLTQAQGVNVKNGGIIFDSAVVNADMAVNQNAY 780
FP-HisN163	-----
AIDA-I	INISDQATINGSVNNNGSIVINNSIINGNITNDADLSFGTAKLLSATVNGSLVNKNIIA 840
FP-HisN163	-----HHHHHHSRRSPEYFKGPPSPRSLNPTKESA 30
	.. * :.: :... : * : *
AIDA-I	GNTLTVSNYTGTPGSVISLGGVLEGDSLTDRLVVKGNTSGQSDIVYVNEGDGSGGQTRDG 900
FP-HisN163	GNTLTVSNYTGTPGSVISLGGVLEGDSLTDRLVVKGNTSGQSDIVYVNEGDGSGGQTRDG 90
	*****
AIDA-I	INIISVEGNSDAEFSCLKNRVVAGAYDYTLQKGNESGTDNKGWYLTSHLPTSDTRQYRPEN 960
FP-HisN163	INIISVEGNSDAEFSCLKNRVVAGAYDYTLQKGNESGTDNKGWYLTSHLPTSDTRQYRPEN 150
	*****
AIDA-I	GSYATNMALANSLFLMDLNERKQFRAMSDNTQPESASVWMKITGGISSGKLNDGQNKTTT 1020
FP-HisN163	GSYATNMTLANSLFLMDLNERKQFRAMSDNTQPESASVWMRITGGRSSGKLNDGQNKTTT 210
	*****:*****
AIDA-I	NQFINQLGGDIYKFHAEQLGDFTLGMGGYANAKGKTINYTSNKAARNTLDGYSVG VYGT 1080
FP-HisN163	NQFINQLGGDIYKFHAEQLGDFTLGMGGYANAKGKTINYTSNKAARNTLDGYSVG VYGT 270
	*****
AIDA-I	WYQNGENATGLFAETWMQYNWFNASVKGDGLEEEKYNLNLGTASAGGGYNLNVHTWTSPE 1140
FP-HisN163	WYQNGENATGLFAETWMQYNWFNASVKGDGLEEEKYNLNLGTASAGGGYNLNVHTWTSPE 330
	*****
AIDA-I	GITGEFWLQPHLQAVWMGVTPDTHQEDNGTVVQGAGKNNIQT KAGIRASWKVKSTL DKDT 1200
FP-HisN163	GITGEFWLQPHLQAVWMGVTPDTHQEDNGTVVQGAGKNNIQT KAGIRASWKVKSTL DKDT 390
	*****
AIDA-I	GRRFRPYIEANWIHNTHFGVKMSDDSQLLSGSRNQGEIKTGIEGVITQNL SVNGGVAYQ 1260
FP-HisN163	GREFSPYIEANWIHNTHFGVKMSDDSQLLSGSRNQGEIKTGIEGVITQNL SVNGGVAYQ 450
	** * *****
AIDA-I	AGGHGSNAISGALGIKYSF 1279
FP-HisN163	AGGHGSNAISGALGIKYSF 469
	.....

Figure S2 Alignment of AIDA-I (Uniprot code Q03155) and FP-HisN163

## References

- Jose, J. & Handel, S. (2003). *ChemBiochem*, 4: 396-405.  
Maurer, J., Jose, J. & Meyer, T. F. (1997). *J Bacteriol*, 179: 794-804.

## Chapter IV

### **Crystal structure of the transport unit of the autotransporter AIDA-I from *Escherichia coli* in a post translocation state**

Published in: *Structure (to be submitted)*

Impact factor: 6.347

Own proportion to this work: 60 %

Cloning and expression in *E. coli*

Protease accessibility assays

Preparation of membranes and solubilization of AIDA-I

Immobilized metal ion and size exclusion chromatography

Crystallization and X-ray diffraction experiments

Structure determination of the transport unit of AIDA-I

Writing of the manuscript

**Crystal structure of the transport unit of the autotransporter AIDA-I  
from *Escherichia coli* in a post translocation state**

**Iris Gawarzewski<sup>1,3</sup>, Frank DiMaio<sup>2</sup>, Elisa Winterer<sup>3</sup>, Britta  
Tschapek<sup>1</sup>, Sander H.J. Smits<sup>1</sup>, Joachim Jose<sup>3</sup> and Lutz Schmitt<sup>1#</sup>**

<sup>1</sup> Institute of Biochemistry, Heinrich-Heine University Düsseldorf, Germany

<sup>2</sup> Department of Biochemistry and HHMI, University of Washington, Seattle, USA

<sup>3</sup> Institute of Pharmaceutical and Medicinal Chemistry, PharmaCampus, Westphalian  
Wilhelms-University Münster, Germany

# Corresponding address:

Lutz Schmitt

Institute of Biochemistry, Heinrich-Heine University Düsseldorf, Universitätsstr. 1, D-40225  
Düsseldorf, Germany

Phone: +49-211-81-10773

Fax: +49-211-81-15310

Email address: lutz.schmitt@hhu.de

---

**Abstract:** Several serious gastrointestinal diseases, which are widespread all over the world, are caused by enteropathogenic *Escherichia coli*. The monomeric autotransporter AIDA-I (*adhesin involved in diffuse adherence*) represents an important virulence factor of those strains and is involved in adhesion, biofilm formation, aggregation and invasion into host cells. Here, we present the crystal structure of the transport unit of AIDA-I at 3.0 Å resolution, which forms a 12-stranded  $\beta$ -barrel harboring the linker domain in its pore. Mutagenesis studies of the C-terminal amino acid demonstrated the great impact of this terminal residue on membrane integration of AIDA-I and passenger translocation.

**Keywords:** AIDA-I, autotransporter, outer membrane (OM), type V secretion

## Introduction

Many diarrheagenic diseases, especially among livestock and infants in third world countries, are caused by Gram-negative enteropathogenic *Escherichia coli* (EPEC) strains (Nataro and Kaper, 1998; Ngeleka *et al.*, 2003). The *adhesin involved in diffuse adherence* (AIDA-I) glycoprotein, which was initially discovered in a patient suffering from infantile diarrhea (Benz and Schmidt, 1989), is an important virulence factor of EPEC strains that mediates auto-aggregation, biofilm formation, adhesion and invasion into host cells (Charbonneau *et al.*, 2006; Charbonneau and Mourez, 2007). AIDA-I was assigned as monomeric autotransporters (AT), which belong to the type V secretion systems (T5SS) (Leo *et al.*, 2012; Gawarzewski *et al.*, 2013a). Like all monomeric AT, preAIDA-I consists of different functional domains (see supplementary information, Figure S1A): (I) an N-terminal signal peptide for Sec-dependent transport across the inner membrane (IM), (II) a passenger ( $\alpha$ -) domain harboring biological activity in the extracellular space, (III) a linker domain and (IV) a  $\beta_2$ -domain, which is predicted to form a  $\beta$ -barrel in the outer membrane (OM) (Jose *et al.*, 1995; Maurer *et al.*, 1997; Henderson *et al.*, 2004; Jose, 2006; Leyton *et al.*, 2012). Additionally, AIDA-I contains an autochaperone (AC) domain termed  $\beta_1$ -domain, which is located at the C-terminus of the  $\alpha$ -domain (Maurer *et al.*, 1997; Konieczny *et al.*, 2001; Benz and Schmidt, 2011). PreAIDA-I is translated as a 132 kDa protein comprising 1286 amino acids (Benz and Schmidt, 1992). After Sec-dependent transport across the IM, the signal peptide (amino acids 1-49) is cleaved off and proAIDA-I is released into the periplasm. Here, the  $\alpha$ -domain of proAIDA-I is glycosylated by the *autotransporter adhesin heptosyl-transferase* (Aah) (Benz and Schmidt, 2001; Charbonneau *et al.*, 2007). The  $\beta_2$ -domain of proAIDA-I is integrated into the OM, while the  $\alpha$ -domain is translocated. Finally, proAIDA-I is auto-proteolytic cleaved at the cell surface to form (I) the 100 kDa mature AIDA-I and (II) the

47.5 kDa AIDA<sub>C</sub>, which remains membrane associated (see supplementary information, Figure S1A) (Benz and Schmidt, 1992; Suhr *et al.*, 1996). Mature AIDA-I mediates adhesion, biofilm formation, aggregation and invasion into host cells (Charbonneau *et al.*, 2006; Charbonneau and Mourez, 2007).

Despite the huge variety of  $\alpha$ -domains among monomeric AT, the transport unit displays a high structural similarity as observed by the structures of NalP, EspP, EstA, BrkA (Oomen *et al.*, 2004; Barnard *et al.*, 2007; van den Berg, 2010; Zhai *et al.*, 2011) and Hbp (PDB code 3AEH). Based on crosslinking experiments, mutational analysis and protease accessibility assays with the monomeric AT EspP, a secretion model was proposed (Ieva *et al.*, 2008; Ieva *et al.*, 2011; Pavlova *et al.*, 2013), which is a combination of the hairpin and the BamA model (Voulhoux *et al.*, 2003; Henderson *et al.*, 2004). This model suggests that the AT adopts a stable conformation in the periplasm by interaction with chaperones forming a partly folded  $\beta$ -barrel with a hairpin-like linker domain in the pore. BamA, also termed Omp85, subsequently integrates this incomplete folded  $\beta$ -barrel into the OM, thereby supporting the translocation of the  $\alpha$ -domain to the cell surface.

Most members of monomeric AT, which are assigned to the subgroup 'a' of T5SS, are involved in virulence processes. Thus, the underlying mechanisms of processing as well as the translocation across the outer membrane are important aspects of pathogenesis. Here, we present the crystal structure of the transport unit AIDA-I-linker- $\beta_2$  at 3.0 Å. Structural analysis revealed a 12-stranded  $\beta$ -barrel with the linker domain accommodated in its hydrophilic pore. Mutagenesis studies proved the impact of the C-terminal amino acid as part of the signature sequence on membrane integration.



---

## Results

We used a truncated version of AIDA-I. The native linker and the  $\beta_2$ -domain of AIDA-I, called AIDA-I-linker- $\beta_2$ , were fused to the C-terminus of the  $\alpha$ -domain carrying a His-tag for purification. For immunodetection, an artificial epitope was inserted at the N-terminus. This recombinant protein was termed FP-HisN163 (see experimental procedures and supplementary information, Figure S1B) (Gawarzewski *et al.*, 2013b). OM localization and surface-exposure of the recombinant  $\alpha$ -domain were confirmed by outer membrane protein (OMP) isolation, proteinase K treatment and immunodetection (see supplementary information, Figure S2).

### ***Purification and determination of the oligomeric state, monodispersity and homogeneity of FP-HisN163***

After constitutive expression, FP-HisN163 was solubilized with n-dodecyl-N,N-dimethylamine-N-oxide (LDAO) and purified using immobilized metal ion affinity chromatography (IMAC) and size exclusion chromatography (SEC) (see experimental procedures) resulting in a highly pure protein sample (Figure 1A). SEC-MALS analysis (size exclusion chromatography coupled to multi-angle light scattering detection) was performed to determine the oligomeric state and monodispersity (Figure 1B). The normalized elution profiles from the UV (blue line), refractive index (black line) and light scattering detectors (red line) revealed one symmetric peak indicating that the protein solution was homogeneous and monodisperse. After determining protein concentration and refractive index, a molecular mass of the protein-detergent complex of  $88.5 \pm 2.4$  kDa was obtained (Figure 1B, violet line). The determined molecular mass of FP-HisN163 ( $49.9 \pm 3.0$  kDa) corresponds well with the theoretical molecular mass of 50.9 kDa for a monomer of FP-

HisN163 (Figure 1B, orange line), while a detergent micelle of  $38.6 \pm 1.0$  kDa (Figure 1B, green line) surrounded AIDA-I.

### ***Overall structure of the transport unit AIDA-I-linker- $\beta_2$***

The purified FP-HisN163 carrying the transport unit AIDA-I-linker- $\beta_2$  was crystallized in a condition containing 0.1 M sodium cacodylate, pH 6.5 and 27.5 % PEG 2000 MME (Gawarzewski *et al.*, 2013b) by hanging drop vapor diffusion. To obtain initial phases, the ROSETTA Molecular Replacement program (DiMaio *et al.*, 2011) was used, with the monomeric autotransporter EspP(N1023S) (PDB code: 3SLT) from *Escherichia coli* as search model (see experimental procedures). The initial structure of AIDA-I-linker- $\beta_2$  was manually corrected using COOT (Emsley *et al.*, 2010) and refined with REFMAC5 (Murshudov *et al.*, 1997; Murshudov *et al.*, 2011) resulting in a  $R_{work}$  of 24.8 % and a  $R_{free}$  of 30.7 % (Table 1). The overall structure of AIDA-I-linker- $\beta_2$  (residues Q962-F1286) represents a 12-stranded antiparallel  $\beta$ -barrel (Figure 2A, highlighted in green) with the linker domain located inside the translocation pore (Figure 2A, highlighted in red). The  $\beta$ -barrel of AIDA-I displays dimensions of approximately 60 Å in height and 30 Å in width with an ellipsoid-shaped pore of  $\approx 20$  Å in diameter. The shortest  $\beta$ -strand (S12) comprises 12 and the longest  $\beta$ -strand (S6) 24 amino acids. Periplasmic turns (T1-T6) and extracellular loops (L1-L6) of various lengths connect the  $\beta$ -strands (see supplementary information, Figure S3). The shear number of the  $\beta$ -barrel is 14 (Schulz, 2002) and the  $\beta$ -strands are tilted at an angle of approximately  $45^\circ$  to the barrel axis. In L4 and L5, short antiparallel  $\beta$ -strands form  $\beta$ -sheets, which protrude into the extracellular space. Likely due to their flexibility, turns T1, T4 and T5 are not resolved in the structure (indicated by an asterisk in Figure 2A). The interior of the  $\beta$ -barrel is occupied by the linker domain (Q962-Q990, Figure 2A, highlighted in red). The N-terminal part forms

an  $\alpha$ -helix (P965-L980), which is slightly twisted and projects into the extracellular space. The remainder of the linker domain (F981-Q990) traverses the pore in an unstructured manner. The linker domain is shifted to the right side of the pore when viewed from the extracellular space and stabilized by several polar interactions.

### ***Comparison with the transport units of other monomeric autotransporter***

During the last decade, several structures of monomeric AT transport units were determined including EspP, NalP, BrkA, EstA (Oomen *et al.*, 2004; Barnard *et al.*, 2007; van den Berg, 2010; Zhai *et al.*, 2011) and Hbp (PDB code: 3AEH). On the sequence level, the amino acid sequence identity between AIDA-I-linker- $\beta_2$  and transport units of the above mentioned monomeric AT is moderate (< 34%). Nevertheless, they share an overall structural similarity with the structure of AIDA-I-linker- $\beta_2$  reflected by the root mean square deviation (RMSD) of the C $\alpha$  atoms after superimposition of the structures (Table 2).

### ***After translocation the extracellular loop 5 resides in an 'open' conformation***

In AIDA-I-linker- $\beta_2$ , the extracellular loop 5 (L5) contains a short  $\beta$ -sheet, which protrudes into the extracellular space adopting an 'open' conformation (Figure 2B, highlighted in blue). The region around L5 is part of crystal contacts but it is likely that it adopts its native conformation as observed in EstA, where L5 is not involved in crystal contact but folds into an 'open' conformation. Interestingly, L5 adopts a similar 'open' conformation in mutated EspP(N1023S)- $\beta$ , whereas in the wild type protein L5 forms a plug from the extracellular side, which stabilizes the pore in a 'closed' conformation (Figure S4, highlighted in blue) and which is due to the presence in one case or absence of the linker domain in the other case of both EspP structures. The role of L5 in  $\alpha$ -domain translocation, cleavage and  $\beta$ -barrel

stability was examined by deletion mutants and thermostability assays (Barnard *et al.*, 2007; Barnard *et al.*, 2012). After deletion of L5 in EspP- $\beta$ , no significant effect on translocation, cleavage or thermostability was observed. In contrast, denaturation analysis of EspP(N1023S)- $\beta$  revealed a significant decrease in temperature stability compared to EspP- $\beta$ . The thermostability of AIDA-I-linker- $\beta_2$  is comparable to that of EspP- $\beta$  (data not shown). Thus, the linker domain of AIDA-I-linker- $\beta_2$  is supposed to perform a sealing function as well, which, in case the linker domain is not present, is mediated by L5 closing the  $\beta$ -barrel to prevent leakage across the OM.

### ***Conservation of essential amino acids between monomeric AT***

A structural alignment between AIDA-I-linker- $\beta_2$  and EspP- $\beta$  revealed 37 identical amino acids at similar positions in the spatial arrangement (see Table S1). Ten of them were characterized for EspP by mutational, crosslinking experiments or bioinformatic comparison with other ATs (Figure 3A, supplementary information Figure S5, highlighted in orange) (Barnard *et al.*, 2007; Ieva *et al.*, 2008; Ieva *et al.*, 2011; Barnard *et al.*, 2012; Pavlova *et al.*, 2013). The results for EspP- $\beta$  indicate that the conserved amino acids are involved in folding and interaction with periplasmic chaperones such as Skp and SurA, lipopolysaccharides (LPS) and BamA, the most important component of the  $\beta$ -barrel assembly machinery (BAM) complex (Wu *et al.*, 2005; Noinaj *et al.*, 2013). Strikingly, all analyzed amino acids are located at similar structural positions in AIDA-I-linker- $\beta_2$  suggesting a similar role in AIDA-I.

The C-terminal phenylalanine (F1286) of the  $\beta$ -barrel of AIDA-I (Figure 3A, highlighted orange) is part of the consensus signature sequence comprising the last 18 amino acids of the  $\beta$ -barrel (G1269-GHGSNAISGALGIKYS-F1286) (Figure 3B, highlighted in black). In ATs, this signature sequence is generally composed of 5-18 amino acids (Gawarzewski *et al.*, 2013a)

and recognized by BamA, which is involved in the insertion of  $\beta$ -barrels in the OM (Struyvé *et al.*, 1991; Hendrixson *et al.*, 1997; Tommassen, 2010). For AIDA-I-linker- $\beta_2$  mutational analyses were conducted to investigate the influence of F1286 on translocation efficiency and membrane integration. F1286 was substituted by different amino acids or deleted (see experimental procedures in supplementary information) resulting in the mutant autotransporter proteins F1286W, F1286Y, F1286H, F1286V and F1286 $\Delta$ . Deletion of the C-terminal phenylalanine was confirmed by mass spectrometry (data not shown). All mutant proteins were expressed in *E. coli* UT5600 (DE3) (see experimental procedures in supplementary information), which lacks the OM protease OmpT (Jose and Handel, 2003). Fluorescence-activated cell sorting (FACS) was performed to confirm the orientation of the mutant autotransporter proteins in the OM (see experimental procedures in supplementary information). Compared to the negative control, the wild type AT showed an eleven-fold increase of fluorescence (Figure 4A). For the mutant AT F1286W, F1286Y and F1286H a seven- to nine-fold increase of fluorescence could be detected. F1286V showed only a three-fold increase of fluorescence, whereas the fluorescence of the deletion mutant F1286 $\Delta$  was in the same range as the fluorescence of the negative control (Figure 4A). These results demonstrated that the  $\alpha$ -domains of the mutant AT F1286W, F1286Y, F1286H and F1286V were facing the extracellular side. The translocation efficacy of F1286V was only 50 % compared to the other mutants. The  $\alpha$ -domain of F1286 $\Delta$  was not detectable at the cell surface. As an additional analysis, the presence of AIDA-I in the outer membrane was tested for each mutant by Western Blot analysis and immunodetection using an antibody against the N-terminal artificial epitope (see experimental procedures in supplementary information). The intensity of the band of the mutants carrying a tryptophan, tyrosine or histidine at the C-terminus was comparable to that of the wild-type protein (Figure 4B, wild

type, F1286W, F1286Y and F1286H). The amount was significantly decreased in F1286V and not detectable in F1286 $\Delta$  (Figure 4B). These findings suggest that the aromatic nature of the C-terminal amino acid directly influenced integration of the AT into the OM. Loss of aromaticity (F1286V) led to a decreased amount of the mutant autotransporter. When the aromatic and the hydrophobic nature of the C-terminal amino acid were removed, the transport unit of AIDA-I was not correctly integrated in the OM (Figure 4B). Thus, the results of the FACS analysis (Figure 4A) were confirmed by the results of immunodetection (Figure 4B). In summary, the membrane integration and translocation efficacy of AIDA-I-linker- $\beta_2$  strongly depends on the properties of the C-terminal amino acid.

The C-terminal phenylalanine of AIDA-I-linker- $\beta_2$  is not part of a  $\beta$ -sheet but protrudes into the periplasm (Figure 3A, highlighted in orange). This is also the case for EstA- $\beta$  and BrkA- $\beta$  (van den Berg, 2010; Zhai *et al.*, 2011). These findings strongly suggest that the hydrophobicity of the C-terminal phenylalanine is not necessary for insertion into the OM. It is more likely that the interaction with BamA requires a certain degree of hydrophobicity and aromaticity, which triggers subsequent integration of the  $\beta$ -barrels in the OM.

***A charged cluster at the extracellular side of AIDA-I-linker- $\beta_2$  might serve as a binding platform for the  $\beta_1$ -domain***

In 1996, Suhr *et al.* investigated the processing of AIDA-I after translocation across the OM. They demonstrated that AIDA<sub>C</sub> remained attached to the OM after auto-cleavage of mature AIDA-I. Protease accessibility assays with externally added TPCK-trypsin and TLCK-chymotrypsin revealed that the cleavage sites in the N-terminal domain of AIDA<sub>C</sub> were only accessible if mature AIDA-I was removed by mild heat treatment after translocation and auto-cleavage (Suhr *et al.*, 1996). These results indicated that mature AIDA-I remained



attached to AIDA<sub>C</sub>, which functions as an anchor site, thereby rendering the cleavage sites inaccessible to exogenous proteases.

In the light of these results, we analyzed the electrostatic surface of AIDA-I-linker- $\beta_2$  to discover potential binding sites. The electrostatic potential of the exterior of the  $\beta$ -barrel (Figure 5) revealed a hydrophobic belt with a width of approximately 30 Å, which matches the hydrophobic part of the OM (White *et al.*, 2001). Additionally, positively (blue) and negatively (red) charged cluster were detected at the extracellular side of the  $\beta$ -barrel (Figure 5). These might serve as a binding platform for AIDA-I domains after cleavage.

To analyze if these charged cluster at the extracellular end of the  $\beta$ -barrel provide such a binding platform for the  $\beta_1$ -domain, docking studies were performed with the structure of AIDA-I-linker- $\beta_2$  and a homology model of the  $\beta_1$ -domain, which is based on the autochaperone (AC) structure of IcsA (Kuhnel and Diezmann, 2011) (see experimental procedures). These simulations indicated that the  $\beta_1$ -domain was placed on a charged cluster, which is composed of the extracellular part of S1-S4 and the connecting loops L1 and L2 forming a specific charged pattern for binding (Figure S6). The positioning is reasonable, because in the AIDA-I primary structure only five amino acids are located between the  $\beta_1$ - and the linker domain and the distance of these ends in our model is in a range, which can be exactly bridged by a stretch of five amino acids (Figure S6B, dotted line). In this hypothetical model, the cleavage sites of TPCK-trypsin and TLCK-chymotrypsin would be covered by the  $\beta_1$ -domain (Figure S6B; the cleavage sites are highlighted by an arrow) and would explain the results of the protease accessibility assays (Suhr *et al.*, 1996). Thus, our interaction simulations imply that, after auto-proteolytic cleavage of the  $\alpha$ -domain, AIDA<sub>C</sub> undergoes a conformational change while the  $\beta_1$ -domain remains attached to the charged cluster at the extracellular side.

---

***Polar interactions between  $\beta$ -sheets of AIDA-I-linker- $\beta_2$*** 

Integral membrane proteins, which contain  $\beta$ -barrels, are known to be very stable and unfold only under harsh denaturing conditions and/or higher temperatures (Mogensen *et al.*, 2005a; Mogensen *et al.*, 2005b). This thermostability is due to the high number of polar interactions within the  $\beta$ -barrel. An analysis of AIDA-I-linker- $\beta_2$  indicates that a stable core can be defined within the  $\beta$ -barrel ranging from S2-S10 (see supplementary information, Table S2 red box and Figure 6A, highlighted in green). The number of polar interactions in this stable core region is significantly higher than between the remaining strands forming the flexible region (Figure 6A, highlighted in light magenta and purple and supplementary information Table S2 green box). Strikingly, the long extracellular loop 5 and the longest periplasmic turn 5 connect S8-S10 (see supplementary information Figure S3), which are presumably able to undergo large conformational changes during the secretion process across the OM. These observations are also true for several other monomeric AT (see supplementary information, Table S2).

**Discussion*****Overall structure of AIDA-I-linker- $\beta_2$*** 

Several hypothetical topology models for the transport unit of AIDA-I were proposed. The  $\beta$ -barrel was predicted to consist of 14 or 15 anti-parallel and amphipathic  $\beta$ -strands, which are connected by short periplasmic turns and longer extracellular loops (Jose *et al.*, 1995; Suhr *et al.*, 1996; Loveless and Saier, 1997; Maurer *et al.*, 1997). By deletion experiments, Maurer *et al.* (1999) could show that all of the 14 predicted  $\beta$ -strands were necessary for correct outer membrane integration of the transport unit (Maurer *et al.*, 1999). The hydrophilic pore was assumed to be occupied by the linker domain, which probably forms an

$\alpha$ -helix. In contrast to these topology models, our crystal structure demonstrates that the transport unit of AIDA-I adopts a 12-stranded  $\beta$ -barrel, which is typical for monomeric ATs (Figure 2A). The disagreement of the number of strands forming the  $\beta$ -barrel can be referred to the observation that S7-S10 contain discontinuous  $\beta$ -strands, interrupted by disordered regions (Figure 2A and see supplementary information Figure S3), which led to a different prediction in the topology models. Furthermore, only half of the linker domain traverses the pore in an  $\alpha$ -helical conformation (Figure 2A, highlighted in red). In 1999, Maurer *et al.* determined the minimal linker length that is necessary to translocate subunit B of cholera toxin (CTB), which was used as an  $\alpha$ -domain, across the OM. They could show that CTB was detectable at the cell surface, when the linker domain comprises a minimal stretch of 48 amino acids lacking the  $\beta_1$ -domain. Furthermore, Jose *et al.* (2005) were able to demonstrate effective translocation of the small peptide P15HA with a linker length, which was shortened by 14 amino acids compared to the minimal linker length of Maurer *et al.* (1999). In light of the crystal structure of AIDA-I-linker- $\beta_2$ , it is reasonable that the  $\beta_1$ -domain is not responsible for the translocation across the outer membrane, but for correct folding of the  $\alpha$ -domain at the cell surface. In case of the hemoglobin binding protein (Hbp) from *E. coli*, which also contains an autochaperone (AC) domain and shares a high structural similarity with AIDA-I (Table 2), Soprova *et al.* (2010) demonstrated that this region is required for the initiation of processive folding of the  $\alpha$ -domain at the cell surface (Soprova *et al.*, 2010). Mutations in the AC region led to accumulation of periplasmic intermediates, which were protease-sensible. For BrkA, deletion of the AC domain led to the formation of an unstable passenger domain after translocation (Oliver *et al.*, 2003). Surface-expression of this domain *in trans* reverted this effect indicating an important role in correct passenger

domain folding. In case of AIDA-I, it is likely that the AC region may play the same role in  $\alpha$ -domain folding.

### ***Comparison with the transport units of other monomeric autotransporter***

An analysis and comparison of AIDA-I-linker- $\beta_2$  with other available monomeric AT  $\beta$ -domains revealed a high overall structural similarity (Table 2). The extracellular loop 5 in AIDA-I-linker- $\beta_2$  contains a short  $\beta$ -sheet (Figure 2B, highlighted in blue), which is also found in the cleavage mutant EspP(N1023S) (see supplementary information, Figure S4, highlighted in blue). In both structures, L5 adopts an 'open' conformation projecting into the extracellular space. The comparison of wild-type EspP with EspP(N1023S) provided insights into the rearrangement of the transport unit after translocation and cleavage of the  $\alpha$ -domain. Here, the extracellular loop L5 undergoes drastic conformational changes from an 'open' to a 'closed' state sealing the pore (see supplementary information Figure S4, highlighted in blue). In AIDA-I-linker- $\beta_2$ , the linker domain, which remains in the pore after cleavage of the  $\alpha$ -domain, functions as a plug. This phenomenon was also observed for other monomeric AT, for example EstA, NalP (Oomen *et al.*, 2004; van den Berg, 2010) and Hbp (PDB code: 3AEH). The thermostability for the transport unit of EspP(N1023S) was significantly lower, whereas the transport units of EspP and AIDA-linker- $\beta_2$  revealed a comparable thermostability. Deletion of L5 in EspP demonstrated that it is not crucial for translocation, cleavage or thermostability (Barnard *et al.*, 2007). Furthermore, several amino acids, which play a key role in the biogenesis of EspP, are structurally conserved in AIDA-I-linker- $\beta_2$  (Figure 3A and supplementary information, Figure S5, highlighted in orange). All of the 10 characterized conserved amino acids were oriented in the same manner indicating that they play the same role in the biogenesis of AIDA-I.

We could demonstrate by mutational analysis that OM integration and  $\alpha$ -domain translocation strongly depends on the hydrophobicity and aromaticity of the C-terminal amino acid in the  $\beta_2$ -domain of AIDA-I (Figure 4), which is part of the consensus signature sequence (Figure 3B) recognized by BamA (Struyvé *et al.*, 1991; Tommassen, 2010). Our results confirm the observations from experiments with PhoE, an *E. coli* porin, and Hap, a monomeric AT from *H. influenza* that the properties of C-terminal amino acid has a major impact on membrane integration (Struyvé *et al.*, 1991; Hendrixson *et al.*, 1997; Robert *et al.*, 2006). Additionally, several conserved amino acids of monomeric AT were also present in FhaC (Gawarzewski *et al.*, 2013a), which belongs to the two-partner secretion systems (TPS), the subgroup Vb of T5SS. The  $\beta$ -barrel of FhaC consists of 16  $\beta$ -strands, which result in different dimensions of the transport unit. Nevertheless, the conserved amino acids are positioned in a comparable spatial arrangement as in EspP. These findings indicate a common translocation mechanism not only for monomeric AT but also for all members of T5SS.

***A charged cluster at the extracellular side of AIDA-I-linker- $\beta_2$  might serve as a binding platform for the  $\beta_1$ -domain***

The analysis of the electrostatic surface of AIDA-I-linker- $\beta_2$  revealed a charged cluster at the extracellular side of the  $\beta$ -barrel (Figure 5). Our simulations implied that the  $\beta_1$ -domain might be bound to such a charged cluster (Figure S6).

At first glance, it seems illogical that the  $\alpha$ -domain of AIDA-I, which mediates e.g. adhesion to target cells, is cleaved after translocation across the OM. However, this cleavage allows the  $\beta_1$ -domain to interact with the  $\beta_2$ -domain in a specific conformation (Figure S6). Suhr *et al.* (1996) demonstrated that the cleavage sites, which are located between the  $\beta_1$ - and the

$\beta_2$ -domain, were protected under non-denaturing conditions. Together with our docking studies, these results indicate that the cleavage of the  $\alpha$ -domain is necessary for the correct positioning of the  $\beta_1$ -domain. Together with the  $\beta_2$ -domain, they could provide a specific binding platform for the cleaved  $\alpha$ -domain. However, the binding position of the  $\beta_1$ -domain needs experimental verification. Nevertheless, the abolishment of  $\alpha$ -domain cleavage by mutation of the cleavage site did not affect the functionality of AIDA-I (Charbonneau *et al.*, 2006). The cleavage could presumably lead to a rearrangement of mature AIDA-I, which then provides a binding platform for other unknown proteins or host factors during infection (Charbonneau *et al.*, 2009). Another possibility is that mature AIDA-I is released due to a specific condition during infection to escape immune response.

#### ***A common secretion mechanism for monomeric AT***

For the transport mechanism of monomeric AT different model pathways were proposed, but recently a novel 'alternative model' was developed based on experimental evidence for the monomeric AT EspP from *E. coli*, which is a combination of the hairpin and the BamA model (Ieva *et al.*, 2008; Ieva *et al.*, 2011; Pavlova *et al.*, 2013). According to this 'alternative model', the AT adopts a stable conformation in the periplasm by interaction with chaperones subsequent to Sec-dependent transport across the IM. The periplasmic intermediate with the incorporated linker domain is integrated into the OM in an 'open' conformation maintained by the BAM complex. Simultaneously to the translocation of the  $\alpha$ -domain to the cell surface, the  $\beta$ -barrel is fully assembled in the OM and the BAM complex is released.

In the light of the 'alternative' model, we analyzed the number of polar interactions within the  $\beta$ -barrel. Strikingly, the number of polar interactions between S2-S10 was significantly



higher than for the remainder of the  $\beta$ -barrel (see supplementary information, Table S2). Thus, the region between S2 and S10 was identified as the stable core of the  $\beta$ -barrel. These observations were confirmed for other monomeric AT (see supplementary information, Table S2). Consequently, it is likely that the stable core of the  $\beta$ -barrel folds in the periplasm and the linker domain is incorporated into the pore of this 'open'  $\beta$ -barrel. Furthermore, the structures of EspP(N1023S) and EspP indicate an overall rearrangement after translocation and  $\alpha$ -domain cleavage due to the different numbers of polar interactions between the  $\beta$ -strands and the different conformation of L5.

The 'alternative' model assumes that the  $\beta$ -barrel is maintained in an 'open' conformation by the BAM complex during translocation of the  $\alpha$ -domain (Pavlova *et al.*, 2013). In consequence, the pore of the  $\beta$ -barrel would be large enough to transport folded or modified  $\alpha$ -domains, which were shown to be effectively translocated through the pore of the intrinsic AT  $\beta$ -barrel (Lindenthal and Elsinghorst, 1999; Lee and Byun, 2003; Skillman *et al.*, 2005). The only possible region for  $\beta$ -barrel opening, without breaking covalent bonds, is between S12 and S1 (Figure 6A, highlighted in purple), which is supported by the low number of polar interactions between these  $\beta$ -strands, which are not part of the stable core (see supplementary information, Table S2). Strikingly, the electrostatic surfaces of S1 and S12 (Figure 6B) strongly differ between these monomeric AT. These observations exclude a dependency of charge on the translocation mechanism. For EspP, interactions of BamA, BamB and BamD at different positions around the  $\beta$ -barrel were identified, which indicate a ring-like complex possibly facilitating the 'open' conformation of the  $\beta$ -barrel in the membrane (Pavlova *et al.*, 2013).

Recently, the crystal structures of two different conformations of BamA were published (Noinaj *et al.*, 2013). Structural and computational studies showed that BamA has a reduced

hydrophobic surface near S16, which decreases lipid order and membrane thickness. In the structure of one conformation, S16 is disordered pointing into the  $\beta$ -barrel lumen. Furthermore, a transient separation of S1 and S16 could be shown by molecular dynamics simulations, which indicate a lateral opening of the  $\beta$ -barrel. Additionally, the POTRA domains and the extracellular loop 6 are able to adopt different conformations assuming a gating mechanism. In conclusion, two modes of action were proposed: the BamA-assisted and the BamA-independent approach (Noinaj *et al.*, 2013). The BamA-assisted approach assumes that the lateral opening of BamA, the conformational switch of L6 and the movement of the POTRA domains thread the OMP through the  $\beta$ -barrel of BamA into the OM. During this process, BamA initiates  $\beta$ -barrel formation of the target OMP resulting in a transient BamA-OMP complex. The second approach suggests that the POTRA domains interact with the OMP targeting it to the OM, which is directly integrated into the destabilized membrane. For AIDA-I, crosslinking experiments did not reveal an interaction with BamA (Muller *et al.*, 2005). Thus, the BamA-independent approach seems reasonable. In contrast, the interaction between EspP and the BAM complex indicate the BamA-assisted approach for membrane integration. By using two different modes of action, the diverse electrostatic surfaces are negligible (Figure 6B) and only the properties of the flexible region are important for membrane integration.

Furthermore, the recently discovered translocation and assembly module (TAM) was shown to be involved in autotransporter secretion (Selkrig *et al.*, 2012) and the crystal structure of TamA revealed conserved structural features, which are also found in other members of the Omp85 superfamily, e.g. FhaC and BamA (Clantin *et al.*, 2007; Gruss *et al.*, 2013; Noinaj *et al.*, 2013). TamA contains a 16-stranded  $\beta$ -barrel and three POTRA domains in a C-shaped arrangement. S16 of the TamA  $\beta$ -barrel forms an inward kink, which is similar to BamA in

one of the two conformations (Noinaj *et al.*, 2013). In consequence, S1 and S16 form a particular weak  $\beta$ -strand pair and an open cleft at the periplasmic end of S1 and S15 is observed (Gruss *et al.*, 2013). Furthermore, the extracellular loop 6 adopts a similar conformation as observed for BamA plugging the pore of the  $\beta$ -barrel from the extracellular side. Taken together, these observations indicate a gating mechanism similar to that for BamA. The proposed model for TamA membrane integration of substrate proteins assumes the formation of a hybrid  $\beta$ -barrel by transient lateral opening of TamA and the substrate OMP, which is in good agreement with our observations concerning the possible lateral opening of monomeric AT due to the lower number of polar interactions between S1 and S12 (see above).

### ***Concluding remarks***

Our investigations of AIDA-I-linker- $\beta_2$  revealed high structural similarity to other monomeric AT. Furthermore, the aromaticity and hydrophobicity of the C-terminal amino acid have a great impact on membrane integration and surface-exposure of an  $\alpha$ -domain. However, our findings cannot explain how the translocation across the OM functions in detail but the structural analyses strongly indicate a common mechanism for membrane integration and  $\alpha$ -domain translocation, which tolerates individual properties of the autotransporter.

---

## Experimental procedures

### ***Cloning, expression and purification of AIDA-I-linker- $\beta_2$***

The sequence of the linker and  $\beta_2$ -domain of AIDA-I encoded by pET-SH3 (Jose and Handel, 2003) was cloned into the plasmid pJM007 for constitutive expression (Maurer *et al.*, 1997). A his<sub>6</sub>-tag was introduced N-terminal to the  $\alpha$ -domain, which carried an epitope (PEYFK) for immunodetection (Gawarzewski *et al.*, 2013b). The expression of the encoded fusion protein FP-HisN163 carrying the transport unit termed AIDA-I-linker- $\beta_2$  (MW: 50.9 kDa) from the resulting plasmid pIG501 was performed in *E. coli* UT5600 (DE3) at 30°C and 170 rpm for 18 hours in shaking flasks. The linker-domain carried one (A255T) and the  $\beta_2$ -domain four naturally occurring amino acid exchanges (K1008R, I1013R, R1210E, R1212S), which had no effect on the transport efficacy compared to the wild type  $\beta_2$ -domain (see supplementary information, Figure S7). Solubilization with n-dodecyl-N,N-dimethylamine-N-oxide (LDAO) and purification were conducted as described (Gawarzewski *et al.*, 2013b).

### ***Crystallization and X-ray analysis***

Purified FP-HisN163 with a final concentration between 7 and 28 mg/ml were mixed with an equal volume of reservoir solution (0.1 M sodium cacodylate, pH 6.5, 27.5% PEG 2000 MME) and incubated at 18°C in hanging-drop vapor diffusion plates (Qiagen). Crystal harvesting, data collection and analysis was performed as described (Gawarzewski *et al.*, 2013b). Data collection and refinement statistics are summarized in Table 1.

### ***Structure determination and refinement***

The initial molecular replacement solution was obtained using a homologous autotransporter structure (EspP(N1023S); PDB code: 3SLT) with 15% sequence identity over

252 residues in the aligned region as template. The initial hit was fairly strong, with a phaser TFZ score of 7.5, but autobuilding was unable to improve this initial solution (McCoy *et al.*, 2007). The model was subsequently refined in MR-Rosetta (DiMaio *et al.*, 2011). Starting from the initial alignment to 3SLT, 1000 homology models were built, constrained by density from the initial molecular replacement hit. Each of these models was then evaluated against the reciprocal space data (using Phaser's MR\_RNP mode). The best model according to this measure was used to rephase the data, and chain tracing was performed with phenix.autobuild (Terwilliger *et al.*, 2008). Starting from the MR-Rosetta model, phenix.autobuild built and placed 294 residues, with an  $R_{work}/R_{free}$  of 0.32/0.39. The subsequent map was readily interpretable. Manual refinement with COOT (Emsley *et al.*, 2010) and REFMAC5 (Murshudov *et al.*, 1997; Murshudov *et al.*, 2011) resulted in a final resolution of 3.0 Å with a crystallographic  $R_{work}/R_{free}$  of 24.8%/30.6% (Table 1). The structure of AIDA-I-linker- $\beta_2$  is accessible in the Protein Data Bank (Berman *et al.*, 2000) via PDB code 4MEE ([www.rcsb.org/pdb](http://www.rcsb.org/pdb)).

### **$\beta_1$ -domain docking onto AIDA-I**

To generate an input model for the  $\beta_1$ -domain the amino acid sequence V50-P956 of native AIDA-I (Universal Protein Knowledgebase reference no. Q03155, <http://www.uniprot.org>) was used in combination with the Protein Homology/analogY Recognition Engine (PHYRE2, <http://www.sbg.bio.ic.ac.uk/phyre2>) (Kelley and Sternberg, 2009). The resulting model based on the autochaperone domain of IcsA (Kuhnel and Diezmann, 2011). The amino acids N803-S846 were removed matching the naturally cleaved N-terminus of the transport unit. Together with the structure of AIDA-I-linker- $\beta_2$  an interaction simulation was conducted

employing the ClusPro server (<http://cluspro.bu.edu>) using standard settings (Comeau *et al.*, 2004).

## Acknowledgements

We thank the beamline scientists at the European Synchrotron Radiation Facility in Grenoble/France and at the European Molecular Biology Laboratory in Hamburg/Germany for assistance in data collection and support during measurement time. We also thank Dr. Astrid Höppner for experimental suggestions as well as stimulating discussions. We thank the crystal and X-ray facility of the Heinrich-Heine-University for the use of the equipment. We also gratefully acknowledge support and training from the International NRW Research School BioStruct, granted by the Ministry of Innovation, Science and Research of the State North Rhine-Westphalia, the Heinrich-Heine University Düsseldorf and the Entrepreneur Foundation at Heinrich-Heine-University of Düsseldorf.

## References

- Barnard, T. J., Dautin, N., Lukacik, P., Bernstein, H. D. and Buchanan, S. K. (2007). Autotransporter structure reveals intra-barrel cleavage followed by conformational changes. *Nat Struct Mol Biol*, 14(12): 1214-1220.
- Barnard, T. J., Gumbart, J., Peterson, J. H., Noinaj, N., Easley, N. C., Dautin, N., Kuszak, A. J., Tajkhorshid, E., Bernstein, H. D. and Buchanan, S. K. (2012). Molecular basis for the activation of a catalytic asparagine residue in a self-cleaving bacterial autotransporter. *J Mol Biol*, 415(1): 128-142.
- Benz, I. and Schmidt, M. A. (1989). Cloning and expression of an adhesin (AIDA-I) involved in diffuse adherence of enteropathogenic *Escherichia coli*. *Infect Immun*, 57(5): 1506-1511.
- Benz, I. and Schmidt, M. A. (1992). AIDA-I, the adhesin involved in diffuse adherence of the diarrhoeagenic *Escherichia coli* strain 2787 (O126:H27), is synthesized via a precursor molecule. *Mol Microbiol*, 6(11): 1539-1546.
- Benz, I. and Schmidt, M. A. (2001). Glycosylation with heptose residues mediated by the aah gene product is essential for adherence of the AIDA-I adhesin. *Mol Microbiol*, 40(6): 1403-1413.
- Benz, I. and Schmidt, M. A. (2011). Structures and functions of autotransporter proteins in microbial pathogens. *Int J Med Microbiol*, 301(6): 461-468.
- Berman, H. M., Westbrook, J., Feng, Z., Gilliland, G., Bhat, T. N., Weissig, H., Shindyalov, I. N. and Bourne, P. E. (2000). The Protein Data Bank. *Nucleic Acids Res*, 28(1): 235-242.
- Charbonneau, M. E., Berthiaume, F. and Mourez, M. (2006). Proteolytic processing is not essential for multiple functions of the *Escherichia coli* autotransporter adhesin involved in diffuse adherence (AIDA-I). *J Bacteriol*, 188(24): 8504-8512.

- Charbonneau, M. E., Girard, V., Nikolakakis, A., Campos, M., Berthiaume, F., Dumas, F., Lepine, F. and Mourez, M. (2007). O-linked glycosylation ensures the normal conformation of the autotransporter adhesin involved in diffuse adherence. *J Bacteriol*, *189*(24): 8880-8889.
- Charbonneau, M. E., Janvire, J. and Mourez, M. (2009). Autoprocessing of the Escherichia coli AIDA-I autotransporter: a new mechanism involving acidic residues in the junction region. *J Biol Chem*, *284*(25): 17340-17351.
- Charbonneau, M. E. and Mourez, M. (2007). Functional organization of the autotransporter adhesin involved in diffuse adherence. *J Bacteriol*, *189*(24): 9020-9029.
- Clantin, B., Delattre, A. S., Rucktooa, P., Saint, N., Meli, A. C., Locht, C., Jacob-Dubuisson, F. and Villeret, V. (2007). Structure of the membrane protein FhaC: a member of the Omp85-TpsB transporter superfamily. *Science*, *317*(5840): 957-961.
- Comeau, S. R., Gatchell, D. W., Vajda, S. and Camacho, C. J. (2004). ClusPro: a fully automated algorithm for protein-protein docking. *Nucleic Acids Res*, *32*(Web Server issue): W96-99.
- DiMaio, F., Terwilliger, T. C., Read, R. J., Wlodawer, A., Oberdorfer, G., Wagner, U., Valkov, E., Alon, A., Fass, D., Axelrod, H., L. Das, D., Vorobiev, S., M. Iwai, H., Pokkuluri, P. R. and Baker, D. (2011). Improved molecular replacement by density- and energy-guided protein structure optimization. *Nature*, *473*(7348): 540-543.
- Emsley, P., Lohkamp, B., Scott, W. G. and Cowtan, K. (2010). Features and development of Coot. *Acta Crystallogr D Biol Crystallogr*, *66*(Pt 4): 486-501.
- Gawarzewski, I., Smits, S. H., Schmitt, L. and Jose, J. (2013a). Structural comparison of the transport units of type V secretion systems. *Biol Chem*, *394*(11): 1385-1398.
- Gawarzewski, I., Tschapek, B., Hoepfner, A., Jose, J., Smits, S. H. and Schmitt, L. (2013b). Purification, crystallization and preliminary X-ray crystallographic analysis of the transport unit of the monomeric autotransporter AIDA-I from Escherichia coli. *Acta Crystallogr F Biol Crystallogr*, *69*: 1159-1162.
- Gruss, F., Zahringer, F., Jakob, R. P., Burmann, B. M., Hiller, S. and Maier, T. (2013). The structural basis of autotransporter translocation by TamA. *Nat Struct Mol Biol*.
- Henderson, I. R., Navarro-Garcia, F., Desvaux, M., Fernandez, R. C. and Ala'Aldeen, D. (2004). Type V protein secretion pathway: the autotransporter story. *Microbiol Mol Biol Rev*, *68*(4): 692-744.
- Hendrixson, D. R., de la Morena, M. L., Stathopoulos, C. and St Geme, J. W., 3rd. (1997). Structural determinants of processing and secretion of the Haemophilus influenzae Hap protein. *Mol Microbiol*, *26*(3): 505-518.
- Ieva, R., Skillman, K. M. and Bernstein, H. D. (2008). Incorporation of a polypeptide segment into the beta-domain pore during the assembly of a bacterial autotransporter. *Mol Microbiol*, *67*(1): 188-201.
- Ieva, R., Tian, P., Peterson, J. H. and Bernstein, H. D. (2011). Sequential and spatially restricted interactions of assembly factors with an autotransporter beta domain. *Proc Natl Acad Sci U S A*, *108*(31): 383-391.
- Jose, J. (2006). Autodisplay: efficient bacterial surface display of recombinant proteins. *Appl Microbiol Biotechnol*, *69*(6): 607-614.
- Jose, J., Betscheider, D. and Zangen, D. (2005). Bacterial surface display library screening by target enzyme labeling: Identification of new human cathepsin G inhibitors. *Anal Biochem*, *346*(2): 258-267.
- Jose, J. and Handel, S. (2003). Monitoring the cellular surface display of recombinant proteins by cysteine labeling and flow cytometry. *Chembiochem*, *4*(5): 396-405.
- Jose, J., Jahnig, F. and Meyer, T. F. (1995). Common structural features of IgA1 protease-like outer membrane protein autotransporters. *Mol Microbiol*, *18*(2): 378-380.
- Kelley, L. A. and Sternberg, M. J. (2009). Protein structure prediction on the Web: a case study using the Phyre server. *Nat Protoc*, *4*(3): 363-371.
- Konieczny, M. P. J., Benz, I., Hollinderbaumer, B., Beinke, C., Niederweis, M. and Schmidt, M. A. (2001). Modular organization of the AIDA autotransporter translocator: the N-terminal beta1-domain is surface-exposed and stabilizes the transmembrane beta2-domain. *Antonie Van Leeuwenhoek*, *80*(1): 19-34.
- Kuhnel, K. and Diezmann, D. (2011). Crystal structure of the autochaperone region from the Shigella flexneri autotransporter IcsA. *J Bacteriol*, *193*(8): 2042-2045.
- Lee, H. W. and Byun, S. M. (2003). The pore size of the autotransporter domain is critical for the active translocation of the passenger domain. *Biochem Biophys Res Commun*, *307*(4): 820-825.
- Leo, J. C., Grin, I. and Linke, D. (2012). Type V secretion: mechanism(s) of autotransport through the bacterial outer membrane. *Philos Trans R Soc Lond B Biol Sci*, *367*(1592): 1088-1101.
- Leyton, D. L., Rossiter, A. E. and Henderson, I. R. (2012). From self sufficiency to dependence: mechanisms and factors important for autotransporter biogenesis. *Nat Rev Microbiol*, *10*(3): 213-225.



- Lindenthal, C. and Elsinghorst, E. A. (1999). Identification of a glycoprotein produced by enterotoxigenic *Escherichia coli*. *Infect Immun*, 67(8): 4084-4091.
- Loveless, B. J. and Saier, M. H., Jr. (1997). A novel family of channel-forming, autotransporting, bacterial virulence factors. *Mol Membr Biol*, 14(3): 113-123.
- Maurer, J., Jose, J. and Meyer, T. F. (1997). Autodisplay: one-component system for efficient surface display and release of soluble recombinant proteins from *Escherichia coli*. *J Bacteriol*, 179(3): 794-804.
- Maurer, J., Jose, J. and Meyer, T. F. (1999). Characterization of the essential transport function of the AIDA-I autotransporter and evidence supporting structural predictions. *J Bacteriol*, 181(22): 7014-7020.
- McCoy, A. J., Grosse-Kunstleve, R. W., Adams, P. D., Winn, M. D., Storoni, L. C. and Read, R. J. (2007). Phaser crystallographic software. *J Appl Crystallogr*, 40(Pt 4): 658-674.
- Mogensen, J. E., Kleinschmidt, J. H., Schmidt, M. A. and Otzen, D. E. (2005a). Misfolding of a bacterial autotransporter. *Protein Sci*, 14(11): 2814-2827.
- Mogensen, J. E., Tapadar, D., Schmidt, M. A. and Otzen, D. E. (2005b). Barriers to folding of the transmembrane domain of the *Escherichia coli* autotransporter adhesin involved in diffuse adherence. *Biochemistry*, 44(11): 4533-4545.
- Muller, D., Benz, I., Tapadar, D., Buddenborg, C., Greune, L. and Schmidt, M. A. (2005). Arrangement of the translocator of the autotransporter adhesin involved in diffuse adherence on the bacterial surface. *Infect Immun*, 73(7): 3851-3859.
- Murshudov, G. N., Skubak, P., Lebedev, A. A., Pannu, N. S., Steiner, R. A., Nicholls, R. A., Winn, M. D., Long, F. and Vagin, A. A. (2011). REFMAC5 for the refinement of macromolecular crystal structures. *Acta Crystallogr D Biol Crystallogr*, 67(Pt 4): 355-367.
- Murshudov, G. N., Vagin, A. A. and Dodson, E. J. (1997). Refinement of macromolecular structures by the maximum-likelihood method. *Acta Crystallogr D Biol Crystallogr*, 53(Pt 3): 240-255.
- Nataro, J. P. and Kaper, J. B. (1998). Diarrheagenic *Escherichia coli*. *Clin Microbiol Rev*, 11(1): 142-201.
- Ngeleka, M., Pritchard, J., Appleyard, G., Middleton, D. M. and Fairbrother, J. M. (2003). Isolation and association of *Escherichia coli* AIDA-I/STb, rather than EAST1 pathotype, with diarrhea in piglets and antibiotic sensitivity of isolates. *J Vet Diagn Invest*, 15(3): 242-252.
- Noinaj, N., Kuszak, A. J., Gumbart, J. C., Lukacik, P., Chang, H., Easley, N. C., Lithgow, T. and Buchanan, S. K. (2013). Structural insight into the biogenesis of beta-barrel membrane proteins. *Nature*.
- Oliver, D. C., Huang, G., Nodel, E., Pleasance, S. and Fernandez, R. C. (2003). A conserved region within the *Bordetella pertussis* autotransporter BrkA is necessary for folding of its passenger domain. *Mol Microbiol*, 47(5): 1367-1383.
- Oomen, C. J., van Ulsen, P., van Gelder, P., Feijen, M., Tommassen, J. and Gros, P. (2004). Structure of the translocator domain of a bacterial autotransporter. *EMBO J*, 23(6): 1257-1266.
- Pavlova, O., Peterson, J. H., Ieva, R. and Bernstein, H. D. (2013). Mechanistic link between beta barrel assembly and the initiation of autotransporter secretion. *Proc Natl Acad Sci U S A*, 110(10): E938-947.
- Robert, V., Volokhina, E. B., Senf, F., Bos, M. P., Van Gelder, P. and Tommassen, J. (2006). Assembly factor Omp85 recognizes its outer membrane protein substrates by a species-specific C-terminal motif. *PLoS Biol*, 4(11): e377.
- Schulz, G. E. (2002). The structure of bacterial outer membrane proteins. *Biochim Biophys Acta*, 1565(2): 308-317.
- Selkrig, J., Mosbahi, K., Webb, C. T., Belousoff, M. J., Perry, A. J., Wells, T. J., Morris, F., Leyton, D., L. Totsika, M., Phan, M., D. Celik, N., Kelly, M., Oates, C., Hartland, E. L., Robins-Browne, R. M., Ramarathinam, S. H., Purcell, A. W., Schembri, M. A., Strugnell, R. A., Henderson, I. R., Walker, D. and Lithgow, T. (2012). Discovery of an archetypal protein transport system in bacterial outer membranes. *Nat Struct Mol Biol*, 19(5): 506-510, S501.
- Skillman, K. M., Barnard, T. J., Peterson, J. H., Ghirlando, R. and Bernstein, H. D. (2005). Efficient secretion of a folded protein domain by a monomeric bacterial autotransporter. *Mol Microbiol*, 58(4): 945-958.
- Soprova, Z., Sauri, A., van Ulsen, P., Tame, J. R., den Blaauwen, T., Jong, W. S. and Luirink, J. (2010). A conserved aromatic residue in the autochaperone domain of the autotransporter Hbp is critical for initiation of outer membrane translocation. *J Biol Chem*, 285(49): 38224-38233.
- Struyvé, M., Moons, M. and Tommassen, J. (1991). Carboxy-terminal phenylalanine is essential for the correct assembly of a bacterial outer membrane protein. *J Mol Biol*, 218(1): 141-148.
- Suhr, M., Benz, I. and Schmidt, M. A. (1996). Processing of the AIDA-I precursor: removal of AIDAc and evidence for the outer membrane anchoring as a beta-barrel structure. *Mol Microbiol*, 22(1): 31-42.
- Terwilliger, T. C., Grosse-Kunstleve, R. W., Afonine, P. V., Moriarty, N. W., Zwart, P. H., Hung, L. W., Read, R. J. and Adams, P. D. (2008). Iterative model building, structure refinement and density modification with the PHENIX AutoBuild wizard. *Acta Crystallogr D Biol Crystallogr*, 64(Pt 1): 61-69.

- Tomassen, J. (2010). Assembly of outer-membrane proteins in bacteria and mitochondria. *Microbiology*, 156(Pt 9): 2587-2596.
- van den Berg, B. (2010). Crystal structure of a full-length autotransporter. *J Mol Biol*, 396(3): 627-633.
- Voulhoux, R., Bos, M. P., Geurtsen, J., Mols, M. and Tomassen, J. (2003). Role of a highly conserved bacterial protein in outer membrane protein assembly. *Science*, 299(5604): 262-265.
- White, S. H., Ladokhin, A. S., Jayasinghe, S. and Hristova, K. (2001). How membranes shape protein structure. *J Biol Chem*, 276(35): 32395-32398.
- Wu, T., Malinverni, J., Ruiz, N., Kim, S., Silhavy, T. J. and Kahne, D. (2005). Identification of a multicomponent complex required for outer membrane biogenesis in *Escherichia coli*. *Cell*, 121(2): 235-245.
- Zhai, Y.Zhang, K.Huo, Y.Zhu, Y.Zhou, Q.Lu, J.Black, I.Pang, X.Roszak, A. W.Zhang, X.Isaacs, N. W. and Sun, F. (2011). Autotransporter passenger domain secretion requires a hydrophobic cavity at the extracellular entrance of the beta-domain pore. *Biochem J*, 435(3): 577-587.

## Table legends

### Table 1 Data collection statistics

Values in parentheses correspond to the highest resolution shell.  $R_{merge} = \frac{\sum_{hkl} \sum_i |I_i(hkl) - \langle I(hkl) \rangle|}{\sum_{hkl} \sum_i I(hkl)}$ , where  $I_i(hkl)$  is the  $i$ th observation of reflection  $hkl$  and  $\langle I(hkl) \rangle$  is the weighted average intensity for all observations  $i$  of reflection  $hkl$ .

### Table 2 Global RMSD calculations of $C\alpha$ atoms of type Va transport units

**Table 1**

Parameter	Value
Cell dimensions	
Space group	P2 <sub>1</sub> 2 <sub>1</sub> 2 <sub>1</sub>
a, b, c (Å)	40.33, 85.83, 134.05
$\alpha = \beta = \gamma$ (°)	90
Data collection	
Wavelength (Å)	0.8726
Resolution range (Å)	50.0-3.0
R <sub>merge</sub> (%)	9.7 (61.9)
(I/ $\sigma$ (I))	13.61 (2.39)
Completeness (%)	92.6 (94.4)
Redundancy	4.65 (4.73)
Matthews coefficient (Å <sup>3</sup> /Da)	2.32
Overall B factor from Wilson plot (Å <sup>2</sup> )	48.29
Refinement	
Resolution (Å)	39.67-3.0 (3.107-3.0)
No. of reflections	36648
R <sub>work</sub> /R <sub>free</sub> (%)	24.8/30.6
No. of atoms	
Protein	2234
B-factors (Å <sup>2</sup> )	61.81
RMSD	
Bond lengths (Å)	0.015
Bond angles (°)	1.65
Residues in Ramachandran plot (%)	
Most favored	96.61
Additional allowed	3.39
Disallowed	0

Table 2

Protein	PDB code	No. of amino acids	No. of C $\alpha$ atoms compared	RMSD (Å)	Reference structure	No. of amino acids
BrkA	3QQ2	245	217	2.6	AIDA-I-linker- $\beta_2$	303
EspP	2QOM	269	229	1.7		
EstA	3KVN	332	269	2.6		
Hbp	3AEH	554	235	1.6		
NalP	1UYN	279	256	1.9		
EspP(N1023S)	3SLT	305	256	2.1		

The lower the RMSD value, the higher the structural similarity is.

## Figure legends

### Figure 1 SDS-PAGE (A) and SEC-MALS analysis (B) of purified FP-HisN163

A: SDS-PAGE after IMAC and SEC; M: PageRuler™ Prestained Protein Ladder (Fermentas)  
 B: Elution profile after SEC-MALS; Black line: refractive index detector signal; blue line: UV absorbance signal; red line: light scattering detector signal; green line: calculated detergent mass; orange line: calculated protein mass; violet line: calculated micelle mass

### Figure 2 Crystal structure of AIDA-I-linker- $\beta_2$

L: extracellular loops; S:  $\beta$ -strand; T: periplasmic turns; red: linker-domain; green:  $\beta_2$ -domain  
 A: The crystal structure of AIDA-I-linker- $\beta_2$  includes amino acids Q962-F1286 and is shown as ribbon presentation. T1, T4 and T5 are not completely modeled as, indicated by an asterisk.  
 B: Loop L5 (highlighted in blue) adopts the same conformation as in the cleavage mutant EspP(N1023S).

### Figure 3 Conserved amino acids and the signature sequence in AIDA-I-linker- $\beta_2$

A: The conserved amino acids, which are labeled with one-letter-code and amino acid number, are shown in stick presentation highlighted in orange.  
 B: Stick presentation of the signature sequence highlighted in black

### Figure 4 Influence of the C-terminal amino acid on membrane integration and $\alpha$ -domain surface-presentation of AIDA-I-linker- $\beta_2$

FACS analyses (A) and immunodetection (B) for OM localization and  $\alpha$ -domain orientation analyses of the C-terminal mutants of AIDA-I-linker- $\beta_2$   
 Negative control: *E. coli* UT5600 (DE3) without any plasmid; F1286 $\Delta$ : deletion mutant; F1286X: substitution of phenylalanine by either tryptophan (F1286W), tyrosine (F1286Y), histidine (F1286H) or valine (F1286V)

### Figure 5 Electrostatic surface of AIDA-I-linker- $\beta_2$

A: same orientation of AIDA-I-linker- $\beta_2$  as in Figure 2; B: rotation by 180° around the y-axis based on the position in A; C: rotation by 90° around the x-axis based on the position in B; blue: positively charged contoured at +5 kT; white; uncharged; red: negatively charged contoured at -5 kT

### Figure 6 Comparison of polar interactions and electrostatic surfaces in type Va transport units

A: ribbon presentation with S1 and S12 highlighted in purple and the adjacent strands of the flexible region are highlighted in light magenta; green: stable core; S:  $\beta$ -strand; dotted lines: polar interaction  
 B: electrostatic surface presentation of S1 and S12; blue: positively charged contoured at +5 kT; white; uncharged; red: negatively charged contoured at -5 kT

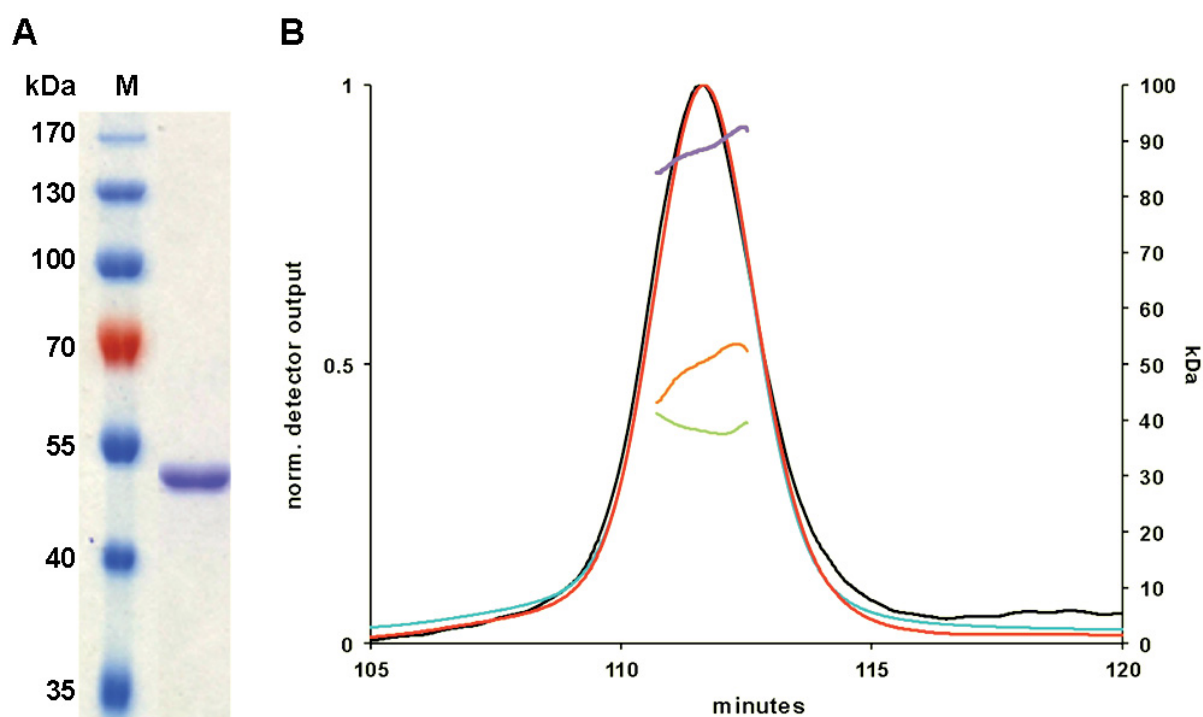


Figure 1

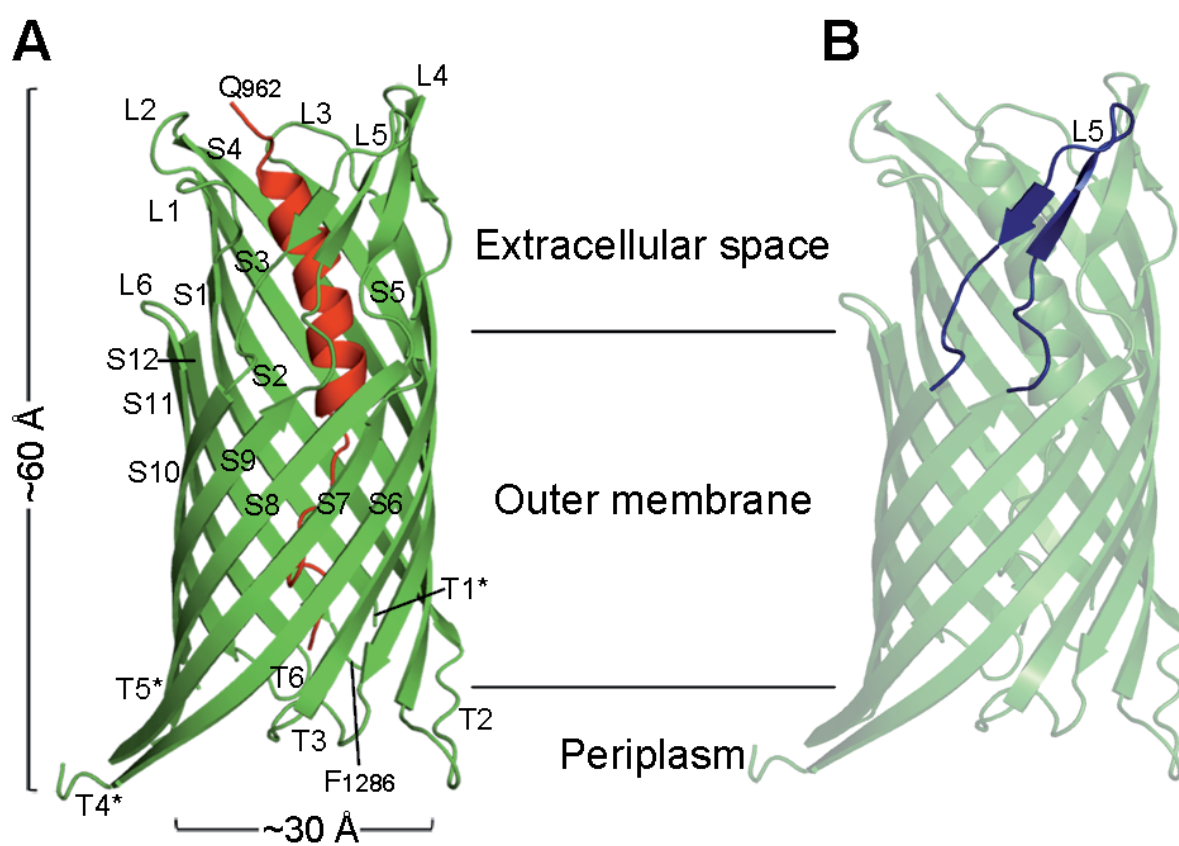


Figure 2

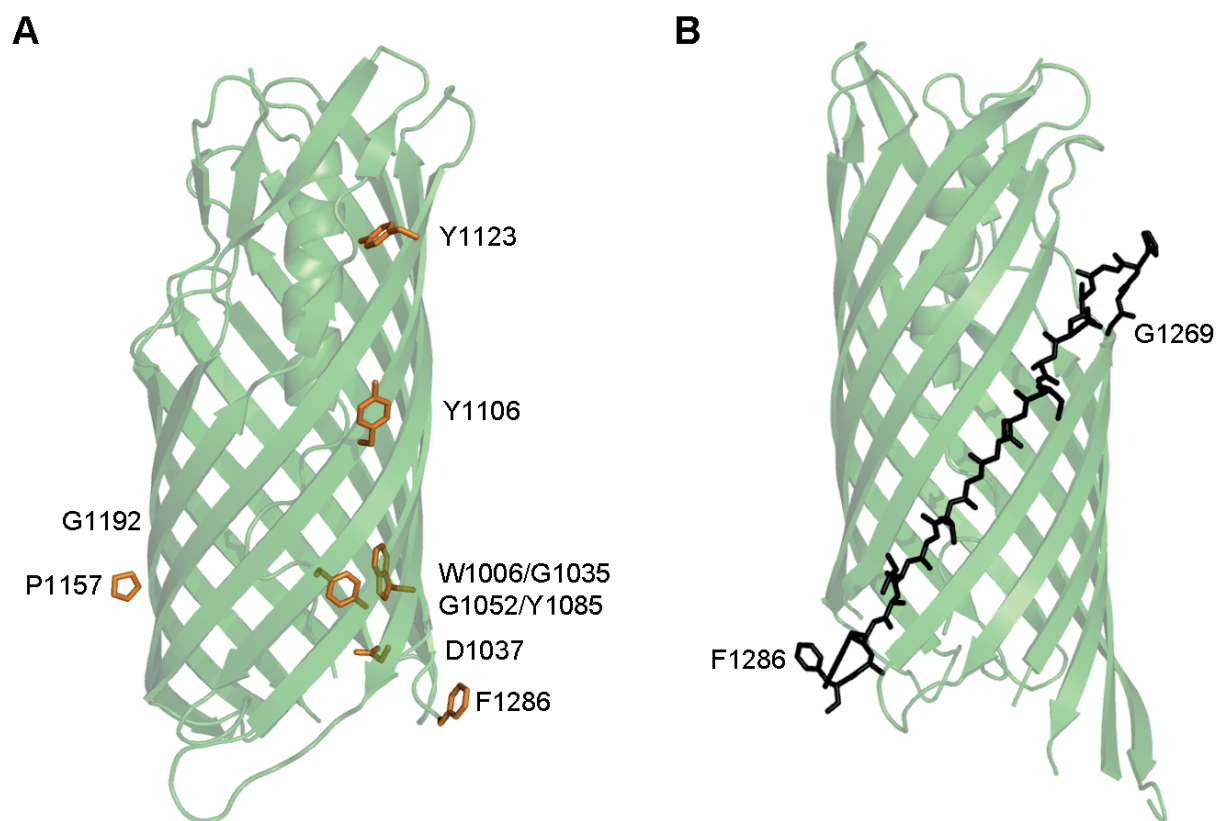


Figure 3

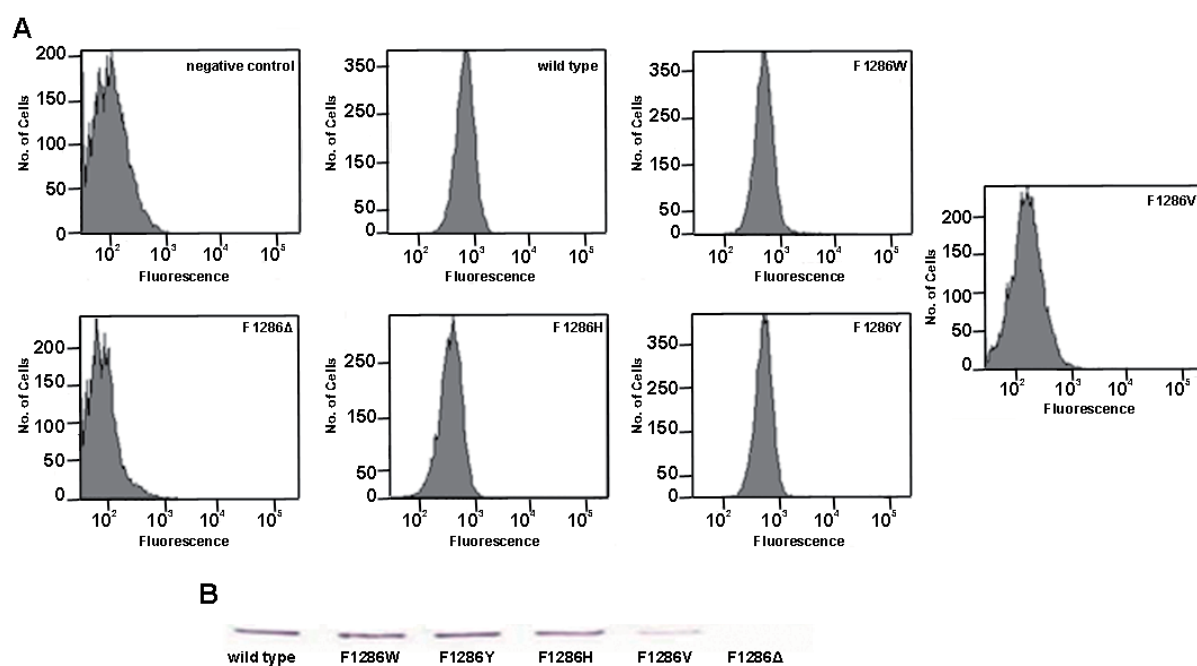


Figure 4



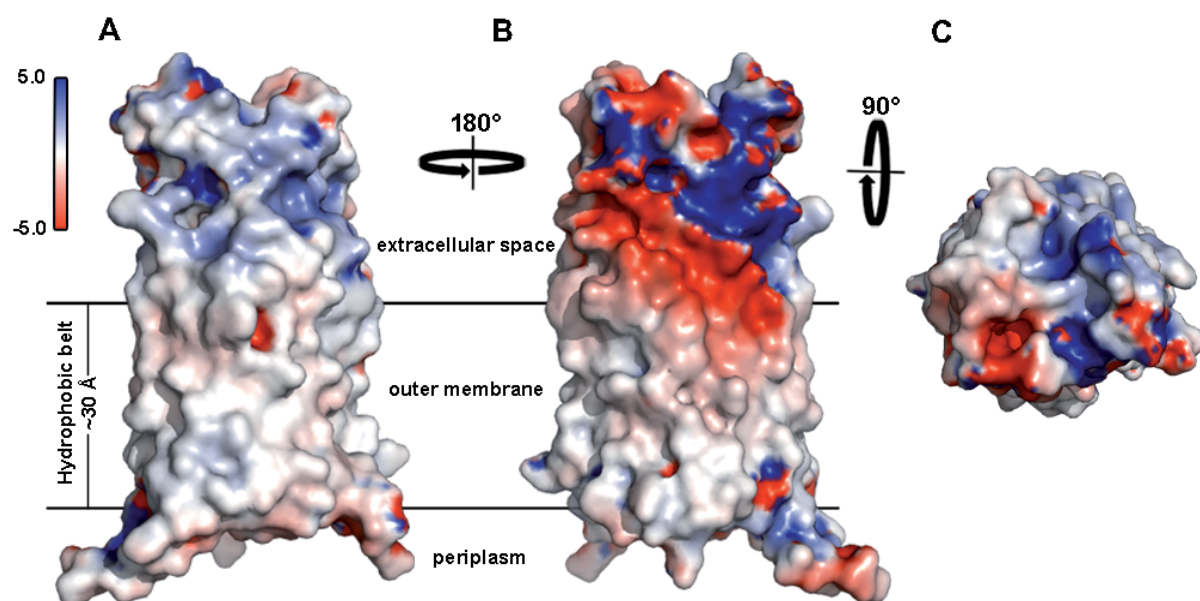
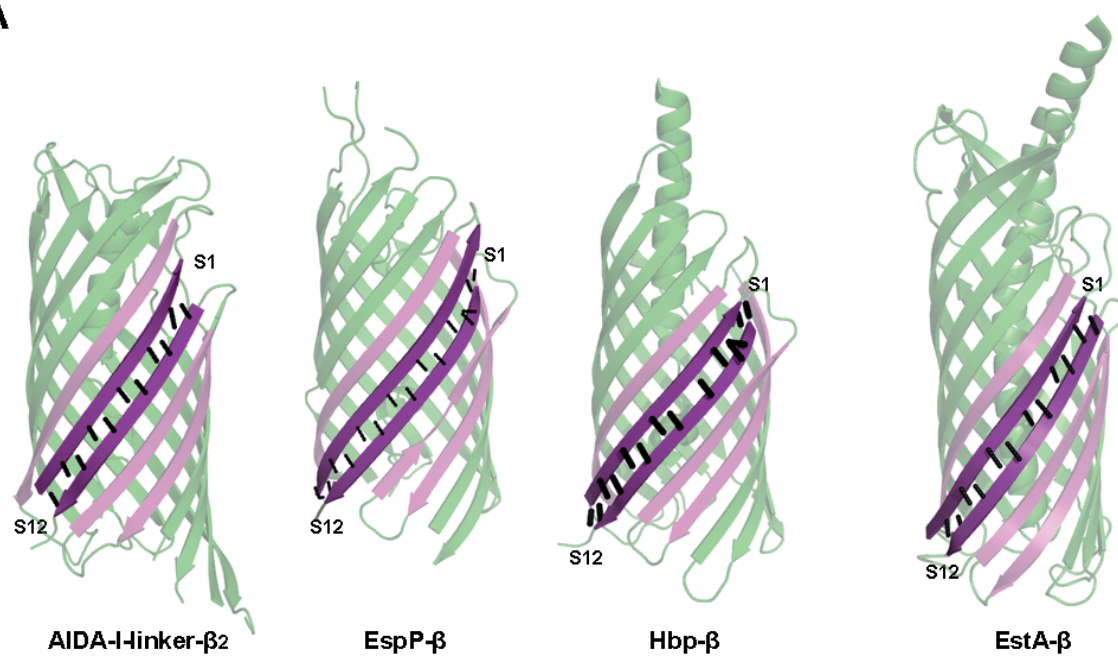
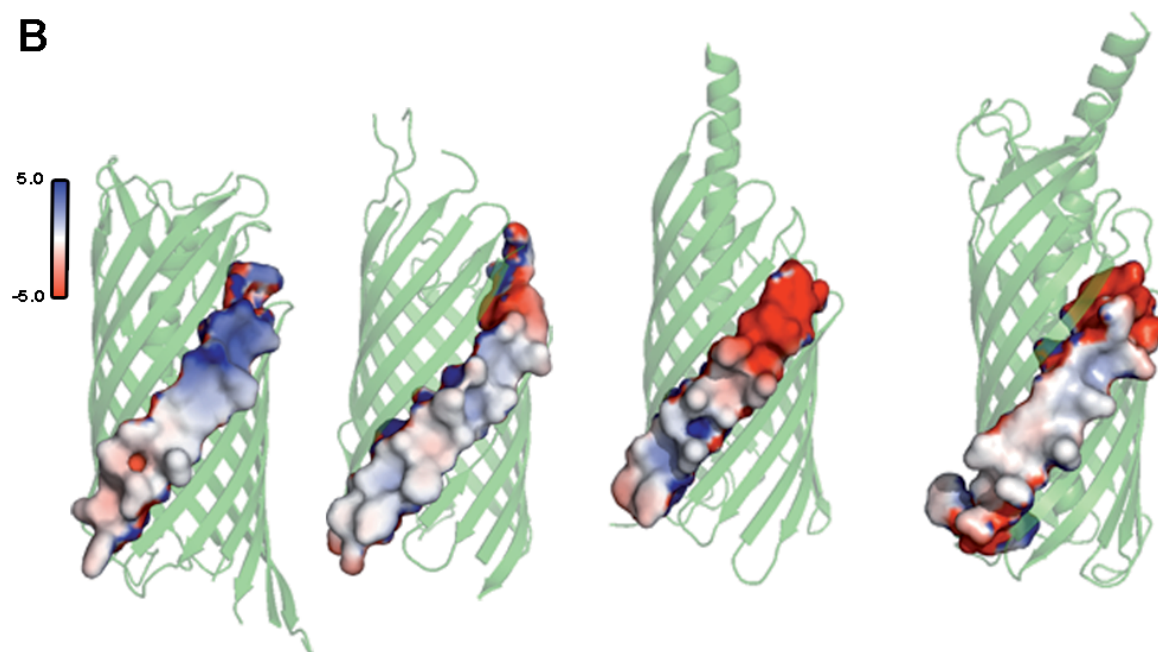


Figure 5

**A****B****Figure 6**

---

## Supplementary information

"Crystal structure of the transport unit of the autotransporter AIDA-I from *Escherichia coli* in a post translocation state"

Iris Gawarzewski, Frank DiMaio, Elisa Winterer, Britta Tschapek, Sander H.J. Smits, Joachim Jose and Lutz Schmitt

## Inventory

- Figures S1 to S7
- Table S1 and S2
- Experimental procedures

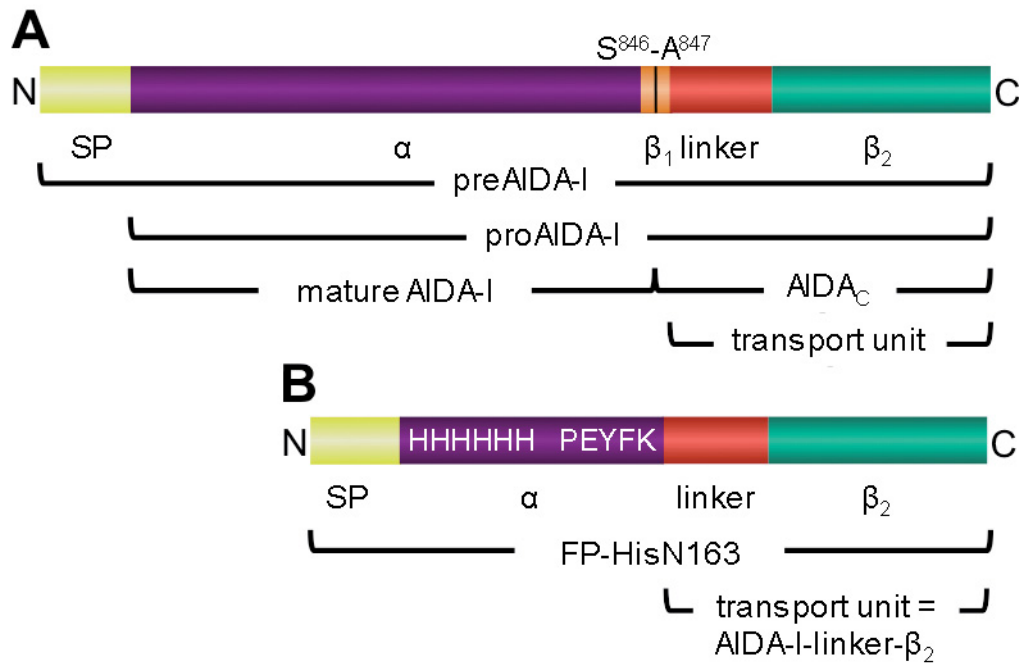


**Figure S1 Organization of native AIDA-I (A) and the truncated construct FP-HisN163 (B) used for crystallization experiments**

SP: signal peptide for Sec-dependent translocation across the inner membrane; α: passenger domain; β<sub>1</sub>: autochaperone domain; linker: connection between β<sub>1</sub>- (A) or α-domain (B) and β<sub>2</sub>-domain; β<sub>2</sub>: β-barrel forming domain in the outer membrane; black vertical line: cleavage site.

HHHHHH: his<sub>6</sub>-tag; PEYFK: epitope for immunodetection.

A: After translation, preAIDA-I is targeted to the inner membrane for Sec-dependent translocation. During this transport process the signal peptide is cleaved off resulting in the periplasmic intermediate proAIDA-I. After translocation across the outer membrane the passenger domain is cleaved by an auto-proteolytic process between S<sup>846</sup>-A<sup>847</sup> (indicated by the black vertical line in the β<sub>1</sub>-domain) resulting in mature AIDA-I, which functions in the extracellular space, and membrane-bound AIDA<sub>C</sub>.

B: Based on the plasmid pET-SH3, the passenger domain was substituted by a his<sub>6</sub>-tag and a PEYFK epitope. The signal peptide was fused to the N-terminus of the histidine tag. At the C-terminus the native linker and the β<sub>2</sub>-domain of AIDA-I were fused. The fusion protein was termed FP-HisN163 containing the transport unit AIDA-I-linker-β<sub>2</sub>. In the crystal structure of AIDA-I-linker-β<sub>2</sub> only the C-terminal part of the linker domain and the β<sub>2</sub>-domain were resolved.

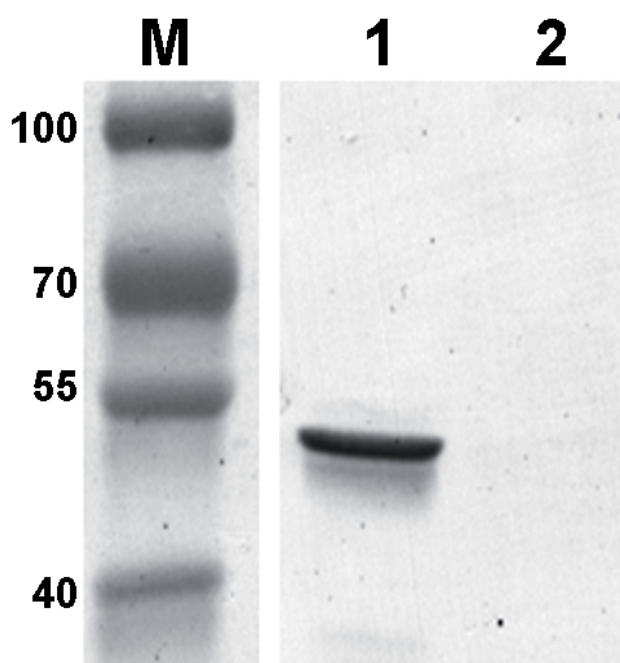


**Figure S2 Validation of membrane localization and correct  $\alpha$ -domain orientation of FP-HisN163 by immunoblotting**

M: PageRuler™ Prestained Protein Ladder (Fermentas); 1: outer membrane protein isolation of *E. coli* UT5600 pIG501 expressing FP-HisN163; 2: outer membrane protein isolation of *E. coli* UT5600 pIG501 expressing FP-HisN163 after proteinase K treatment.

The correct localization of FP-HisN163 and the surface-presentation of the  $\alpha$ -domain were confirmed by outer membrane protein isolation, proteinase K treatment and immunodetection using an anti-Histidine antibody. For this, FP-HisN163, which carried a PEYFK epitope for immunodetection as  $\alpha$ -domain, was constitutively expressed from plasmid pIG501 in *E. coli* UT5600 (DE3). Outer membranes of whole cells were isolated and analyzed by immunodetection (lane 1). A strong protein band with an apparent molecular mass of 50 kDa was detectable, which was assigned to FP-HisN163. The  $\alpha$ -domain presentation at the cell surface was validated by treatment of whole cells with proteinase K before outer membrane protein isolation. This treatment resulted in the removal of the surface-exposed his<sub>6</sub>-tag that was not protected by membrane lipids. In consequence, no protein band was detectable (lane 2). Together, these results show that the recombinant autotransporter FP-HisN163 localized to the outer membrane and that the  $\alpha$ -domain was presented at the cell surface confirming the correct folding and functionality of FP-HisN163.

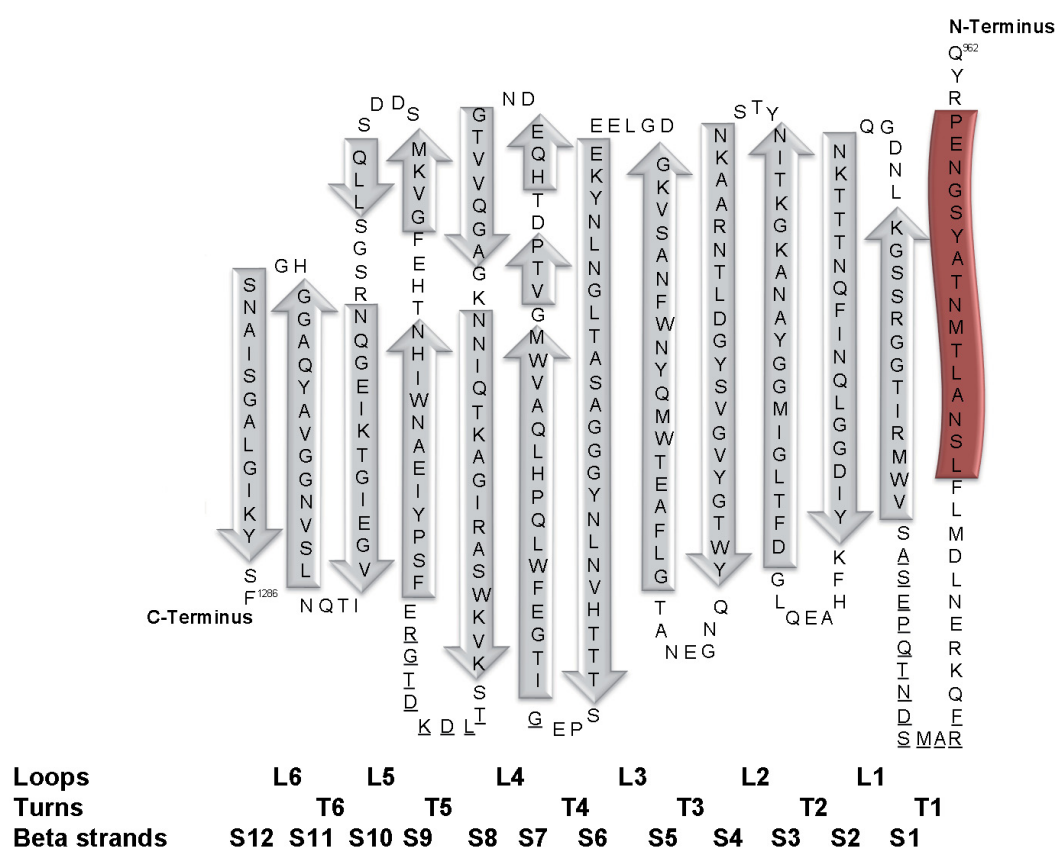


**Figure S3 Topology of AIDA-I-linker- $\beta_2$**

Grey arrows:  $\beta$ -strands; red box:  $\alpha$ -helical part of the linker domain

Missing amino acids in the crystal structure of AIDA-I-linker- $\beta_2$  are underlined.

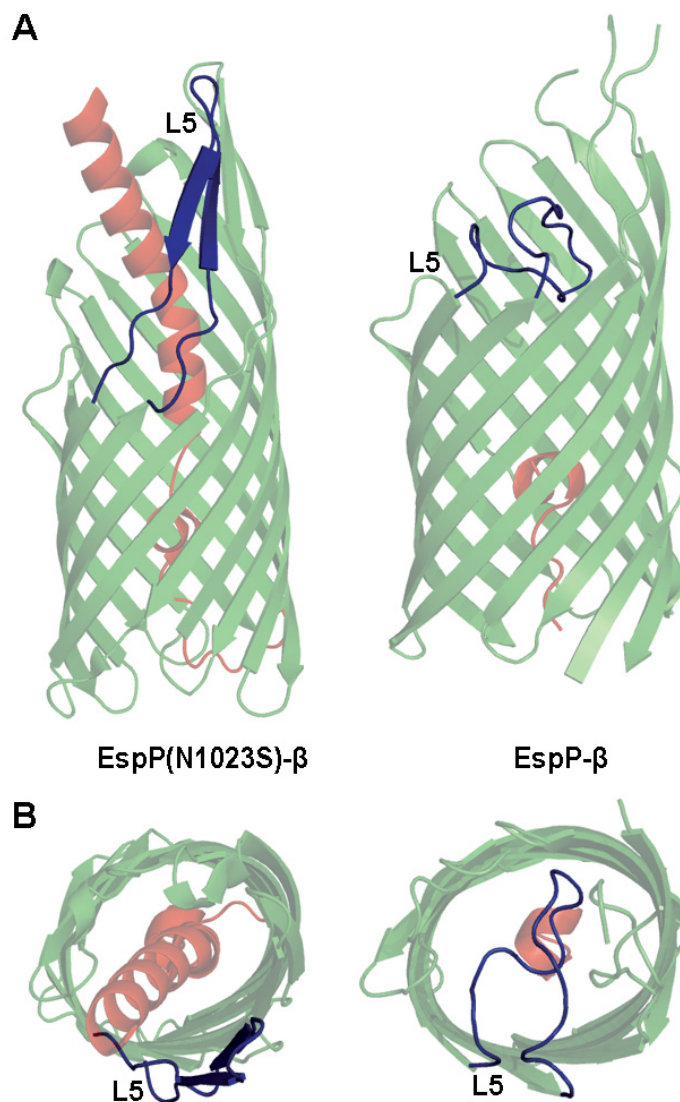
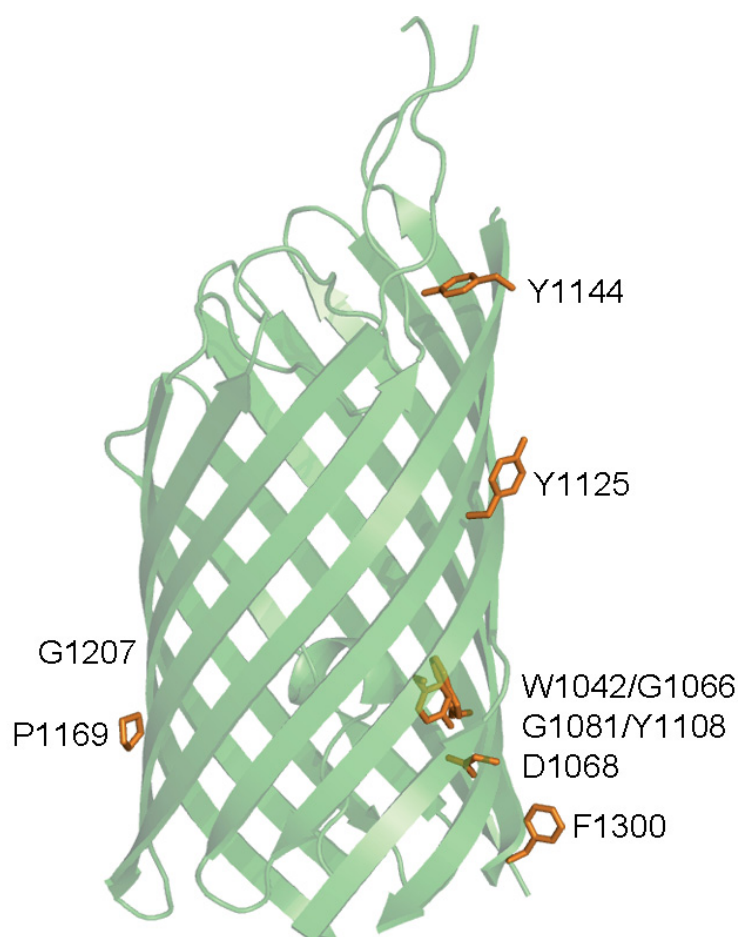


**Figure S4 Different conformations of L5 in EspP wild type and in the cleavage mutant EspP(N1023S)**

The crystal structures of the transport units of EspP wild type and the cleavage mutant EspP(N1023S) are shown in side view (A) and top view from the extracellular side (B); Loop L5 is highlighted in blue and the linker domain in red.

In the mutant, the post-translocational cleavage of the  $\alpha$ -domain is abolished due to an amino acid exchange in the cleavage site. In consequence, the linker domain (highlighted in red) remains in the pore of the  $\beta$ -barrel in an  $\alpha$ -helical conformation and projects into the extracellular space. Thus, L5 adopts an 'open' conformation. In case of the EspP wild type, the linker domain is cleaved and only a small portion remains in the pore close to the periplasm, which allows L5 (highlighted in blue) to plug the pore from the extracellular side in a 'closed' conformation.





## EspP-β

### Figure S5 Conserved amino acids within the transport units of AIDA-I and EspP

The conserved amino acids (highlighted in orange) are labeled with the amino acid in one-letter code and the position number in the sequence.

It was shown that the replacement of G1066 or G1081 by alanine, serine or aspartate led to transient stalling and a slight decrease in  $\beta$ -barrel stability due to steric clashes involving W1042, D1068 and Y1108. Furthermore, Y1125, which is located in the midbarrel region with the side chain facing to the outer membrane, could be crosslinked to the periplasmic chaperone Skp and lipopolysaccharides (LPS) of the outer membrane. Bioinformatic analysis identified Y1144, P1169 and G1207 to be highly conserved among monomeric ATs (see superfamily entry pfam03797 in the Conserved Domain Database, <http://www.ncbi.nlm.nih.gov/cdd>) but their role in AT biogenesis needs to be determined.

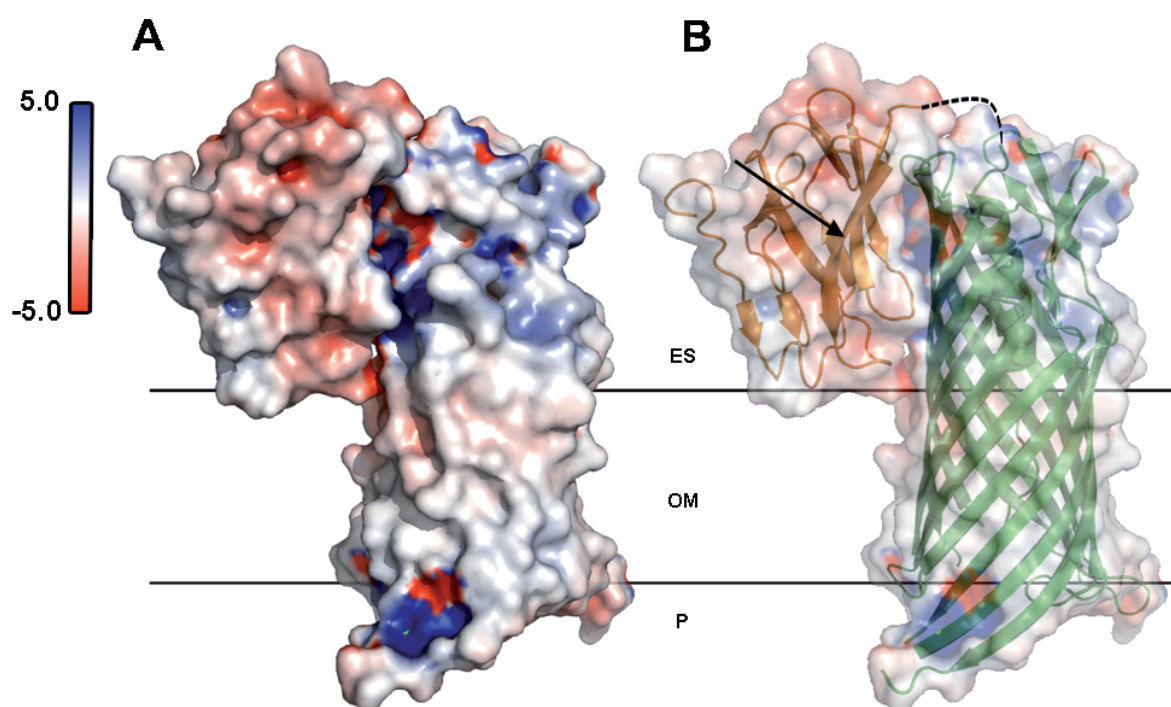


**Figure S6 Interaction of the  $\beta_1$ -domain with the  $\beta_2$ -domain of AIDA-I-linker- $\beta_2$**

A: Electrostatic surface of AIDA-I-linker- $\beta_2$  (green) and the interacting  $\beta_1$ -domain (orange); B: ribbon presentation with an transparent overlay of the electrostatic surface; blue: positively charged contoured at +5 kT; white; uncharged; red: negatively charged contoured at -5 kT; ES: extracellular space; OM: outer membrane; P: periplasm

The missing connection between the  $\beta_1$ - and the  $\beta_2$ -domain is indicated by a dotted line. The arrow points to protease cleavage sites for TPCK-trypsin and TLCK-chymotrypsin.

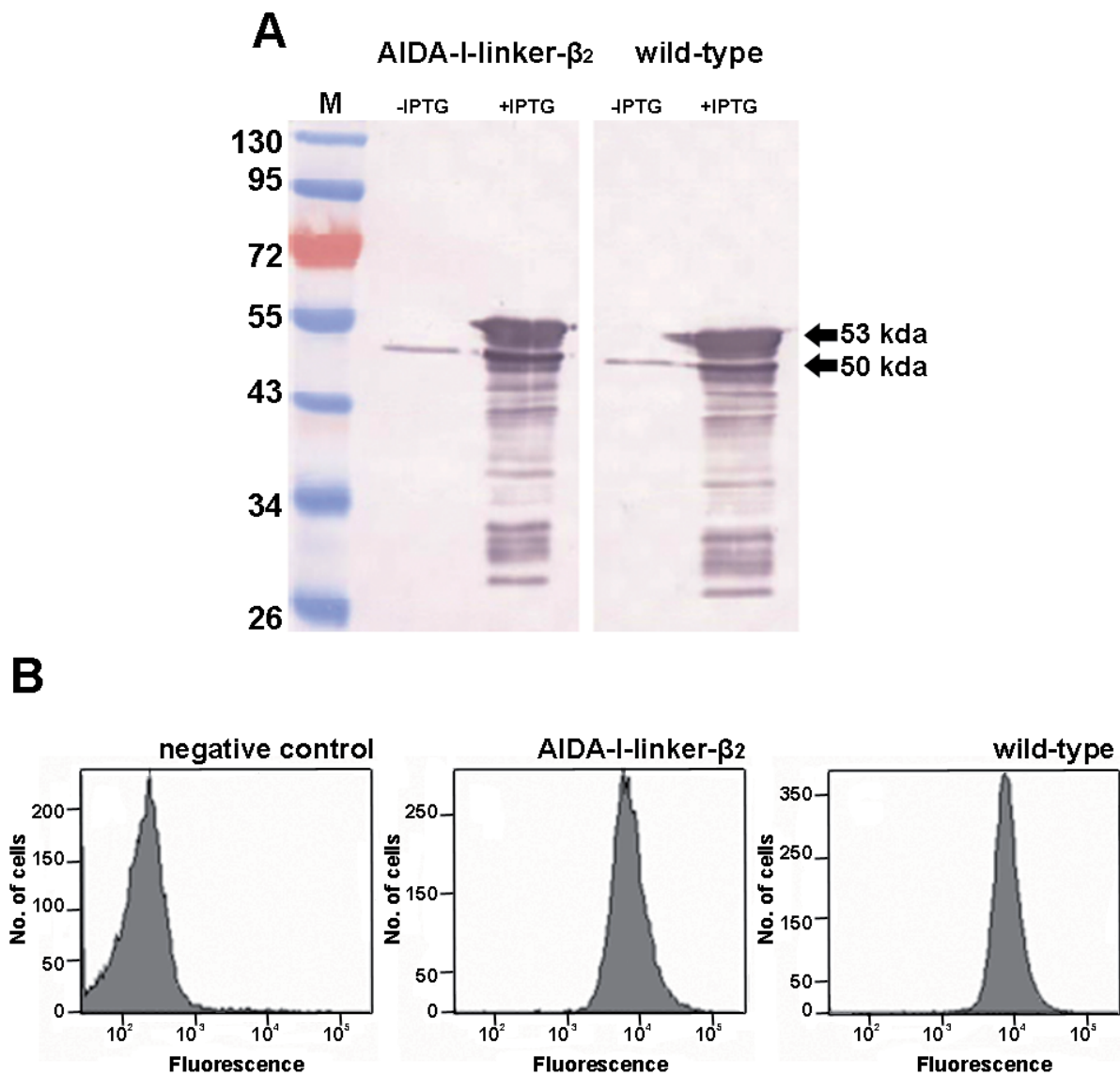


**Figure S7 Validation of the functionality of AIDA-I-linker- $\beta_2$**

A: Immunodetection of AIDA-I-linker- $\beta_2$  and the wild-type  $\beta_2$ -domain; B: FACS analyses of *E. coli* UT5600 (DE3) carrying no plasmid (negative control), *E. coli* UT5600 (DE3) pIG501 (expressing AIDA-I-linker- $\beta_2$ ) and *E. coli* UT5600 (DE3) pEW010 (expressing wild-type  $\beta_2$ -domain).

Protein expression was induced by addition of 1mM IPTG to cell cultures. For immunodetection outer membrane protein preparations were applied to SDS-PAGE and Western Blot and the epitopes in the  $\alpha$ -domain of both autotransporters were detected with an anti-PEYFK antibody. For FACS analyses, whole cells were labeled with the primary mouse anti-PEYFK antibody and a secondary goat anti-mouse antibody, which was coupled to a red fluorescence dye.

**Table S1 Conserved amino acids between AIDA-I-linker- $\beta_2$  and EspP- $\beta$** 

AIDA-I-linker- $\beta_2$	EspP- $\beta$	AIDA-I-linker- $\beta_2$	EspP- $\beta$
L985	L1025	A1132	A1153
N986	N1062	G1135	G1156
R1008	R1044	Y1136	Y1157
I1009	I1045	V1140	V1161
G1112	G1048	W1154	W1166
S1115	S1051	P1157	P1169
N1028	N1059	V1162	V1174
Q1033	Q1064	V1166	V1178*
G1035	G1066	Q1180	Q1182
D1037	D1068	N1185	N1200
K1040	K1070	G1192	G1207
D1048	D1077*	G1249	G1263
G1052	G1081	N1257	N1271*
G1083	G1106	A1268	A1282*
Y1085	Y1108	N1274	N1287
G1097	G1116*	Y1284	Y1298
Y1106	Y1125	S1285	S1299
Y1123	Y1144	F1286	F1300
A1130	A1151		

\* No exact overlay in spatial arrangement; position shifted

**Table S2 Comparison of polar interactions within type Va  $\beta$ -barrels**

A stable core region (red box) and a flexible region (green box) can be defined within the  $\beta$ -barrels for AIDA-I, EspP(N1023S), EspP, EstA and Hbp.

	S1-S2	S2-S3	S3-S4	S4-S5	S5-S6	S6-S7	S7-S8	S8-S9	S9-S10	S10-S11	S11-S12	S12-S1
AIDA-I-linker- $\beta_2$	15	20	20	18	19	16+3*	16+5	12+4*	11+4	12	12	11
EspP(N1023S)	16	20	18	19	21	6+8	14+8	14+5	14+7	11	10	15
EspP	15	12+7*	7+12	12+7	17*	15	14+7*	18*	15	4+6	9	16
EstA	16	15	18	19	23	1+14	17+4	13+4	12+7	13	12	14
Hbp	15	19	19	19	12+4	16	12+3*	16	16*	12	10	15

\* incomplete connection between  $\beta$ -strands

---

## Experimental procedures

### ***Mutagenesis of the C-terminal phenylalanine of the $\beta$ -barrel and expression of the mutant autotransporter proteins***

Based on the autotransporter sequence encoded on plasmid pET-SH3, five different autotransporter mutants were generated using the Quick Change Site-Directed Mutagenesis Kit as described in the manufactures' manual (Stratagene). Customized primer pairs (Sigma Aldrich) for every point mutation in the DNA-sequence were applied resulting in an exchange or the deletion of the C-terminal phenylalanine. The resulting plasmids pEW006 (F1286W), pEW003 (F1286Y), pEW004 (F1286H), pEW008 (F1286V) and pEW005 (F1286 $\Delta$ ) were transferred in *E. coli* UT5600 (DE3) for protein expression. Cultures carrying one of the plasmids were incubated at 37°C and 200 rpm in LB media with 100  $\mu$ g/ml ampicillin and 10 mM 2-mercaptoethanol to an optical density of 0.5 at 578 nm. The protein expression of the mutant autotransporter proteins was induced by addition of 1 mM isopropyl  $\beta$ -D-1-thiogalactopyranoside (IPTG). After incubation for 1 hour at 37 °C and 200 rpm the cell cultures were incubated at 4°C for 15 min to stop protein expression.

### ***Labeling of cells for the fluorescence-activated cell sorting (FACS)***

Cells carrying a plasmid for the wild type or a mutant autotransporter protein were incubated in LB, 10 mM 2-mercaptoethanol and 100  $\mu$ g/ml ampicillin at 37°C and 200 rpm to an optical density of 0.5 at 578 nm. Protein expression was induced by addition of 1 mM IPTG for one hour at 37°C and 200 rpm. The cells were cooled on ice for 15 min to stop the protein expression. Afterwards, aliquots of an optical density of 0.6 were washed with PBS and incubated with 3 % Bovine serum albumin (BSA) in PBS to block unspecific binding sites. Subsequently, the cell pellets were incubated for 30 min in a mouse-anti PEYFK antibody,

---

which detects the  $\alpha$ -domain of the autotransporter proteins used in these studies. The cell pellets were washed for three times in 3 % BSA in PBS and a goat-anti mouse secondary antibody, which was labeled with a red dye (Dylight 647), was added. After 30 min of incubation the labeled cells were washed with PBS and adjusted to an optical density of 1 at 578 nm. As a negative control *E. coli* UT5600 (DE3) without any plasmid was treated in the same manner. Subsequently, all samples were analyzed by fluorescence-activated cell sorting (FACS).



### 3. General discussion

This doctoral thesis deals with the structural determination of the transport unit of *adhesin involved in diffuse adherence* (AIDA-I) glycoprotein from *Escherichia coli*. AIDA-I was discovered in 1989 and assigned to the group of monomeric autotransporter (AT) within the type V secretion systems (T5SS) [39; 77]. For immunodetection, purification and crystallization experiments, the transport unit, termed AIDA-I-linker- $\beta_2$ , was fused to a his<sub>6</sub>-tag and a peptide antigen-tag (see Figure 6 in the introduction). The resulting fusion proteins were called FP-HisN163 and FP-HisC163. Intensive investigation focused on the expression of quantitative amounts of fully processed and correctly folded AT. The expression tests using an inducible promotor resulted in the expression of two differently processed forms (see chapter II), which was shown before [78]. Mass spectrometry revealed that the protein form with a higher molecular weight still carried the signal peptide, which should have been cleaved off by the signal peptidase during Sec-dependent transport across the inner membrane. Furthermore, heat modifiability assays confirmed that this protein form was not properly folded (chapter II). To promote the expression of the fully processed and correctly folded form of FP-HisN163 and FP-HisC163, various induction conditions and different kinds of *E. coli* strains were tested. However, in none of these experiments quantitative amounts of the fully processed and correctly folded forms of FP-HisN163 and FP-HisC163 sufficient for purification and crystallization were detected. Therefore, a constitutive expression system was tested yielding only the fully processed and correctly folded forms of FP-HisN163 and FP-HisC163 in quantitative amounts sufficient for purification experiments (chapter II). To release the AT from the OM, solubilization with the detergent LDAO was performed, which was also successfully applied for solubilization of e.g. the reaction center from *Rhodobacter sphaeroides* and the long-chain fatty acid transporter FadL from *Escherichia coli* [79; 80]. The purification of FP-HisN163 was conducted with immobilized metal ion affinity chromatography (IMAC) and size exclusion chromatography (SEC). SEC-MALS analysis of purified FP-HisN163 revealed that the protein solution was homogeneous and monodisperse and FP-HisN163 was a monomer in solution (see Figure II-19 in chapter II). The identity of the purified FP-HisN163 was confirmed by mass spectrometry (see Figure II-20 in chapter II). Since the developed purification protocol was sufficient to isolate quantitative amounts of pure FP-HisN163 suitable for crystallization, various crystallization conditions were tested using hanging drop vapor diffusion (chapter II). Several of the initial crystallization conditions were optimized yielding different kinds of crystals with varying diffraction quality. Finally, the data set of a single crystal needle, which was obtained in 100 mM sodium cacodylate, pH 6.5 and 27.5 (v/v) % PEG 2000 MME (chapter III), was used to solve the structure of AIDA-I-linker- $\beta_2$  at 3.0 Å resolution (chapter III and IV).

### 3.1 Crystal package

For structural determination of the transport unit of AIDA-I, the fusion protein FP-HisN163 comprising a short passenger domain and the transport unit of AIDA-I (residue L840-F1286) was crystallized (chapter III and IV). However, the crystal structure of AIDA-I-linker- $\beta_2$  only contains residues Q962-F1286 (see Figure 2A in chapter IV). The missing linker and passenger domain were not visible in the electron density presumably due to their high flexibility. The crystal package reveals that the contact between the monomers in the crystal is made by interaction of the extracellular loops 4 and 5 and  $\beta$ -strand 6 (Figure 10, circle 1) and by interaction of the periplasmic turn 3 with the extracellular loops L1 and L6 of (Figure 10, circle 2). It is likely that the missing linker and passenger domain are located in between the interacting monomers contributing to the crystal contact (Figure 10).

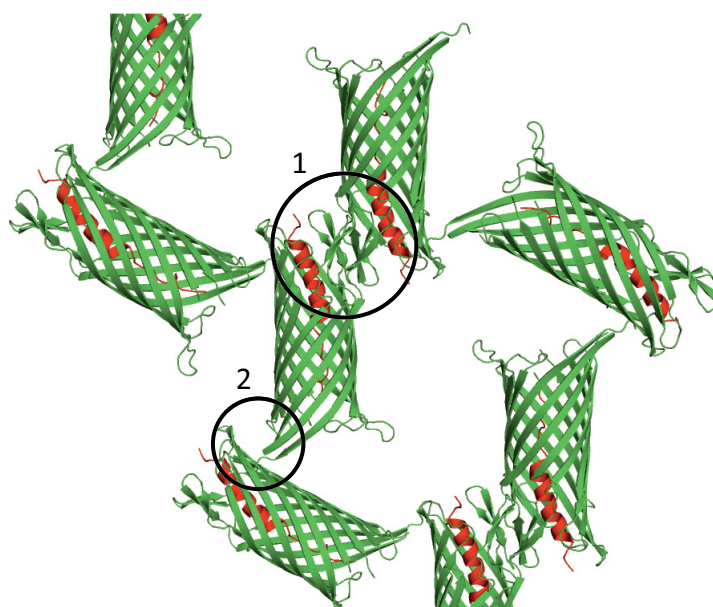


**Figure 10 Crystal packing of the transport unit of AIDA-I**

Green:  $\beta$ -barrel; red: linker

The contacts within the crystal is made by interaction of L4 and L5 (circle 1) and T3 with L1 and L6 (circle 2).

A single crystal needle of FP-HisN163 with dimensions of  $20 \times 20 \times 200 \mu\text{m}^3$  diffracted the X-rays to a final resolution of  $3.0 \text{ \AA}$  (chapter III and IV). During the last decade, several crystal structures of outer membrane proteins were solved at higher resolution ranging from  $1.85$  to  $2.7 \text{ \AA}$  [60; 61; 81-84]. The crystal quality concomitant with the resolution limit strongly depends on various parameters, such as crystal size, tightness of protein packing, order inside the crystal and also on the treatment during crystal harvesting, cryo-cooling and X-ray diffraction experiments [85]. Since the crystal needle of FP-HisN163 was very thin, it is reasonable that larger crystals would diffract to a higher resolution. However, optimization of the crystallization condition did not result in larger and therefore no higher resolution could be achieved.

## 3.2 Structural analysis of the transport unit of AIDA-I

### 3.2.1 The overall structure of AIDA-I-linker- $\beta_2$

The crystal structure of AIDA-I-linker- $\beta_2$  (residues Q962-F1286) contains a 12-stranded antiparallel  $\beta$ -barrel with the linker domain accommodated in the pore (see Figure 2A in chapter IV). These observations contradict the topology models proposed by different groups [38; 47; 52]. The  $\beta$ -barrel was predicted to be composed of 14  $\beta$ -strands comprising residues (Figure 11A). The difference in the number of strands forming the  $\beta$ -barrel is presumably due to the discontinuous  $\beta$ -strands S7-S10 interrupted by unstructured sections (Figure 11B), which resulted in a different prediction for the topology models (chapter IV). Nevertheless, Maurer *et al.* (1999) could show with deletion mutants that all of the predicted 14  $\beta$ -strands were necessary for correct outer membrane integration [54]. The linker domain was thought to adopt an  $\alpha$ -helical conformation in the pore [53], which was also observed for other monomeric AT (see Figure 7 in the introduction). For AIDA-I, only the N-terminal half of the linker reveals an  $\alpha$ -helical fold. The C-terminal end traverses the pore in an unstructured manner (see Figure 2A in chapter IV) due to missing polar interactions required for the formation of an  $\alpha$ -helix. It was shown that mutations affecting the linker domain did not abolish translocation of proAIDA-I (see Figure 4 in the introduction) [73]. However, proAIDA-I showed an abnormal protease sensitivity, which was interpreted that the mutations in the linker region lead to an incorrect conformation of the extracellular portion of AIDA-I. For the surface exposure of MalE using the transport unit of AIDA-I, none of the mutations had a significant effect on the translocation or folding properties. These observations were also made for the translocation of the cholera toxin B subunit (CTB) using a truncated linker domain of AIDA-I [54]. The results indicate that the translocation and folding of recombinant passenger domains do not require the same properties of the linker domain as necessary for efficient AIDA-I translocation and passenger domain folding.

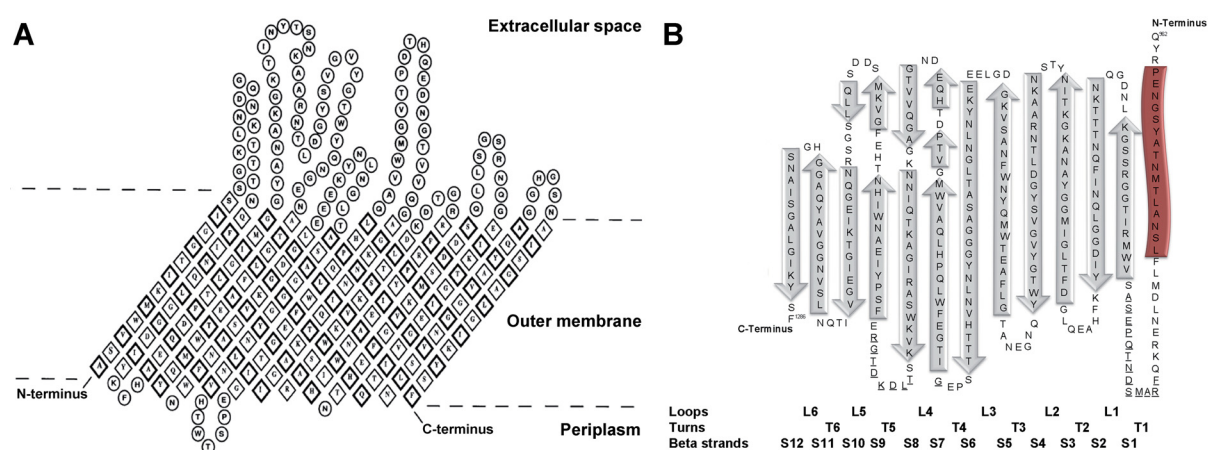


**Figure 11 Hypothetical topology (A) and topology determined from crystal structure (B) of the transport unit of AIDA-I**

A: Amino acids (one-letter code) within the membrane are indicated by diamonds and non-membrane-embedded regions by circles. Hydrophobic (boldface typesetting) and hydrophilic (lightface typesetting) amino acids are denoted. Picture taken from [38].

B: Grey arrows:  $\beta$ -strands; red box:  $\alpha$ -helical part of the linker domain; missing amino acids in the crystal structure of AIDA-I-linker- $\beta_2$  are underlined. Taken from chapter IV.

AIDA-I is predicted to contain a conserved autochaperone (AC) domain, termed  $\beta_1$ -domain, which is also found in other monomeric AT and seems to be involved in folding of passenger domains [43-45]. The  $\beta_1$ -domain is located between the C-terminal end of the  $\alpha$ -domain and the N-terminus of the linker domain (see Figure 4 in the introduction) comprising the residues A847-Y950 [40]. In 2005, Mogensen *et al.*, demonstrate that the  $\beta_1$ -domain stabilizes the  $\beta_2$ -domain and *in vitro* refolding of the  $\beta_2$ -domain in absence of the  $\beta_1$ -domain can only occur if a solid support is present [75]. These results indicate that not only the presence of the  $\beta_1$ -domain is sufficient for proper folding but another component, presumably the linker domain (see above), is required for the correct conformation of AIDA-I. For the monomeric AT Hbp from *E. coli*, it was shown that mutations affecting this region resulted in the accumulation of protease-sensitive periplasmic intermediates [45]. Oliver *et al.* (2003) investigated the role of the AC domain for BrkA by deletion experiments and protease accessibility assays [43]. They could show that this domain promotes folding of the BrkA passenger domain into a stable conformation. For AIDA-I, it is likely that not only the predicted  $\beta_1$ -domain seems to be involved in the correct folding of the  $\alpha$ -domain but the linker domain also has an impact on the proper conformation of the extracellular part of AIDA-I.

### 3.2.2 Comparison with other monomeric AT

In contrast to the variety in structure and function of the passenger domains, the transport units of monomeric AT share a high structural similarity (see chapter I and Table 2 in chapter IV). The extracellular loop 5, which was found to adopt a similar conformation in AIDA-I-linker- $\beta_2$  and the cleavage mutant EspP(N1023S) projecting into the extracellular space, undergoes drastic conformational changes from an 'open' to a 'closed' conformation in the wild type EspP (see Figure 2B and Figure S4 in chapter IV). In wild type EspP, only a small portion of the linker domain remains in the pore close to the periplasmic end after cleavage of the passenger domain (see Figure S4 in chapter IV). The conformational change moving L5 into the 'closed' state plugs the pore from the extracellular side and rearranges the polar interactions within the  $\beta$ -barrel. Thus, in  $\beta$ -strand 9 and 10 of EspP additional four and three amino acids are involved in the formation of the  $\beta$ -sheet compared to AIDA-I-linker- $\beta_2$  and EspP(N1023S). For AIDA-I-linker- $\beta_2$ , the sealing function is conducted by the linker domain, which resides in the pore (see Figure 2B in chapter IV). This observation is also true for other monomeric AT, e.g. EstA, NalP [61; 62] and Hbp (PDB code: 3AEH) (see Figure 7 in the introduction). Although L5 is involved in crystal contact in AIDA-I-linker- $\beta_2$  (Figure 10), it is likely that it adopts its native conformation as observed in EstA and EspP(N1023S), where this loop is not involved in crystal contact but also projects into the extracellular space due to the presence of the linker domain in the pore of their  $\beta$ -barrels [60; 62]. The linker domains of different monomeric AT share a similar  $\alpha$ -helical conformation (Figure 12). In case of EstA and NalP, the complete linker domains comprise an  $\alpha$ -helix. In contrast, only the N-terminal half of the linker domain adopts an  $\alpha$ -helical fold in AIDA-I, whereas the C-terminus remains unstructured (Figure 12).

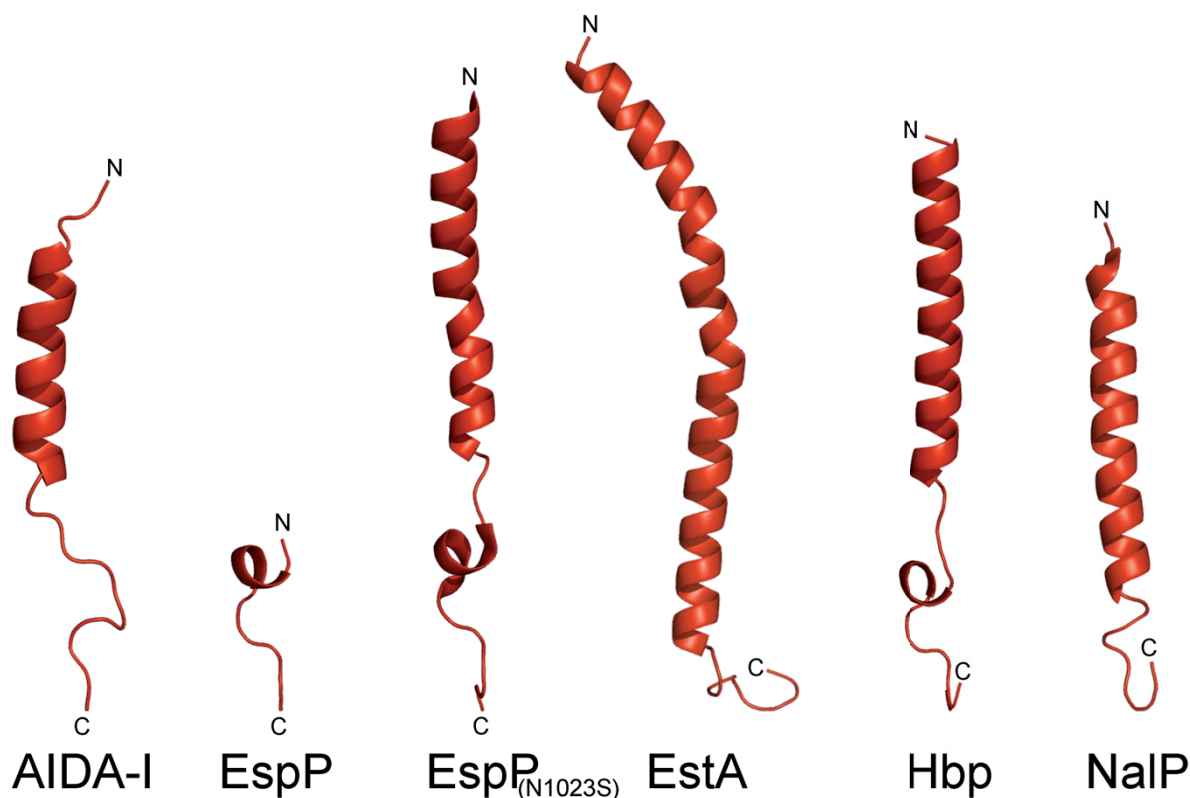


**Figure 12 Comparison of linker domains from monomeric AT**  
The N- and C-termini are labeled.

Due to post-translocational passenger cleavage of the EspP passenger domain, only the C-terminus of the  $\alpha$ -helical linker domain resides in the pore (Figure 12). In EspP(N1023S) and Hbp, the  $\alpha$ -helix is disrupted by an unstructured region and the same motif as observed in EspP is found at the C-terminal end of the linker domain. As described in chapter IV, the linker domains plug the pore to avoid leakage of ions and nutrients. In case of AIDA-I, the unstructured C-terminus of the linker domain can be extended, which is presumably necessary during adhesion to avoid disruption of the outer membrane. Furthermore, several amino acids, which play a key role in the biogenesis of EspP, were also conserved in AIDA-I-linker- $\beta_2$  (see Figure 3A and Figure S5 in chapter IV) and FhaC from *Bordetella pertussis* (see Figure 4 in chapter I), which belongs to the subgroup 'b' of T5SS [86] indicating the same role in the biogenesis not only for monomeric AT but for all members of T5SS. Mutational analysis of the C-terminal phenylalanine of AIDA-I revealed a strong impact of the hydrophobicity and aromaticity on outer membrane integration and passenger domain translocation, which was also shown for the *E. coli* porin PhoE and the monomeric AT Hap from *H. influenza* [87; 88]. The C-terminal phenylalanine is part of a consensus signature sequence typical for outer membrane proteins [52; 89; 90]. The signature sequence comprises the last 18 amino acids of the C-terminal end and is recognized by the outer membrane factor Omp85/BamA indicating a similar mechanism for membrane integration of OMPs in general.

### 3.2.3 A charged cluster at the extracellular side of AIDA-I-linker- $\beta_2$ serves as a binding platform for the $\beta_1$ -domain

In 1996, Suhr *et al.* demonstrate that AIDA<sub>C</sub> remains in the outer membrane after translocation and cleavage and is protected against proteolytic digestion when mature AIDA-I is present [47]. Thus, it was assumed that mature AIDA-I remains attached to AIDA<sub>C</sub> indicating a specific binding site. The analysis of the electrostatic surface of AIDA-I-linker- $\beta_2$  revealed charged clusters at the extracellular end of the  $\beta_2$ -domain, which could serve as binding platform (see Figure 13A-C). Interaction simulations with a model of the  $\beta_1$ -domain, which based on the AC domain of IcsA [44], and the structure of AIDA-I-linker- $\beta_2$  were performed resulting in the placement of the  $\beta_1$ -domain on such a charge cluster (Figure 13D/E).

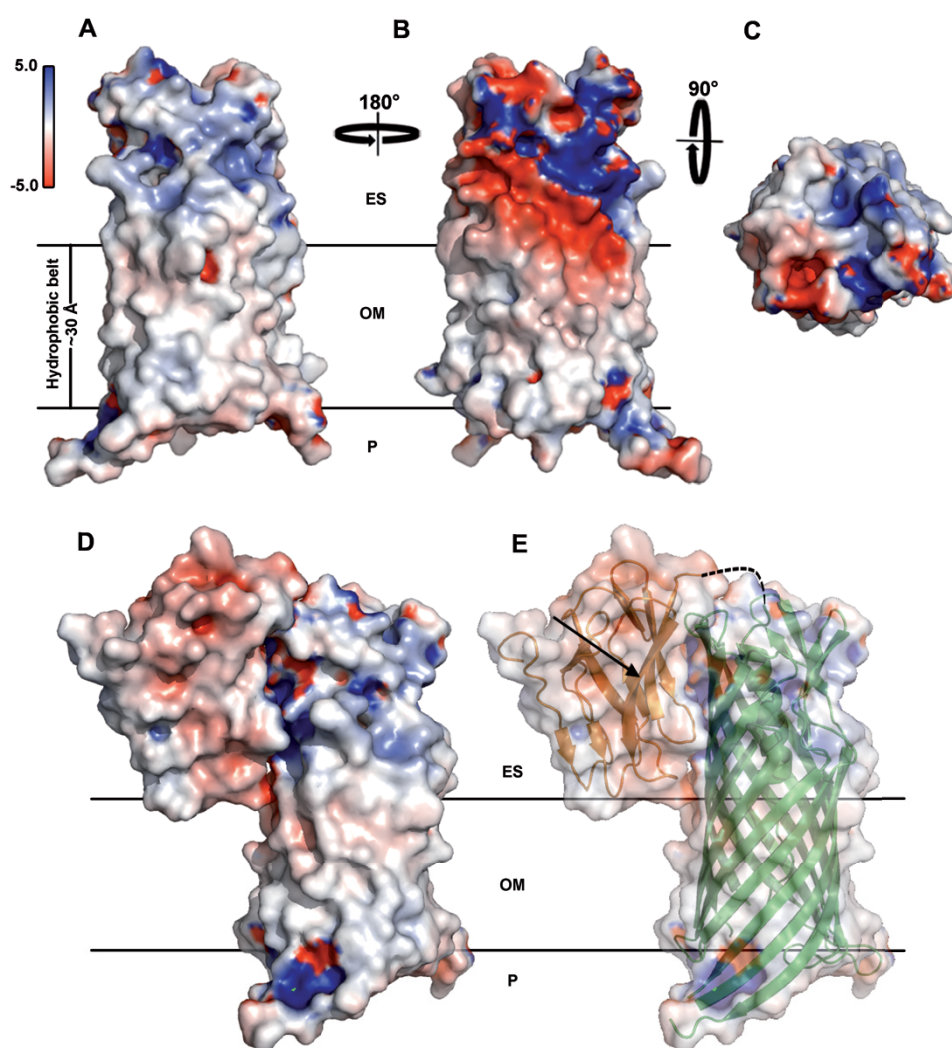


**Figure 13 Electrostatic surface of AIDA-I-linker- $\beta_2$  interacting with the  $\beta_1$ -domain**

A: Electrostatic surface of AIDA-I-linker- $\beta_2$ ; B: rotation by 180° around y-axis based on the position in A; C: rotation by 90° around x-axis based on the position in B; D: Electrostatic surface of AIDA-I-linker- $\beta_2$  and the interacting  $\beta_1$ -domain; E: ribbon presentation of AIDA-I-linker- $\beta_2$  (green) and the  $\beta_1$ -domain (orange) with an transparent overlay of the electrostatic surface; blue: positively charged contoured at +5 RT; white: uncharged; red: negatively charged contoured at -5 RT; ES: extracellular space; OM: outer membrane; P: periplasm. The missing connection between the  $\beta_1$ - and the  $\beta_2$ -domain is indicated by a dotted line (E). The arrow points to protease cleavage sites for TPCK-trypsin and TLCK-chymotrypsin (E). Picture adapted from chapter IV.



In consequence, the cleavage of the  $\alpha$ -domain is required for the correct positioning of the  $\beta_1$ -domain, which, together with the  $\beta_2$ -domain, could provide a binding platform for mature AIDA-I. Since the abolishment of  $\alpha$ -domain cleavage has no influence on the functionality of AIDA-I, the question why cleavage occurs remains open. One possibility is that mature AIDA-I itself serves as a binding platform for other unknown proteins or host factors during infection requiring a unique orientation, which is established after cleavage and attachment to the  $\beta_1$ - $\beta_2$ -binding platform but which is independent from the functionality of mature AIDA-I [91]. Although no condition could be determined for release of mature AIDA-I, another possibility is that during infection mature AIDA-I is released to enable the bacteria escaping from immunity response.

### 3.2.4 A common secretion mechanism for monomeric AT

In recent years, numerous investigations focused on the biogenesis of monomeric AT. Different model pathways were proposed, which try to consider all data obtained by biochemical, structural and bioinformatic analyses (see introduction and chapter I). A combination of the hairpin and the Omp85 model [24; 65] termed the 'alternative' model was proposed, which based on recently obtained data with the monomeric AT EspP from *E. coli* (see Figure 9 in the introduction) [69-71]. The formation of a periplasmic intermediate consisting of a prefolded  $\beta$ -barrel with an incorporated linker domain was shown [92], which is in good agreement to the 'alternative' model. Regarding the number of polar interactions within the transport units of monomeric AT, a stable core region could be defined comprising S2-S10 (see Figure 6A in chapter IV). It is reasonable that the prefolded  $\beta$ -barrel consists of the stable core region, which is subsequently integrated into the outer membrane in an 'open' conformation maintained by the BAM complex or probably TamA. This assumption is supported by observations made from the recently solved crystal structures of BamA and TamA [84; 93]. In both proteins, S16 is unstructured and points into the lumen of the 16-stranded  $\beta$ -barrel. In consequence, S1 and S16 form a shorter  $\beta$ -sheet, which creates an open cleft at the periplasmic end between S1 and S15. Furthermore, the extracellular loop 6 adopts a similar conformation in BamA and TamA sealing the  $\beta$ -barrel pore from the extracellular side. For BamA, a reduced hydrophobic surface near S16 was shown indicating a decrease in lipid order and membrane thickness [93]. Additionally, molecular dynamic simulations show that L6 and the POTRA domains are able to adopt different conformations. Two different modes of action for membrane integration of target OMPs were proposed. The BamA-assisted approach assumes a formation of a transient OMP-BamA complex after initiation of  $\beta$ -barrel formation of the target OMP. By lateral opening of BamA, the conformational switch of L6 and the movement of the POTRA domains the target OMP is threaded through the hybrid  $\beta$ -barrel pore and released into the disordered outer membrane near S16 of the BamA  $\beta$ -barrel [93]. In contrast, the BamA-independent approach suggests that the POTRA domains target the substrate OMP to the OM, which is directly integrated into the destabilized membrane. For TamA, a gating mechanism similar to the BamA-assisted approach with formation of a hybrid  $\beta$ -barrel was proposed [84]. For AIDA-I, no interaction with BamA could be shown by crosslinking



experiments until now [76]. Thus, the interaction with TamA or the BamA-independent approach needs to be analyzed.

The only possible region for lateral opening of the target AT  $\beta$ -barrel without breaking covalent bonds is between S12 and S1 (see Figure 6A in chapter IV). This hypothesis is supported by the significantly lower number of polar interactions between these  $\beta$ -strands within the flexible region (Table 1, green box) observed in the transport unit of AIDA-I and other monomeric AT. Furthermore, a stable core region can be defined for these transport units comprising S2-S10 (Table 1, red box). For EspP, a prefolded  $\beta$ -barrel was detected in the periplasm with an incorporated part of the linker domain in its pore [92]. It is reasonable that the prefolded  $\beta$ -barrel is composed of the stable core region. Other members of T5SS, e.g. intimin from *Escherichia coli* and FhaC from *Bordetella pertussis* [81; 86], which belong to the subgroup of reversed AT and to the two-partner secretion systems, also contain a stable core and a flexible region (Table 1). The stable core region comprises S2-S12 for intimin and S2-S14 for FhaC (Table 1, red box). The flexible region of intimin is composed of S12-S2 and for FhaC, it comprises S14-S2 (Table 1, green box). These findings indicate a common mechanism for membrane integration of the transport units of T5SS, for which a minimum flexible region of two  $\beta$ -sheets is sufficient. In contrast, the  $\beta$ -barrels of the *E. coli* porins PhoE [82] and OmpG [83] do not comprise a stable core and a flexible region (Table 1). Consequently, for the membrane integration of these porins the BamA-independent approach seems possible (see above).

**Table 1 Comparison of polar interactions within type Va  $\beta$ -barrels**

A stable core region (red box) and a flexible region (green box) can be defined within the  $\beta$ -barrels. Adapted from Table S2 in chapter IV.

	S1-S2	S2-S3	S3-S4	S4-S5	S5-S6	S6-S7	S7-S8	S8-S9	S9-S10	S10-S11	S11-S12	S12-13/ S12-S1	S13-S14/ S14-S1	S14-S15	S15-S16	S16-S1
AIDA-I	15	20	20	18	19	16+3*	16+5	12+4*	11+4	12	12	11				
EspP(N1023S)	16	20	18	19	21	6+8	14+8	14+5	14+7	11	10	15				
EspP	15	12+7*	7+12	12+7	17*	15	14+7*	18*	15	4+6	9	16				
EstA	16	15	18	19	23	1+14	17+4	13+4	12+7	13	12	14				
Hbp	15	19	19	19	12+4	16	12+3*	16	16*	12	10	15				
Intimin	8	14	13	13	13	9	4+9	10	9	9	12	8				
FhaC	8	10	9	13	14	17	20	12	12*	14	9	12	12	8	9	7
PhoE	9+3	11	13	8	8	9	13	11	11	12	13	12	16	11	9	9
OmpG	12*	11	6+3+2*	10+5	16	13	12	15	8+3	5+9	10*	11	13*			

\* incomplete connection between  $\beta$ -strands

The analysis of the pore of different monomeric AT revealed an ellipsoid shape except for NalP and comparable pore diameters (Figure 14). Regarding the linker domains, which traverse the pores, the diameter is too small to accommodate folded or modified passenger domains [61]. According to the BamA-assisted approach, the formation of a hybrid  $\beta$ -barrel would result in a pore, which would be large enough to translocate partially folded or modified passenger domains.

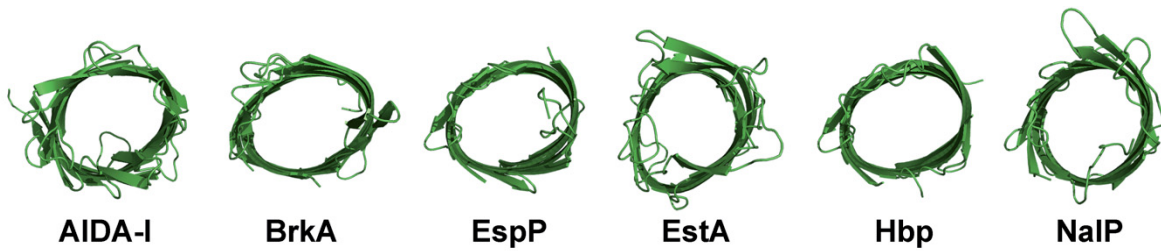


**Figure 14 Comparison of the transport unit pores from monomeric AT**

The crystal structures are shown in a similar orientation. The linker domains and in case of EspP L5 were removed from the pore.

Studies with AIDA-I and another monomeric AT TibA demonstrated that glycosylated passengers were efficiently secreted by *E. coli* [49; 66]. Furthermore, experimental evidence for successful translocation of folded passenger domains was obtained from experiments with the subunit of cholera toxin B (CTB), which is known to contain disulfide bonds generated in the periplasm [67].

### 3.3 Outlook

Despite lots of biochemical, structural and bioinformatic data, several details of the biogenesis of monomeric AT remains unclear. However, a common mechanism for membrane integration and passenger translocation, which tolerates individual properties of the AT, is reasonable. To clarify the details of these processes, the role of the BAM complex and the TAM should be further investigated by crosslinking experiments and mutational analyses. Furthermore, structural determination of AT intermediates should give more insight into the biogenesis of monomeric AT in Gram-negative bacteria.

## 4. References

1. Gram, C. (1884). Ueber die isolierte Faerbung der Schizomyceten in Schnitt- und Trockenpraeparaten. *Fortschritte der Medizin*, 2: 185-189.
2. Remaut, H. and Waksman, G. (2004). Structural biology of bacterial pathogenesis. *Curr Opin Struct Biol*, 14(2): 161-170.
3. Desvaux, M., Hebraud, M., Talon, R. and Henderson, I. R. (2009). Secretion and subcellular localizations of bacterial proteins: a semantic awareness issue. *Trends Microbiol*, 17(4): 139-145.
4. Cordwell, S. J. (2006). Technologies for bacterial surface proteomics. *Curr Opin Microbiol*, 9(3): 320-329.
5. Bingle, L. E., Bailey, C. M. and Pallen, M. J. (2008). Type VI secretion: a beginner's guide. *Curr Opin Microbiol*, 11(1): 3-8.
6. Christie, P. J. and Vogel, J. P. (2000). Bacterial type IV secretion: conjugation systems adapted to deliver effector molecules to host cells. *Trends Microbiol*, 8(8): 354-360.
7. Galan, J. E. and Collmer, A. (1999). Type III secretion machines: bacterial devices for protein delivery into host cells. *Science*, 284(5418): 1322-1328.
8. Holland, I. B., Schmitt, L. and Young, J. (2005). Type 1 protein secretion in bacteria, the ABC-transporter dependent pathway (review). *Mol Membr Biol*, 22(1-2): 29-39.
9. Sandkvist, M. (2001). Biology of type II secretion. *Mol Microbiol*, 40(2): 271-283.
10. Simeone, R., Bottai, D. and Brosch, R. (2009). ESX/type VII secretion systems and their role in host-pathogen interaction. *Curr Opin Microbiol*, 12(1): 4-10.
11. Thanassi, D. G., Stathopoulos, C., Karkal, A. and Li, H. (2005). Protein secretion in the absence of ATP: the autotransporter, two-partner secretion and chaperone/usher pathways of gram-negative bacteria (review). *Mol Membr Biol*, 22(1-2): 63-72.
12. Busch, A. and Waksman, G. (2012). Chaperone-usher pathways: diversity and pilus assembly mechanism. *Philos Trans R Soc Lond B Biol Sci*, 367(1592): 1112-1122.
13. Dalbey, R. E. and Kuhn, A. (2012). Protein traffic in Gram-negative bacteria--how exported and secreted proteins find their way. *FEMS Microbiol Rev*, 36(6): 1023-1045.
14. Rego, A. T., Chandran, V. and Waksman, G. (2010). Two-step and one-step secretion mechanisms in Gram-negative bacteria: contrasting the type IV secretion system and the chaperone-usher pathway of pilus biogenesis. *Biochem J*, 425(3): 475-488.
15. Pugsley, A. P. (1993). The complete general secretory pathway in gram-negative bacteria. *Microbiol Rev*, 57(1): 50-108.
16. Kudva, R., Denks, K., Kuhn, P., Vogt, A., Muller, M. and Koch, H. G. (2013). Protein translocation across the inner membrane of Gram-negative bacteria: the Sec and Tat dependent protein transport pathways. *Res Microbiol*.
17. Gerlach, R. G. and Hensel, M. (2007). Protein secretion systems and adhesins: the molecular armory of Gram-negative pathogens. *Int J Med Microbiol*, 297(6): 401-415.
18. Sandkvist, M. (2001). Type II secretion and pathogenesis. *Infect Immun*, 69(6): 3523-3535.
19. Cornelis, G. R. (2006). The type III secretion injectisome. *Nat Rev Microbiol*, 4(11): 811-825.
20. Cascales, E. and Christie, P. J. (2003). The versatile bacterial type IV secretion systems. *Nat Rev Microbiol*, 1(2): 137-149.
21. Alvarez-Martinez, C. E. and Christie, P. J. (2009). Biological diversity of prokaryotic type IV secretion systems. *Microbiol Mol Biol Rev*, 73(4): 775-808.
22. Christie, P. J. (2004). Type IV secretion: the *Agrobacterium* VirB/D4 and related conjugation systems. *Biochim Biophys Acta*, 1694(1-3): 219-234.
23. Desvaux, M., Parham, N. J. and Henderson, I. R. (2004). Type V protein secretion: simplicity gone awry? *Curr Issues Mol Biol*, 6(2): 111-124.
24. Henderson, I. R., Navarro-Garcia, F., Desvaux, M., Fernandez, R. C. and Ala'Aldeen, D. (2004). Type V protein secretion pathway: the autotransporter story. *Microbiol Mol Biol Rev*, 68(4): 692-744.
25. Leo, J. C., Grin, I. and Linke, D. (2012). Type V secretion: mechanism(s) of autotransport through the bacterial outer membrane. *Philos Trans R Soc Lond B Biol Sci*, 367(1592): 1088-1101.
26. Basler, M., Ho, B. T. and Mekalanos, J. J. (2013). Tit-for-tat: type VI secretion system counterattack during bacterial cell-cell interactions. *Cell*, 152(4): 884-894.
27. MacIntyre, D. L., Miyata, S. T., Kitaoka, M. and Pukatzki, S. (2010). The *Vibrio cholerae* type VI secretion system displays antimicrobial properties. *Proc Natl Acad Sci U S A*, 107(45): 19520-19524.

28. Basler, M., Pilhofer, M., Henderson, G. P., Jensen, G. J. and Mekalanos, J. J. (2012). Type VI secretion requires a dynamic contractile phage tail-like structure. *Nature*, **483**(7388): 182-186.
29. Kostakioti, M., Newman, C. L., Thanassi, D. G. and Stathopoulos, C. (2005). Mechanisms of protein export across the bacterial outer membrane. *J Bacteriol*, **187**(13): 4306-4314.
30. Stathopoulos, C., Hendrixson, D. R., Thanassi, D. G., Hultgren, S. J., St Geme, J. W., 3rd and Curtiss, R., 3rd. (2000). Secretion of virulence determinants by the general secretory pathway in gram-negative pathogens: an evolving story. *Microbes Infect*, **2**(9): 1061-1072.
31. Lo, A. W., Moonens, K. and Remaut, H. (2013). Chemical attenuation of pilus function and assembly in Gram-negative bacteria. *Curr Opin Microbiol*, **16**(1): 85-92.
32. Chapman, M. R., Robinson, L. S., Pinkner, J. S., Roth, R., Heuser, J., Hammar, M., Normark, S. and Hultgren, S. J. (2002). Role of *Escherichia coli* curli operons in directing amyloid fiber formation. *Science*, **295**(5556): 851-855.
33. Jose, J., Maas, R. M. and Teese, M. G. (2012). Autodisplay of enzymes--molecular basis and perspectives. *J Biotechnol*, **161**(2): 92-103.
34. Lee, S. Y., Choi, J. H. and Xu, Z. (2003). Microbial cell-surface display. *Trends Biotechnol*, **21**(1): 45-52.
35. Tanaka, T., Yamada, R., Ogino, C. and Kondo, A. (2012). Recent developments in yeast cell surface display toward extended applications in biotechnology. *Appl Microbiol Biotechnol*, **95**(3): 577-591.
36. Loset, G. A. and Sandlie, I. (2012). Next generation phage display by use of pVII and pIX as display scaffolds. *Methods*, **58**(1): 40-46.
37. Smith, G. P. (1985). Filamentous fusion phage: novel expression vectors that display cloned antigens on the virion surface. *Science*, **228**(4705): 1315-1317.
38. Maurer, J., Jose, J. and Meyer, T. F. (1997). Autodisplay: one-component system for efficient surface display and release of soluble recombinant proteins from *Escherichia coli*. *J Bacteriol*, **179**(3): 794-804.
39. Jose, J., Jahnig, F. and Meyer, T. F. (1995). Common structural features of IgA1 protease-like outer membrane protein autotransporters. *Mol Microbiol*, **18**(2): 378-380.
40. Konieczny, M. P. J., Benz, I., Hollinderbaumer, B., Beinke, C., Niederweis, M. and Schmidt, M. A. (2001). Modular organization of the AIDA autotransporter translocator: the N-terminal beta1-domain is surface-exposed and stabilizes the transmembrane beta2-domain. *Antonie Van Leeuwenhoek*, **80**(1): 19-34.
41. Benz, I. and Schmidt, M. A. (2011). Structures and functions of autotransporter proteins in microbial pathogens. *Int J Med Microbiol*, **301**(6): 461-468.
42. Charbonneau, M. E., Girard, V., Nikolakakis, A., Campos, M., Berthiaume, F., Dumas, F., Lepine, F. and Mourez, M. (2007). O-linked glycosylation ensures the normal conformation of the autotransporter adhesin involved in diffuse adherence. *J Bacteriol*, **189**(24): 8880-8889.
43. Oliver, D. C., Huang, G., Nodel, E., Pleasance, S. and Fernandez, R. C. (2003). A conserved region within the *Bordetella pertussis* autotransporter BrkA is necessary for folding of its passenger domain. *Mol Microbiol*, **47**(5): 1367-1383.
44. Kuhnel, K. and Diezmann, D. (2011). Crystal structure of the autochaperone region from the *Shigella flexneri* autotransporter IcsA. *J Bacteriol*, **193**(8): 2042-2045.
45. Soprova, Z., Sauri, A., van Ulsen, P., Tame, J. R., den Blaauwen, T., Jong, W. S. and Luirink, J. (2010). A conserved aromatic residue in the autochaperone domain of the autotransporter Hbp is critical for initiation of outer membrane translocation. *J Biol Chem*, **285**(49): 38224-38233.
46. Benz, I. and Schmidt, M. A. (1992). AIDA-I, the adhesin involved in diffuse adherence of the diarrhoeagenic *Escherichia coli* strain 2787 (O126:H27), is synthesized via a precursor molecule. *Mol Microbiol*, **6**(11): 1539-1546.
47. Suhr, M., Benz, I. and Schmidt, M. A. (1996). Processing of the AIDA-I precursor: removal of AIDAc and evidence for the outer membrane anchoring as a beta-barrel structure. *Mol Microbiol*, **22**(1): 31-42.
48. Charbonneau, M. E., Berthiaume, F. and Mourez, M. (2006). Proteolytic processing is not essential for multiple functions of the *Escherichia coli* autotransporter adhesin involved in diffuse adherence (AIDA-I). *J Bacteriol*, **188**(24): 8504-8512.
49. Charbonneau, M. E. and Mourez, M. (2007). Functional organization of the autotransporter adhesin involved in diffuse adherence. *J Bacteriol*, **189**(24): 9020-9029.
50. Junker, M., Besingi, R. N. and Clark, P. L. (2009). Vectorial transport and folding of an autotransporter virulence protein during outer membrane secretion. *Mol Microbiol*, **71**(5): 1323-1332.
51. Klemm, P., Vejborg, R. M. and Sherlock, O. (2006). Self-associating autotransporters, SAATs: functional and structural similarities. *Int J Med Microbiol*, **296**(4-5): 187-195.
52. Loveless, B. J. and Saier, M. H., Jr. (1997). A novel family of channel-forming, autotransporting, bacterial virulence factors. *Mol Membr Biol*, **14**(3): 113-123.

53. Kostakioti, M. and Stathopoulos, C. (2006). Role of the alpha-helical linker of the C-terminal translocator in the biogenesis of the serine protease subfamily of autotransporters. *Infect Immun*, *74*(9): 4961-4969.
54. Maurer, J., Jose, J. and Meyer, T. F. (1999). Characterization of the essential transport function of the AIDA-I autotransporter and evidence supporting structural predictions. *J Bacteriol*, *181*(22): 7014-7020.
55. Jose, J., Betscheider, D. and Zangen, D. (2005). Bacterial surface display library screening by target enzyme labeling: Identification of new human cathepsin G inhibitors. *Anal Biochem*, *346*(2): 258-267.
56. Henderson, I. R., Navarro-Garcia, F. and Nataro, J. P. (1998). The great escape: structure and function of the autotransporter proteins. *Trends Microbiol*, *6*(9): 370-378.
57. Leyton, D. L., Rossiter, A. E. and Henderson, I. R. (2012). From self sufficiency to dependence: mechanisms and factors important for autotransporter biogenesis. *Nat Rev Microbiol*, *10*(3): 213-225.
58. Meng, G., Surana, N. K., St Geme, J. W., 3rd and Waksman, G. (2006). Structure of the outer membrane translocator domain of the Haemophilus influenzae Hia trimeric autotransporter. *EMBO J*, *25*(11): 2297-2304.
59. Thanassi, D. G. and Hultgren, S. J. (2000). Multiple pathways allow protein secretion across the bacterial outer membrane. *Curr Opin Cell Biol*, *12*(4): 420-430.
60. Barnard, T. J., Dautin, N., Lukacik, P., Bernstein, H. D. and Buchanan, S. K. (2007). Autotransporter structure reveals intra-barrel cleavage followed by conformational changes. *Nat Struct Mol Biol*, *14*(12): 1214-1220.
61. Oomen, C. J., van Ulsen, P., van Gelder, P., Feijen, M., Tommassen, J. and Gros, P. (2004). Structure of the translocator domain of a bacterial autotransporter. *EMBO J*, *23*(6): 1257-1266.
62. van den Berg, B. (2010). Crystal structure of a full-length autotransporter. *J Mol Biol*, *396*(3): 627-633.
63. Zhai, Y., Zhang, K., Huo, Y., Zhu, Y., Zhou, Q., Lu, J., Black, I., Pang, X., Roszak, A. W., Zhang, X., Isaacs, N. W. and Sun, F. (2011). Autotransporter passenger domain secretion requires a hydrophobic cavity at the extracellular entrance of the beta-domain pore. *Biochem J*, *435*(3): 577-587.
64. Bernstein, H. D. (2007). Are bacterial 'autotransporters' really transporters? *Trends Microbiol*, *15*(10): 441-447.
65. Voulhoux, R., Bos, M. P., Geurtsen, J., Mols, M. and Tommassen, J. (2003). Role of a highly conserved bacterial protein in outer membrane protein assembly. *Science*, *299*(5604): 262-265.
66. Lindenthal, C. and Elsinghorst, E. A. (1999). Identification of a glycoprotein produced by enterotoxigenic Escherichia coli. *Infect Immun*, *67*(8): 4084-4091.
67. Skillman, K. M., Barnard, T. J., Peterson, J. H., Ghirlando, R. and Bernstein, H. D. (2005). Efficient secretion of a folded protein domain by a monomeric bacterial autotransporter. *Mol Microbiol*, *58*(4): 945-958.
68. Peterson, J. H., Tian, P., Ieva, R., Dautin, N. and Bernstein, H. D. (2010). Secretion of a bacterial virulence factor is driven by the folding of a C-terminal segment. *Proc Natl Acad Sci U S A*, *107*(41): 17739-17744.
69. Ieva, R., Tian, P., Peterson, J. H. and Bernstein, H. D. (2011). Sequential and spatially restricted interactions of assembly factors with an autotransporter beta domain. *Proc Natl Acad Sci U S A*, *108*(31): 383-391.
70. Pavlova, O., Peterson, J. H., Ieva, R. and Bernstein, H. D. (2013). Mechanistic link between beta barrel assembly and the initiation of autotransporter secretion. *Proc Natl Acad Sci U S A*, *110*(10): E938-947.
71. Gawarzewski, I., Smits, S. H., Schmitt, L. and Jose, J. (2013). Structural comparison of the transport units of type V secretion systems. *Biol Chem*, *394*(11): 1385-1398.
72. Selkrig, J., Mosbahi, K., Webb, C. T., Belousoff, M. J., Perry, A. J., Wells, T. J., Morris, F., Leyton, D. L., Totsika, M., Phan, M. D., Celik, N., Kelly, M., Oates, C., Hartland, E. L., Robins-Browne, R. M., Ramarathnam, S. H., Purcell, A. W., Schembri, M. A., Strugnell, R. A., Henderson, I. R., Walker, D. and Lithgow, T. (2012). Discovery of an archetypal protein transport system in bacterial outer membranes. *Nat Struct Mol Biol*, *19*(5): 506-510, S501.
73. Berthiaume, F., Rutherford, N. and Mourez, M. (2007). Mutations affecting the biogenesis of the AIDA-I autotransporter. *Res Microbiol*, *158*(4): 348-354.
74. Mogensen, J. E., Kleinschmidt, J. H., Schmidt, M. A. and Otzen, D. E. (2005). Misfolding of a bacterial autotransporter. *Protein Sci*, *14*(11): 2814-2827.
75. Mogensen, J. E., Tapadar, D., Schmidt, M. A. and Otzen, D. E. (2005). Barriers to folding of the transmembrane domain of the Escherichia coli autotransporter adhesin involved in diffuse adherence. *Biochemistry*, *44*(11): 4533-4545.
76. Muller, D., Benz, I., Tapadar, D., Buddenborg, C., Greune, L. and Schmidt, M. A. (2005). Arrangement of the translocator of the autotransporter adhesin involved in diffuse adherence on the bacterial surface. *Infect Immun*, *73*(7): 3851-3859.
77. Benz, I. and Schmidt, M. A. (1989). Cloning and expression of an adhesin (AIDA-I) involved in diffuse adherence of enteropathogenic Escherichia coli. *Infect Immun*, *57*(5): 1506-1511.

- 
78. Winterer, E. (2009). Untersuchung zur Struktur und Funktion der Transportdomänen des Autodisplay Systems. Dissertation, Heinrich-Heine-University, Duesseldorf.
  79. Camara-Artigas, A., Brune, D. and Allen, J. P. (2002). Interactions between lipids and bacterial reaction centers determined by protein crystallography. *Proc Natl Acad Sci U S A*, 99(17): 11055-11060.
  80. van den Berg, B., Black, P. N., Clemons, W. M., Jr. and Rapoport, T. A. (2004). Crystal structure of the long-chain fatty acid transporter FadL. *Science*, 304(5676): 1506-1509.
  81. Fairman, J. W., Dautin, N., Wojtowicz, D., Liu, W., Noinaj, N., Barnard, T. J., Udho, E., Przytycka, T. M., Cherezov, V. and Buchanan, S. K. (2012). Crystal structures of the outer membrane domain of intimin and invasins from enterohemorrhagic *E. coli* and enteropathogenic *Y. pseudotuberculosis*. *Structure*, 20(7): 1233-1243.
  82. Cowan, S. W., Schirmer, T., Rummel, G., Steiert, M., Ghosh, R., Pauptit, R. A., Jansonius, J. N. and Rosenbusch, J. P. (1992). Crystal structures explain functional properties of two *E. coli* porins. *Nature*, 358(6389): 727-733.
  83. Subbarao, G. V. and van den Berg, B. (2006). Crystal structure of the monomeric porin OmpG. *J Mol Biol*, 360(4): 750-759.
  84. Gruss, F., Zahringer, F., Jakob, R. P., Burmann, B. M., Hiller, S. and Maier, T. (2013). The structural basis of autotransporter translocation by TamA. *Nat Struct Mol Biol*.
  85. Rupp, B. 2010. Biomolecular Crystallography. New York/USA: Garland Science. 978-0-8153-4081-2
  86. Clantin, B., Delattre, A. S., Rucktooa, P., Saint, N., Meli, A. C., Locht, C., Jacob-Dubuisson, F. and Villeret, V. (2007). Structure of the membrane protein FhaC: a member of the Omp85-TpsB transporter superfamily. *Science*, 317(5840): 957-961.
  87. Hendrixson, D. R., de la Morena, M. L., Stathopoulos, C. and St Geme, J. W., 3rd. (1997). Structural determinants of processing and secretion of the *Haemophilus influenzae* hsp protein. *Mol Microbiol*, 26(3): 505-518.
  88. Struyvé, M., Moons, M. and Tommassen, J. (1991). Carboxy-terminal phenylalanine is essential for the correct assembly of a bacterial outer membrane protein. *J Mol Biol*, 218(1): 141-148.
  89. Robert, V., Volokhina, E. B., Senf, F., Bos, M. P., Van Gelder, P. and Tommassen, J. (2006). Assembly factor Omp85 recognizes its outer membrane protein substrates by a species-specific C-terminal motif. *PLoS Biol*, 4(11): e377.
  90. Tommassen, J. (2010). Assembly of outer-membrane proteins in bacteria and mitochondria. *Microbiology*, 156(Pt 9): 2587-2596.
  91. Charbonneau, M. E., Janvare, J. and Mourez, M. (2009). Autoprocessing of the *Escherichia coli* AIDA-I autotransporter: a new mechanism involving acidic residues in the junction region. *J Biol Chem*, 284(25): 17340-17351.
  92. Ieva, R., Skillman, K. M. and Bernstein, H. D. (2008). Incorporation of a polypeptide segment into the beta-domain pore during the assembly of a bacterial autotransporter. *Mol Microbiol*, 67(1): 188-201.
  93. Noinaj, N., Kuszak, A. J., Gumbart, J. C., Lukacik, P., Chang, H., Easley, N. C., Lithgow, T. and Buchanan, S. K. (2013). Structural insight into the biogenesis of beta-barrel membrane proteins. *Nature*.

## 5. Abbreviations

Å	Angstrom
ABC	<u>A</u> TP <u>b</u> inding <u>c</u> assette
AIDA-I	<u>A</u> dhesin <u>i</u> nvolved in <u>d</u> iffuse <u>a</u> dherence <u>I</u>
AIDA-I-linker-β <sub>2</sub>	transport unit of <u>A</u> dhesin <u>i</u> nvolved in <u>d</u> iffuse <u>a</u> dherence <u>I</u> consisting of the linker and the β-barrel forming domain
AmmSO <sub>4</sub>	ammonium sulfate
AT	<u>a</u> uto <u>t</u> ransporter
ATP	<u>A</u> denosine-5'-triphosphate
CHAPSO	3-[(3- <u>c</u> holamidopropyl)-dimethyl <u>a</u> mmonio]-1-propanesulfonate
CU	<u>c</u> haperone- <u>u</u> sher
DDM	n- <u>d</u> odecyl-β-D- <u>m</u> altoside
DM	n- <u>d</u> ecyl-β-D- <u>m</u> altoside
<i>E. coli</i>	<i>Escherichia coli</i>
e.g.	<u>e</u> xempli gratia
eh	<u>e</u> xperimental <u>h</u> utch
ESI	<u>e</u> lectro <u>s</u> pray <u>i</u> onisation
FC-14	<u>F</u> OS- <u>C</u> holine 14
FP-HisN163	<u>f</u> usion <u>p</u> rotein with <u>N</u> -terminal His tag and a linker length of <u>163</u> amino acids
FP-HisC163	<u>f</u> usion <u>p</u> rotein with <u>C</u> -terminal His tag and a linker length of <u>163</u> amino acids
g	gram
GSP	<u>g</u> eneral <u>s</u> ecretory <u>p</u> athway
His/his <sub>6</sub> tag	<u>h</u> istidine tag
IMAC	<u>i</u> mmobilized <u>m</u> etal ion <u>c</u> hromatography
IPTG	<u>I</u> sopropyl-β-D- <u>t</u> hiogalactopyranoside
K	<u>K</u> elvin
kDa	<u>k</u> ilo <u>D</u> alton
LDAO	<u>L</u> auryl <u>d</u> imethyl <u>a</u> mine- <u>o</u> xide
M	<u>m</u> olar
MFP	<u>m</u> embrane <u>f</u> usion <u>p</u> rotein
mg	<u>m</u> illigram

---

μg	microgram
min	<u>min</u> utes
mM	<u>milli</u> molar
MS	<u>mass</u> <u>spectrometry</u>
nm	<u>nanometer</u>
OD	<u>optical</u> <u>density</u>
OM	<u>outer</u> <u>membrane</u>
Omp	<u>outer</u> <u>membrane</u> <u>protein</u>
oriT	<u>origin</u> of <u>transfer</u>
PAGE	<u>polyacrylamide</u> <u>gel</u> <u>electrophoresis</u>
PCR	<u>polymerase</u> <u>chain</u> <u>reaction</u>
PEYFK	peptide antigen tag for immunodetection consisting of proline ( <u>P</u> ), glutamic acid ( <u>E</u> ), tyrosine ( <u>Y</u> ), phenylalanine ( <u>F</u> ) and lysine ( <u>K</u> )
PVDF	<u>polyvinylidene</u> <u>difluoride</u>
QqTOF	<u>quadrupole</u> <u>time-of-flight</u>
RNA	<u>ribonucleic</u> <u>acid</u>
rpm	<u>revolutions</u> per <u>minute</u>
SDS	<u>sodium</u> <u>dodecyl</u> <u>sulfate</u>
SEC	<u>Size</u> <u>exclusion</u> <u>chromatography</u>
SP	<u>signal</u> <u>peptide</u>
ssDNA	single-stranded DNA
Tat	<u>T</u> win <u>A</u> rginine <u>T</u> ranslocation
TDM	n- <u>tri</u> <u>decyl</u> -β-D- <u>mal</u> toside
TXSS	type X secretion system
V	<u>volts</u>
v/v	volume per volume
w/v	weight per volume
X-ray	electromagnetic radiation with wavelengths in the range of 0.1-10 nm



## 6. Acknowledgement

Zunächst möchte ich Prof. Dr. Lutz Schmitt danken. Getreu Lutz' Motto "Der Tag hat 24 Stunden und die Nacht ist ja auch noch da!" weiß ich jetzt, wie er es geschafft hat trotz seiner Verpflichtungen mein "exotisches" Projekt mit großen Interesse zu verfolgen und bei jedem Messtrip mit zu fiebern! Danke, für die experimentelle Freiheit, das Vertrauen, den ab und an nötigen "Motivations"tritt und den Glauben an den "einen" Kristall!

Prof. Joachim Jose möchte ich für die das interessante Projekt, die freundliche Aufnahme in seiner Arbeitsgruppe zu Beginn der Promotion und die Unterstützung danken.

Sander: du schaffst es mit deiner "holländischen" Gelassenheit und den richtigen Worten das Chaos in meinem Kopf zu ordnen und die Dinge auf den Punkt zu bringen! Ich danke dir für deine Unterstützung auf unseren gemeinsamen Messtrips, deine unendliche Geduld meine geistigen Ergüsse Korrektur zu lesen und deine Fähigkeit meine oft pessimistische Denkweise aufzulockern!

Ein besonderer Dank gilt auch meinem "Trio crystallographica" Dr. Britta Ries, Dr. Astrid Höppner und Isabell Wingartz. Britta, ohne deine Hilfe bei den ersten Schritten der Reinigung und Kristallographie wäre das Projekt nicht so schnell voran geschritten! Astrid: "Et kütt wie et kütt, et is wie et is un et hätt noch imma joot jejange!" Mit deiner absolute Seelenruhe, deinen offenen Ohren und deinem positives Denken hast du mir durch etliche Enttäuschungen und Rückschläge geholfen! Mein Kristallographie-Küken Isa hat mich so manches Mal zum Lachen gebracht und mit ihrer positiven und hilfsbereiten Art immer für gute Stimmung gesorgt! Ohne euch drei wären die Messtrips nicht so lustig gewesen und die Arbeit nicht so leicht von der Hand gegangen!

Marianne Kluth und Ricarda Moseler möchte ich für die tolle Zusammenarbeit, das gute Klima in Labor und Büro und für die unzähligen Stunden bei Tee und Kaffee danken! Danke für eure Unterstützung, offenen Ohren und Ablenkung, wenn wie so oft nichts funktionieren wollte!

Allen jetzigen und ehemaligen Mitarbeitern der AG Schmitt und der AG Jose danke ich für die tolle Arbeitsatmosphäre und die vielen Gespräche: Martina Wesemann, Ananda Ayyappan, Dr. Nacera Infed, Zainab Al-Kathib, Sven Reimann, Dr. Diana Kleinschrodt, Iris Fey, Susanne Przybylla, Sabrina Thomas, Sakshi Khosa, Kerstin Kanonenberg, Sadber Rasid, Michael Lenders, André Abts, Dr. Christian Schwarz, Miroslav Kirov, Dr. Nils Hanekop, Rakeshkumar Gupta, Dr. Ulrich Schulte, Dr. Philipp Ellinger, Tatu Meyer, Dr. Jan Stindt, Dr. Patrick Bakkes, Dr. Antonino Mavaro, Dr. Veronika Kemke, Irina Altendorfer, Bertan Bopp, Achim Braukmann, Michael Goblirsch, Zoya Orlando, Agne Tubeleviciute, Dr. Claas

Hundsdoerfer, Dr. Tatjana Brossette, Dr. Ruth Maas, Dr. Tanja Völker, Dr. Mark Teese, Dr. Andreas Gratz, Dr. Sarah Thömmes, Dr. Claudia Reicheneder, Dr. Stephanie Schumacher, Dr. Eva Kranen, Dr. Christian Detzel, Dr. Klaudia Petermann, Nora Stellisch, Karin Voigt, Heinz Matthew, Peter Sippel, Gaby Zerta

Dr. Cordula Kruse danke ich für die tolle Betreuung und Organisation im Rahmen des BioStruct-Stipendiums, die stets offene Tür und die motivierenden Gespräche!

Zum Schluss möchte ich meiner Familie und meinen Freunden danken, die mich immer aufgefangen und, was noch viel wichtiger ist, wieder aufgebaut haben. Danke an meine Eltern Gerd und Gudrun, an meinen Bruder Axel und an Gabriele und Christian Hauptelshofer. Ihr habt mir den Rücken immer freigehalten und mich dabei unterstützt meine Ziele zu verfolgen und zu erreichen!

Zum Schluss möchte ich mich bei dem Menschen bedanken, der mich immer aufgefangen und aufgebaut und all (!!!!) meine Launen ertragen hat: Steffen Hauptelshofer! Danke für die Unterstützung, unendliche Geduld, Ablenkung und Liebe.

## 7. Curriculum Vitae

### Personal data

Date and place of birth	11.10.1984 in Leverkusen, Germany
Nationality	German

### Work Experience

Sep 2009 - Dec 2013	PhD student in the Department of Pharmaceutical and Medical Chemistry with Prof. Dr. Joachim Jose and in the Institute of Biochemistry with Prof. Dr. Lutz Schmitt, Heinrich-Heine University Düsseldorf, Germany
---------------------	---

### Academic education

Oct 2004 - Mar 2009	Diploma studies in Biology at the Heinrich-Heine University Düsseldorf, Germany Degree: <b>Diplom-Biologin</b>
---------------------	---

### School Education

Aug 1991 – Jul 2004	Elementary and secondary school in Leverkusen, Germany Degree: <b>Abitur</b>
---------------------	---

### Further Training and Commitments

since Oct 2010	Member of the graduate school iGRAD
since Sep 2009	Member of the International Research School 'BioStruct'
Apr 2005 – Okt 2008	Member of the student council for biology

### List of publications

Articles	<p><b>Gawarzewski I</b>, Smits SHJ, Schmitt L and Jose J. Structural comparison of the transport units of type V secretion systems. <b>Biological Chemistry</b> (2013); 394(11): 1385-1398</p> <p><b>Gawarzewski I</b>, Tschapek B, Hoeppner A, Jose J, Smits SHJ and Schmitt, L. Purification, crystallization and preliminary X-ray crystallographic analysis of the transport unit of the monomeric autotransporter AIDA-I from <i>Escherichia coli</i>. <b>Acta Crystallographica Section F</b> (2013); 69: 1159-1162</p>
----------	---

- 
- Poster presentations
- Gawarzewski I**, Jose J (2010) Overexpression of the His-tagged AIDA-I  $\beta$ -barrel in the outer membrane of *E. coli*. Biostruct's Master Class 2010, 06.-09. September, Düsseldorf, Poster BSMS2010-23
- Gawarzewski I**, Jose J, Tschapek B, Smits SHJ, Schmitt L (2011) Purification and Crystallization of the AIDA-I  $\beta$ -barrel in the outer membrane of *E. coli*. Biostruct's Master Class 2011, 12.-15. September, Düsseldorf, Poster MC2011-17
- Gawarzewski I**, Jose J, Tschapek B, Smits SHJ, Schmitt L (2011) Purification and Crystallization of the AIDA-I  $\beta$ -barrel in the outer membrane of *E. coli*. Molecular Life Sciences 2011, 25.-28. September, Frankfurt, Poster DOI®: 10.3288/contoo.paper1353
- Gawarzewski I**, Jose J, Smits SHJ, Schmitt L (2013) The crystal structure of the membrane protein AIDA-I from *Escherichia coli*. Biostruct Symposium 2013, 04.-06. November, Düsseldorf, Poster BS2013-05
- Oral presentations
- Gawarzewski I**, Jose J, Tschapek B, Smits SHJ, Schmitt L (2011) Purification and Crystallization of the AIDA-I  $\beta$ -barrel in the outer membrane of *E. coli*. Biostruct's Master Class 2011, 12.-15. September, Düsseldorf.
- Gawarzewski I**, Jose J, Smits SHJ, Schmitt L (2013) The crystal structure of the membrane protein AIDA-I from *Escherichia coli*. Biostruct Symposium 2013, 04.-06. November, Düsseldorf.

## 8. Statement

Ich versichere an Eides Statt, dass die Dissertation von mir selbstständig und ohne unzulässig fremde Hilfe unter Beachtung der „Grundsätze zur Sicherung guter wissenschaftlicher Praxis“ an der Heinrich-Heine-Universität Düsseldorf erstellt worden ist. Die Dissertation wurde in der vorgelegten oder in ähnlicher Form noch bei keiner anderen Institution eingereicht. Ich habe bisher keine erfolglosen Promotionsversuche unternommen.

Düsseldorf, den

---

Iris Gawarzewski